DEVELOPMENT OF CELLULOSE AS SUBSTRATES FOR ADSORBENTS AND SENSORS

Mr. Jadetapong Klahan

จุฬาลงกรณ์มหาวิทยาลัย
CHULALONGKORN UNIVERSITY

A Dissertation Submitted in Partial Fulfillment of the Requirements

for the Degree of Doctor of Philosophy in Petrochemistry

Common Course

FACULTY OF SCIENCE

Chulalongkorn University

Academic Year 2020

Copyright of Chulalongkorn University

การพัฒนาเซลลูโลสเป็นซับสเตรตสำหรับเป็นตัวดูดซับและตัวรับรู้

นายเจตพงษ์ กล้าหาญ

จุฬาลงกรณ์มหาวิทยาลัย
CHULALONGKORN UNIVERSITY

วิทยานิพนธ์นี้เป็นส่วนหนึ่งของการศึกษาตามหลักสูตรปริญญาวิทยาศาสตรดุษฎีบัณฑิต
สาขาวิชาปิโตรเคมี ไม่สังกัดภาควิชา/เทียบเท่า
คณะวิทยาศาสตร์ จุฬาลงกรณ์มหาวิทยาลัย
ปีการศึกษา 2563

Thesis Title	DEVELOPMENT OF CELLULOSE AS SUBSTRATES FOR ADSORBENTS AND SENSORS
By	Mr. Jadetapong Klahan
Field of Study	Petrochemistry
Thesis Advisor	Professor MONGKOL SUKWATTANASINITT, Ph.D.
Thesis Co Advisor	Gamolwan Tumcharern, Ph.D.

Accepted by the FACULTY OF SCIENCE, Chulalongkorn University in Partial Fulfillment of the Requirement for the Doctor of Philosophy

.. Dean of the FACULTY OF SCIENCE

(Professor POLKIT SANGVANICH, Ph.D.)

DISSERTATION COMMITTEE

.. Chairman

(Assistant Professor WARINTHORN CHAVASIRI, Ph.D.)

.. Thesis Advisor

(Professor MONGKOL SUKWATTANASINITT, Ph.D.)

.. Thesis Co-Advisor

(Gamolwan Tumcharern, Ph.D.)

.. Examiner

(Associate Professor SIRILUX POOMPRADUB, Ph.D.)

.. Examiner

(Professor DUANGDAO AHT-ONG, Ph.D.)

.. External Examiner

(Rungnapa Pimsen, Ph.D.)

เจตพงษ์ กล้าหาญ : การพัฒนาเซลลูโลสเป็นซับสเตรตสำหรับเป็นตัวดูดซับและตัวรับรู้. (DEVELOPMENT OF CELLULOSE AS SUBSTRATES FOR ADSORBENTS AND SENSORS) อ.ที่ปรึกษาหลัก : ศ. ดร.มงคล สุข วัฒนาสินิทธิ์, อ.ที่ปรึกษาร่วม : ดร.กมลวรรณ ธรรมเจริญ

วิทยานิพนธ์นี้ได้ทำการพัฒนาเซ็นเซอร์ โดยใช้เซลลูโลสเป็นซับสเตรต ซึ่งได้แบ่งเป็นสองหัวข้อคือ: ส่วนแรกคือ การพัฒนาฟลูออเรสเซนต์เซ็นเซอร์และตัวดูดซับไอออนโลหะ โดยใช้เซลลูโลสจากแบคทีเรียเป็นซับสเตรต และส่วนที่สอง คือ การพัฒนาเซนเซอร์ที่เปลี่ยนสีได้บนเซลลูโลสกระดาษเพื่อใช้ตรวจวัดปริมาณสารบ่งชี้ประเภทของน้ำมัน โดยใช้สมาร์ทโฟนเป็น เครื่องตรวจจับ

ส่วนที่หนึ่ง, เซลลูโลสจากแบคทีเรีย เป็นวัสดุธรรมชาติที่น่าสนใจอย่างมาก เพราะมีสมบัติเด่นหลายประการ อาทิ เช่น เส้นใยมีความบริสุทธิ์สูง มีสมบัติเชิงกลที่ดี การมีพื้นที่ผิวและรูพรุนสูง ดูดซับน้ำได้มาก เนื่องจากมีโครงสร้างแบบเส้นใย สามมิติระดับนาโน ส่งผลให้เซลลูโลสจากแบคทีเรียเป็นตัวเลือกที่น่าสนใจ ในงานวิจัยนี้ได้นำประโยชน์ของ เซลลูโลสจาก แบคทีเรีย มาใช้เป็นซับสเตรตในการตรึงอนุพันธ์ควิโนลีน ด้วยปฏิกิริยาการแทนที่ด้วยนิวคลีโอไฟล์ โดยใช้โพแทสเซียม คาร์บอเนตเป็นเบส เซลลูโลสจากแบคทีเรียที่ตรึงด้วยอนุพันธ์ควิโนลีน ถูกนำมาขึ้นรูปเป็นแผ่นฟิล์ม เพื่อใช้เป็นฟลูออเรสเซนต์ เซ็นเซอร์แบบเปิด ที่ให้สัญญาณการเรืองแสงสีเขียวอย่างจำเพาะกับไอออนสังกะสี และจากการหาค่าความสามารถในการดูด ซับด้วยเทคนิค ICP-AES พบว่ามีค่าความสามารถในการดูดซับ ไอออนสังกะสีและแคดเมียม เท่ากับ 38.2 และ 56.8 มิลลิกรัมต่อ กรัม ตามลำดับ เซลลูโลสจากแบคทีเรียที่ตรึงด้วยอนุพันธ์ควิโนลีนจึงมีประโยชน์ สำหรับการดึงไอออนสังกะสีและไอออน แคดเมียม ออกจากสารละลาย เช่นแหล่งน้ำหรือระบบบำบัดน้ำ เป็นต้น

ส่วนที่สอง, ได้ทำการพัฒนากระบวนการตรวจวัดปริมาณสารบ่งชี้ประเภทของน้ำมัน โดยใช้สมาร์ทโฟน เป็น เครื่องตรวจจับร่วมกับการประมวลผลภาพด้วยโปรแกรม โดยใช้สารละลายฟีนอล์ฟทาลีนซึ่งไม่มีสี เป็นสารบ่งชี้ประเภทของ น้ำมัน เมื่อทำการตรวจวัด โดยแช่แถบกระดาษด้านหนึ่งลงในสารละลายโซเดียมไฮดรอกไซด์ ส่วนอีกด้านหนึ่งแช่ลงในน้ำมันที่มี สารบ่งชี้ประเภทของน้ำมัน เมื่อสารทั้งสองไหลแพร่มาบรรจบกัน จะเกิดอันตรกิริยาระหว่างฟีนอล์ฟทาลีนและโซเดียมไฮดรอก ไซด์โดยปรากฏเป็นแถบสีบนกระดาษ ซึ่งค่าต่ำสุดที่สามารถอ่านปริมาณสารบ่งชี้ประเภทของน้ำมัน บนแถบสีด้วยตาเปล่าคือ 1 ppm หากทำการตรวจวัดด้วยสมาร์ทโฟนและแสดงผลออกมาเป็นค่า CMYK โดยใช้โปรแกรม ImageJ ค่าต่ำสุดที่สามารถ ตรวจวัด (LOD) คือ 0.31 ppm โดยความสามารถในการตรวจวัดที่สูงของกระบวนการนี้ เกิดเนื่องจากการสะสมของฟีนอล์ฟ ทาลีนในบริเวณที่สารทั้งสองได้ไหลแพร่มาบรรจบกัน จึงเกิดการสะสมความเข้มของสีขึ้น กระบวนการ ไหลแพร่มาบรรจบกัน บนกระดาษนี้ จึงถือเป็นวิธีการวิเคราะห์แบบใหม่ที่สะดวก มีผลต่อ ความสามารถในการตรวจวัดที่เพิ่มขึ้นแก่การตรวจวัดทางเคมี

5772809323 : MAJOR PETROCHEMISTRY

KEYWORD: FLUORESCENCE SENSORS, AMINOQUINOLINE, ZINC ION, CADMIUM ION, PETROLEUM MARKER, COLOR IMAGE ANALYSIS, PAPER-BASED SENSOR, SMARTPHONE-BASED DETECTOR, PHENOLPHTHALEIN

Jadetapong Klahan : DEVELOPMENT OF CELLULOSE AS SUBSTRATES FOR ADSORBENTS AND SENSORS. Advisor: Prof. MONGKOL SUKWATTANASINITT, Ph.D. Co-advisor: Gamolwan Tumcharern, Ph.D.

This thesis deals with two parts of development of novel sensors based on cellulose substrate platform. The first part is the development of fluorescence sensors and adsorbents for metal ions using bacterial cellulose as the platform. The second part is the development of colorimetric sensors for smartphone detection of oil marker using filter paper as the platform.

In the first part, bacterial cellulose (BC) has several advantageous properties over plant cellulose such as high purity, high surface area, high porosity, and high water-holding capacity due to its three-dimensional network of nanofibrils structure, that make BC appealing for applications related to surface capacity. In this work, BC is utilized as a substrate for immobilization of a 2-chloro-N-(quinolin-8-yl)acetamide (QA) via a nucleophilic substitution reaction using K_2CO_3 as a base. The QA modified BC film exhibit green fluorescence turn-on emission upon addition of Zn^{2+}. The metal ion adsorption study by the ICP-OES analysis showed the adsorption capacity of 38.2 and 56.8 mg/g for Zn^{2+} and Cd^{2+}, respectively. The functionalized BC sheet is thus potentially useful for detection of Zn^{2+} and retrieving or removal of Zn^{2+} and Cd^{2+} from aqueous solution.

In the second part, a convenient method for sensitive detection of gasoline marker using a smartphone camera and image processing application are developed. Phenolphthalein (PhP) is used as a colorless dye marker in commercial gasoline. The color was developed by the interaction of PhP with NaOH on filter paper strips and evaluated based on the CMYK color system by ImageJ program. The counter-flowing technique, in which a gasoline sample and NaOH solution are allowed to travel on a filter paper strip from the opposite end, give the naked eye detection concentration of PhP as low as 1 ppm with the LOD of 0.31 ppm using a smartphone camera. The high sensitivity is attributed to the preconcentration derived from accumulation of PhP at the immiscible liquid interface. The counter-flowing method can thus be a new facile analytical technique for enhancing chemical detection sensitivity.

Field of Study:	Petrochemistry	Student's Signature ....
Academic Year:	2020	Advisor's Signature ....
		Co-advisor's Signature ....

ACKNOWLEDGEMENTS

Jadetapong Klahan

TABLE OF CONTENTS

จุฬาลงกรณ์มหาวิทยาลัย

CHULALONGKORN UNIVERSITY

LIST OF TABLES

จุฬาลงกรณ์มหาวิทยาลัย

CHULALONGKORN UNIVERSITY

LIST OF FIGURES

CHAPTER 1
INTRODUCTION

1.1 Cellulose substrate

Cellulose constitutes the most abundant renewable polymer resource available today. As a chemical raw material, it is generally well-known that it has been used in the form of fibers or derivatives for nearly 150 years for a wide spectrum of products and materials in daily life.

1.1.1 Plant cellulose

Cellulose is well known as one of the most abundant natural polysaccharide, being the major structural component of plants. Cellulose is biodegradable materials in nature, and the most abundant renewable organic material produced in the biosphere. Cellulose is widely distributed in higher plants, in several marine animals, and to a lesser degree in algae, fungi, bacteria, invertebrates, and even amoeba. In general, cellulose is a fibrous, tough, water-insoluble substance that plays an essential role in maintaining the structure of plant cell walls. It was first discovered and isolated by Anselme Payen in 1838, and since then, multiple physical and chemical aspects of cellulose have been extensively studied; indeed, discoveries are constantly being made with respect to its biosynthesis, assembly, and structural features that have inspired a number of research efforts among a broad number of disciplines. Cellulose has thus been the topic of extensive investigations in macromolecular chemistry. Over the past 30 years, developments in molecular biology and the application of cell systems in vitro have resulted in extensive exploration of the mechanisms underlying the biosynthesis of cellulose in nature. Cellulose based polymers have wide applications in tissue engineering, controllable delivery system, sensor, agriculture, as well as water purification [1]

Structure and morphology of celluloses

Cellulose can be characterized as a high molecular weight homopolymer of β-1,4-linked anhydro-D-glucose units in which every unit is corkscrewed 180° with

respect to its neighbors, and the repeat segment is frequently taken to be a dimer of glucose, known as cellobiose (Figure 1.1). Each cellulose chain possesses a directional chemical asymmetry with respect to the termini of its molecular axis:one end is a chemically reducing functionality (i.e., a hemiacetal unit) and the other has a pendant hydroxyl group, the nominal nonreducing end. The number of glucose units or the degree of polymerization (DP) is up to 20 000, but shorter cellulose chains can occur and are mainly localized in the primary cell walls [2].
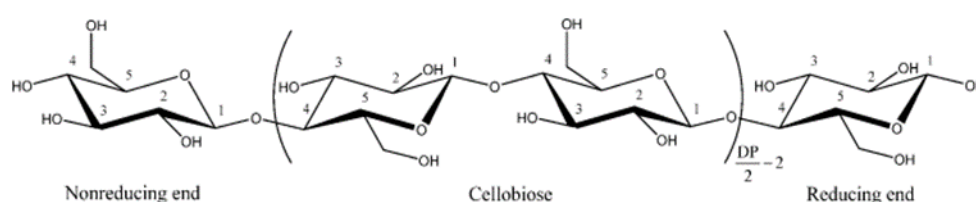
Figure 1.1 Chemical structure of cellulose.

All β-D-glucopyranose rings adopt a 4C1 chair conformation, and consequently, the hydroxyl groups are positioned in the ring (equatorial) plane, while the hydrogen atoms are in the vertical position (axial). This structure is stabilized by an intramolecular hydrogen bond network extending from the $O(3')$-H hydroxyl to the $O(5)$ ring oxygen of the next unit across the glycosidic linkage and from the $O(2)$-H hydroxyl to the $O(6')$ hydroxyl of the next residue (Figure 1.2). Additionally, Cellulose was found 43.6–45% carbon, 6.0–6.5% hydrogen, and the remainder was oxygen (theoretical C 44.4%, H 6.2%) [2].
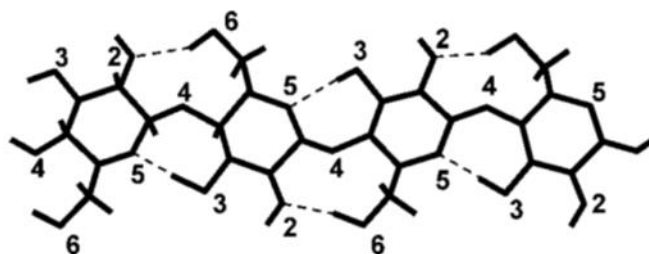
Figure 1.2 Intramolecular hydrogen-bonding network in a representative cellulose structure.

Paper has shown potential as a ubiquitous material for fabricating micro analytical devices for diagnostic and screening applications for resource-limited regions; paper-based sensing technology has become a hot research field since 2007. Intensive research in the past decade has accumulated a large number of scientific publications. However, usability of paper-based indicator for real applications is important. The ASSURED criteria (i.e., affordable, sensitive, specific, user-friendly, rapid and robust, equipment-free, deliver to the users who need them), set by the World Health Organization (WHO), specified the whole spectrum of requirements for a low-cost sensor designed for use in developing countries.

Paper is a material typically made of cellulose fibers; it is universal and low-cost and can be created on a large scale. From as early as the 1930s to 1940s, researchers started exploring using paper to build multi welled assay plates and fluidic systems for chemical analysis. The first paper-based diagnostic device for semiquantitative glucose assay in urine was demonstrated in the 1950s, this invention was further developed into immunological paper test devices, and commercialized. Since 2007, a renewed interest in using paper to design paper-based indicators has been initiated and pursued by many research groups in the world.

The original motivation for paper-based indicator was to provide low-cost, disposable, and simple-to-use diagnostic and analytical devices to people living in resource-limited areas, and for point-of-care applications in developed countries. Low-cost sensors for diagnostic use in resource-limited settings must be affordable, sensitive, specific, user-friendly, robust, and rapid, equipment-free or desire minimal equipment that can be powered by batteries and delivered to those who need them. These criteria are the guidelines for improving human health in both developing and developed regions through research on low cost and user-operated diagnostic and environmental analytical devices.

In many methods, supporting equipment, including electrochemical stations and color intensity analyzers are required to perform a test, capture the signals, and analyze results. Such equipment often requires a high level of professional skills, usually beyond the adaptive ability of general nonprofessional users. Therefore,

although most new paper-based analytical devices demonstrated high level analytical performance in the assured criteria in the hands of researchers and professionals, considerable efforts are urgently required to improve their features to make them acceptable to nonprofessional users. For a laboratory-validated method to become a user accepted device, the device should be able to analyze real samples (e.g., human blood and urine, etc.).

1.1.2 Bacterial cellulose (BC)

It has been well known that bacteria (Acetobacter xylinum) could synthesize cellulose. Specifically, when being fermented in a culture rich in polysaccharides, these bacteria produce pellicles of **BC**. **BC** has distinctive advantages over plants cellulose, even though they have the same chemical structure. In particular, **BC** has lower density, higher crystallinity, very high surface area per unit mass, higher water holding capacity, higher mechanical strength due to its web-like network structure and higher purity as it is pure cellulose and does not associate with lignin or hemicelluloses [3, 4]. Thanks to these properties, bacterial cellulose fibrils are increasingly being used in various areas, such as biomedicine, paper industry and many others. Its applications in the food industry are recently investigated. **BC** could be used to improve rheology of food as a thickening, stabilizing or gelling agent.

The biosynthetic pathways of **BC**, including those involving enzymes and precursors, have previously been described in detail by Chawla (2009) [5]. Nevertheless, it has been well known that bacteria Acetobacter xylinum is the only species known to be capable of producing cellulose in commercial quantities. Specifically, when being fermented in a culture rich in polysaccharides, these bacteria produce pellicles of **BC**. The fibrous structure of **BC** consists of a three-dimensional non-woven network of nanofibrils, sharing the same chemical structure as plant cellulose, which is held together by inter- and intra-fibrilar hydrogen bonding, resulting in a hydrogel state with high strength. The cellulose pellicle consists of random assembled fibrils, less than 100 nm wide [6].

This quality, combined with its highly hydrophilic nature, results in a very high liquid loading capacity. The hydrophilic ability of **BC** is decided by its high water

content, while only 10% out of the 99 wt% water presented in **BC** gels behave like free bulk water [7]. Moreover, its biocompatibility, hydrophilicity, transparency and non-toxicity, From these properties, make it an attractive candidate for a wide range of applications in various fields, especially those related to biomedical, environmental, and biotechnology applications [8]. Its applications in the food industry are recently investigated. Also **BC** could produce low-calorie and low cholesterol foods [9]. Additionally, efficiency in the production of **BC** is indispensable in determining its potential applications. Carreira et al. evaluated several residues from agro-forestry industries as economic carbon and nutrient sources for the production of **BC**: namely grape skins aqueous extract, cheese whey, crude glycerol and sulfite pulping liquor. Agro-forestry residues were successfully used as carbon sources to produce **BC** [10].

1.2 Digital imaging and processing in sensing application

Digital imaging is quite different from photographic imaging in many aspects. A digital image is made up of many small square picture elements or pixels. Many of these picture elements are combined in a two-dimensional field to produce an image. A computer can store the pixel data in a file and the image can be easily processed or reproduced on a computer.

However, the resolution of a digital image is dependent on two factors. The first is the number of pixels used to create the two-dimensional field or pixel resolution. The pixel resolution of a digital image is expressed as horizontal times vertical numbers of pixels (e.g., 1024×1024). Obviously, the higher these numbers are, the better the resolution will be. The second factor upon which digital image resolution depends is the color resolution or color depth. This is defined as the number of different colors (or shades of gray for black and white images) that can be assigned to a pixel. Color depth is determined by the number of binary digits or bits which are assigned to a pixel by the hardware or software in a computer. Computers store data as binary digits of which there are only two choices, a 1 or a 0. Because of this, the number of possible colors that can be assigned to a pixel is a power of 2. For instance, a color depth of 8 bits would

give 256 possible colors 2 to the eighth power. 24-bit color depth (224) would allow 16,777,216 possible colors. This color depth is considered true color as it provides a greater number of colors and shades than the human eye can distinguish.

1.2.1 RGB color model

This is an additive color system based on tri-chromatic theory. RGB is easy to implement and very common, being used in virtually every computer system as well as television, video etc. According to development of paper based colorimetric respond of a simple method and suitable to use as a sensors application, since evaluate the results into a quantitative analysis can be collected by using the RGB color model. The RGB color model is an additive color model in which red, green, blue color are added together in various component ratio to reproduce a broad array of colors as shown in Figure 1.3. The name of the model comes from the initials of the three additive primary colors, red, green, and blue. The main purpose of the RGB color model is for the sensing, representation, and display of images. The RGB color model was used to descript how much of each red, green, and blue color is included in the photographic images.

The basic of the RGB value, the color is black when the intensity of each component is zero (0, 0, 0) and the color is white when the intensity of each component is full (255, 255, 255). When the intensities are the same, the result is a shade of gray, darker or lighter depending on the intensity [11].
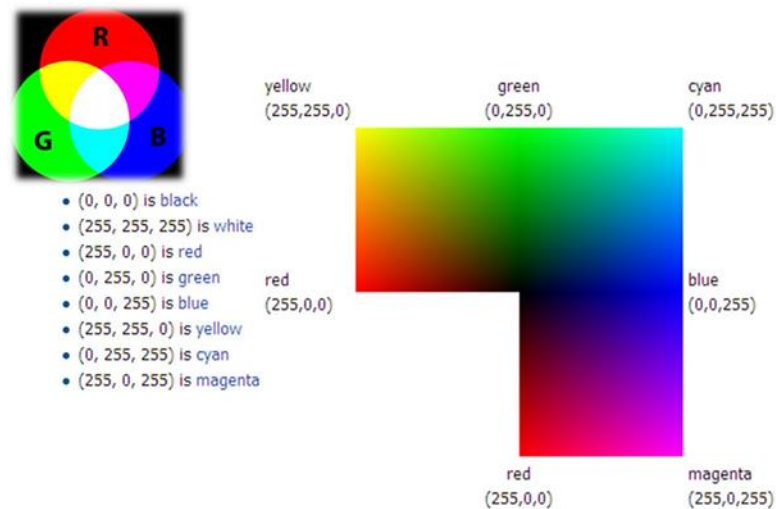
Figure 1.3 The RGB color model.

1.2.2 CMYK color model

The CMYK color model (also known as process color, or four color) is a subtractive color model, based on the CMY color model, used in color printing, and is also used to describe the printing process itself. CMYK refers to the four ink plates used in some color printing: cyan, magenta, yellow, and key (black). The CMYK model works by partially or entirely masking colors on a lighter, usually white, background. The ink reduces the light that would otherwise be reflected. Such a model is called subtractive because inks subtract the colors red, green and blue from white light. White light minus red leave cyan, white light minus green leave magenta, and white light minus blue leave yellow (Figure 1.4). In additive color models, such as RGB, white is the additive combination of all primary-colored lights, black is the absence of light. In the CMYK model, it is the opposite: white is the natural color of the paper or other background, black results from a full combination of colored inks. To save cost on ink, and to produce deeper black tones, unsaturated and dark colors are produced by using black ink instead of the combination of cyan, magenta, and yellow [12].
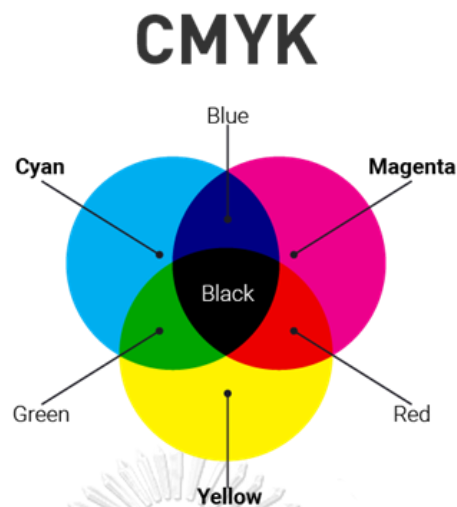
Figure 1.4 The CMYK color model

1.2.3   Color difference

The CIELAB color space also referred to as L*a*b* is a color space defined by the International Commission on Illumination (CIE) in 1976. It expresses color as three values: L* for perceptual lightness, and a* and b* for the four unique colors of human vision: red, green, blue, and yellow. CIELAB was intended as a perceptually uniform space, where a given numerical change corresponds to similar perceived change in color. While the LAB space is not truly perceptually uniform, it nevertheless is useful in industry for detecting small differences in color. The non-linear relationships for L* a* and b* are intended to mimic the logarithmic response of the eye.
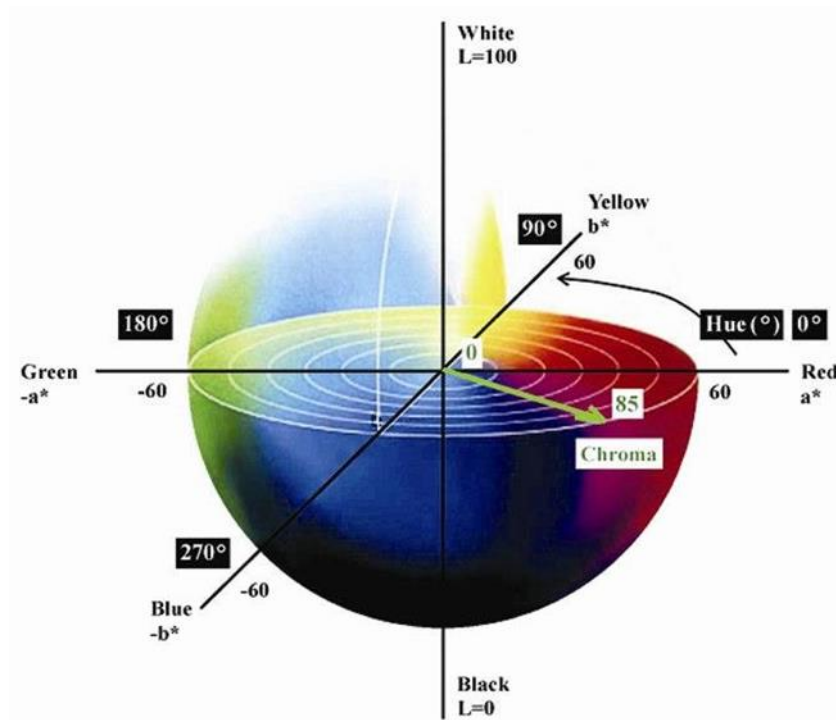
Figure 1.5 The three-dimensional of CIE L*a*b* color space.

The difference or distance between two colors is a metric of interest in color science. It allows quantified examination of a notion that formerly could only be described with adjectives. Quantification of these properties is of great importance to those whose work is color-critical. Common definitions make use of the Euclidean distance in a device independent color space.

The CIE calls their distance metric ΔE*ab (also called ΔE*, dE*, dE, or "Delta E"). Perceptual non-uniformities in the underlying CIELAB color space have led to the CIE refining their definition over the years, leading to the superior (as recommended by the CIE) 1994 and 2000 formulas. These non-uniformities are important because the human eye is more sensitive to certain colors than others. CIELAB metric is used to define color tolerance of CMYK solids. A good metric should take this into account in order for the notion of a just noticeable difference to have meaning. Otherwise, a certain ΔE may be insignificant between two colors in one part of the color space while being significant in some other part [13].
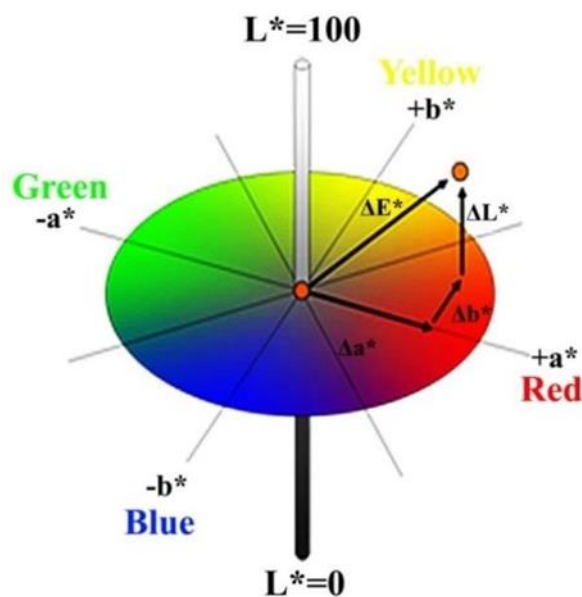
Figure 1.6 The three-dimensional of ΔE*ab.

1.3 Colorimetric sensor

In 2013, Cate et al. [14] presented paper-based analytical devices (PADs) represent a growing class of elegant, yet inexpensive chemical sensor technologies designed for point-of-use applications. Most PADs, however, still utilize some form of instrumentation such as a camera for quantitative detection. They describe here a simple technique to render PAD measurements more quantitative and straightforward using the distance of color development as a detection motif. The so-called distance-based detection enables PAD chemistries that are more portable and less resource intensive compared to classical approaches that rely on the use of peripheral equipment for quantitative measurement (Figure 1.7). They demonstrate the utility and broad applicability of this technique with measurements of glucose, nickel, and glutathione using three different detection chemistries: enzymatic reactions, metal complexation, and nanoparticle aggregation, respectively. The results show excellent quantitative agreement with certified standards in complex sample matrices. This work provides the first demonstration of distance-based PAD detection with broad application as a class of new, inexpensive sensor technologies designed for point-of-use applications.
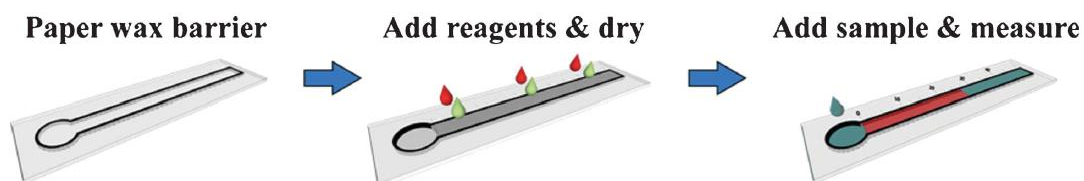
Figure 1.7 Operational concept of the device. Device fabrication and use are simple, inexpensive, and fast, consisting of printing a hydrophobic barrier on filter paper, patterning reagents, and adding a sample for analysis.

In 2015, Morales-Narvaez et al. [15] reported various nanopaper-based optical sensing platforms and describe how they can be tuned, using nanomaterials, to exhibit plasmonic or photoluminescent properties that can be exploited for sensing applications. They also describe several nanopaper configurations, including cuvettes, plates and spots that thay printed or punched on **BC**. The platforms include a colorimetric-based sensor based on nanopaper containing embedded silver and gold nanoparticles; a photoluminescent-based sensor, comprising CdSe@ZnS quantum dots conjugated to nanopaper; and a potential up-conversion sensing platform constructed from nanopaper functionalized with $NaYF_4:Yb^{3+}@Er^{3+}\&SiO_2$ nanoparticles (Figure 1.8). Moreover, they prove that **BC** is and advantageous preconcentration platform that facilitates the analysis of small volumes of optically active materials ($\sim$4 μL). They are confident that these platforms will pave the way to optical (bio)sensors or theranostic devices that are simple, transparent, flexible, disposable, lightweight, miniaturized and perhaps wearable.
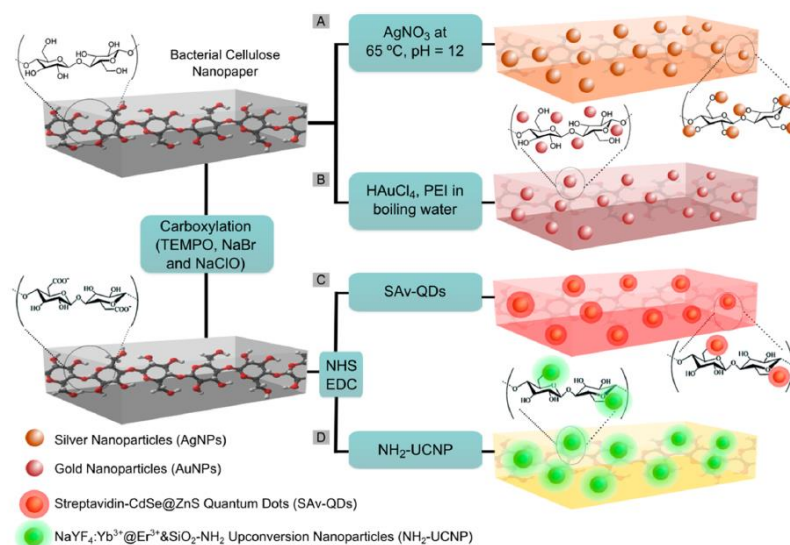
Figure 1.8 Schematic of the proposed nanopaper-based composites. (A and B) Fabrication of plasmonic nanopaper: (A) silver nanoparticle/**BC** nanopaper conjugate (AgNP-**BC**); (B) gold nanoparticle/**BC** nanopaper conjugate (AuNP-**BC**). (C and D) Fabrication of photoluminescent nanopaper: (C) streptavidin-coated CdSe@ZnS quantum dot/**BC** nanopaper conjugate (QD-**BC**); (D) aminosilica-coated NaYF4:Yb^{3+}@Er^{3+} up-conversion nanoparticle/**BC** nanopaper conjugate (UCNP-**BC**).

1.4   Smart phone

Smart phones are now widely used all over the world. According to the International Telecommunication Union (ITU), by the end of 2010 the number of cell-phone subscribers reached almost 5 billion worldwide, and the majority of these users are actually located in developing countries. Because of this massive volume, smart phones are now having a central role in many applications, especially for developing countries and resource limited locations. Among several examples, the use of smart phones for remote monitoring of various medical data/images has already been well-established in current. In addition to these, together with the recent advances in hardware and software capabilities of smart phones, there is also a growing interest in converting smart phones into microscopic analysis tools for imaging of, e.g., bodily fluids or water samples.

These previous efforts, however, focused on microscopic imaging of static objects (with significantly limited sample volumes), using a cell-phone-enabled optical microscope. On the other hand, there is also an important need today for translating colorimetric based into smart phones to enable specific and sensitive analysis of large sample volumes through. Toward this goal, development, and integration of device onto a smart phone using compact device attachments is interested. The main reason of using a smart phone camera, instead of a digital camera, for signal readout is to avoid the ambient light effect and to operate under fixed conditions.

Some examples of literature related to smart phone-based detector are as follows:

In 2014, Guan et al. [16] introduced a barcode-like design into a paper based blood typing device by integrating with smartphone-based technology. The concept of presenting a paper-based blood typing assay in a barcode-like pattern significantly enhanced the adaptability of the assay to the smartphone technology. The fabrication of this device involved the use of a printing technique to define hydrophilic bar channels which were, respectively, treated with Anti-A, -B, and -D antibodies. These channels were then used to perform blood typing assays by introducing a blood sample. Blood type can be visually identified from eluting lengths in bar channels (Figure 1.9). A smartphone-based analytical application was designed to read the bar channels, analogous to scanning a barcode, interpret this information, and then report results to users. The proposed paper-based blood typing device is rapidly read by smartphones and easy for the user to operate. They envisage that the adaptation of paper-based devices to the widely accepted smartphone technology will increase the capability of paper-based diagnostics with rapid assay result interpretation, data storage, and transmission.
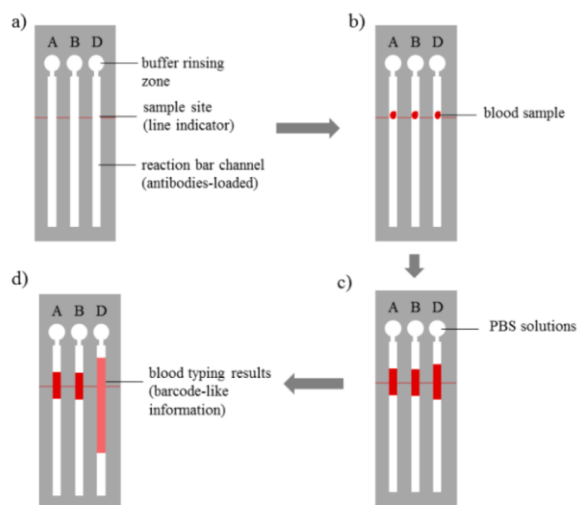
Figure 1.9 Schematic diagram of the barcode-like blood typing device. *(a)* Anti-A, Anti-B, and Anti-D antibodies were introduced into the reaction bar channels. *(b)* 3 µL of blood samples was introduced in the sample sites for the blood typing test and allowed to wick and react for 30 s. *(c)* 10 µL of PBS solutions was added as eluting buffer for 1 min of elution. *(d)* Reading the blood typing test results.

In 2019, Rathod et al. [17] efforted to get the learners to become independent in evaluating their titration experiments, in this paper, the design, development, and implementation of a new smartphone tutor application named Titration Color-Darts (TCD) has been presented. TCD uses the camera function to analyze the pink color of the titration solution to provide learners with a feedback report on their experimental conduct. TCD maps the gradient of pink (from light to dark) to a corresponding performance score (on a scale of 1 to 10) (Figure 1.10). An exploratory pilot study conducted with undergraduate chemistry students indicated that TCD is useful in helping students attain the learning goals of identifying the optimal pink color of a phenolphthalein-based-titration end point and detecting potential experimental errors to be minimized. As a smartphone tool that can easily be accessed and installed, TCD has the potential to be an effective method of helping students who are performing phenolphthalein-based titration experiments independently with minimal support from the instructor.
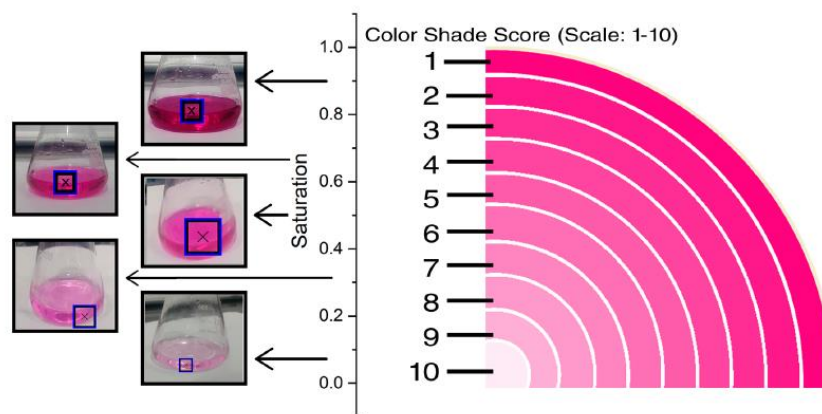
Figure 1.10 Increasing saturation values as the solution turns darker pink and corresponding score on a scale of $1-10$.

1.5 Image processing/Analysis software

For material characterization, various features (shape, size, area, surface area, volume, profile, texture, etc.) of objects of interest must be quantified rather than using visual inspection by human eyes. Visual inspection is very subjective and cannot be used as quantitative data in a reliable manner. A computer-aided decision-making process is highly desired. Quantitative characterization using image processing/analysis software must be implemented for objective analysis and record keeping. For large amounts of image data acquisition, processing, and analysis, automation capability is also a very important feature to have as a useful image processing/analysis software. From these perspectives, a new image processing/analysis software development project was initiated by ImageJ.

ImageJ, a freely available Java-based image processing program, was developed at the National Institutes of Health (NIH) in collaboration with the Laboratory for Optical and Computational Instrumentation. Since the initial implementation of NIH Image in 1987 and the public release of ImageJ in 1997, this processing system has become a potent and pervasive tool for the scientific community. In this protocol was create a necessary bridge between ImageJ and the biochemical/bioanalytical research community, making this technology more accessible for objective analysis of colorimetric responses across these analytical fields.

Finallly, these methods serve as a convenient, easily implemented precursor for subsequent development of more sophisticated algorithms and applications to automate image processing of bioanalytical colorimetric responses. Some examples of literature related to image processing and analysis software are as follows:

In 2015, Choodum et al. [18] proposed a sol–gel colorimetric sensor was successfully developed for the detection of methamphetamine (MA). Simon's reagents were entrapped within the polymeric network of the sol–gel matrix. The sol–gel MA sensor was fabricated within a micro-PCR tube to which the sample solution could be directly added for in-tube detection. This resulted in a small and easy to carry sensor. The sensor was used to demonstrate the rapid quantitative analysis of MA in illicit methamphetamine tablets (Yaba) in conjunction with digital image colorimetry. Real-time Red-Green-Blue (RGB) basic color data of the colorimetric product from the sensor was obtained using an application installed on a mobile phone (Figure 1.11). The sensor was also applied to spiked urine samples and low relative errors in the range of +4 to −9% were obtained. The sol–gel sensor was capable of being stored for almost 3 months (84 days) in a freezer (−18 °C) with only a 4.89% change in the results compared to analysis carried out on the day of preparation. These results demonstrate that the sol–gel MA sensor has the potential to be used as a colorimetric sensor for MA detection in a variety of media. When the sensor was used in combination with a color analysis application installed on a mobile phone, it provided an ideal novel platform for the rapid quantitative analysis of MA.
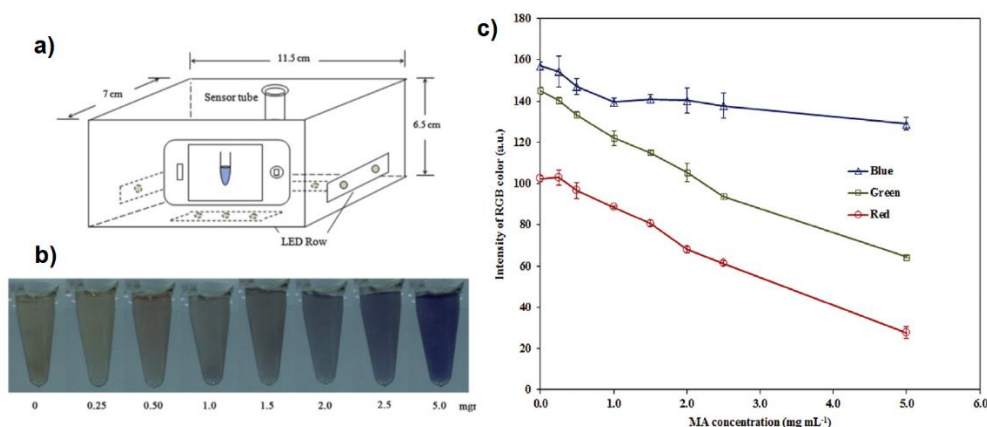
Figure 1.11 a) Real time on-mobile color analysis system for methamphetamine detection. b) Colorimetric products obtained from the use of the sol–gel MA sensor with various concentrations of methamphetamine (0–5.0 mg mL^{-1}). c) Relationships between MA concentrations and individual RGB values.

In 2020, Li et al. [19] proposed that saliva identification provides significant evidence for forensic examinations, especially in sexual assault events. Herein, they developed a rapid and cost-effective smartphone-based bacteria sensor for saliva identification that assays for two oral bacteria in real samples. This bacteria sensor was constructed by the blue-emitting silicon carbide quantum dots (**SiC Qds**) and red-emitting gold nanoclusters (**AuNCs**) to form a series of test strips. This method can be selectively detected two oral bacteria species (S. salivarius and S. sanguinis) with good sensitivity. Exposure of the test strips to bacteria solutions promoted dose sensitive color evolution under a 365 nm UV lamp, which was imaged by a smartphone camera and analyzed by a color detector application (Figure 1.12). Additional studies on 29 real samples from 4 different forensic body fluids (saliva, semen, urine, and serum) demonstrated the feasibility of the method. These findings indicate the proposed approach provides a new way for rapid and visual detection of two bacteria in saliva and screening saliva samples among forensic body fluids.
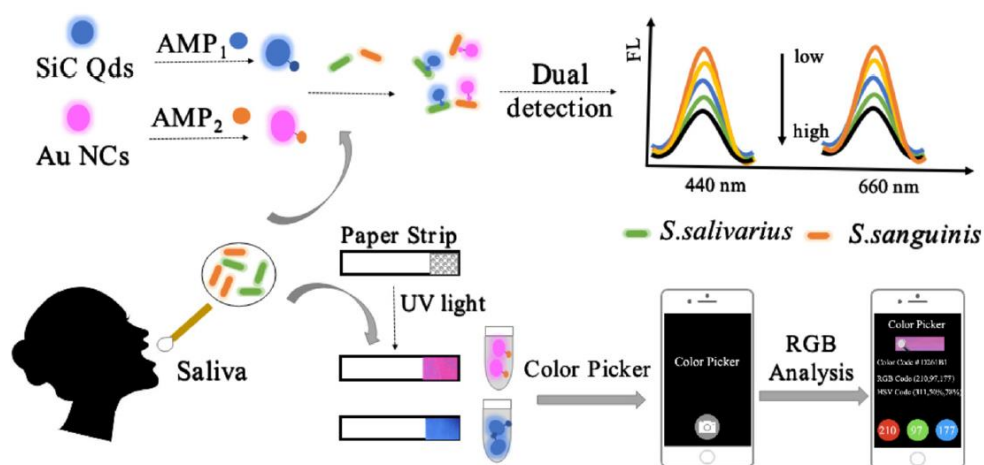
Figure 1.12 Schematic principle of the simultaneous detection of S.salivarius and S.sanguini in saliva based on the smartphone sensing platform.

1.6 Fluorescent sensor

Nowadays, fluorescent sensors have been developed for easy to use, short response time and no sample destruction. They were designed for detection of several analytes in chemical, biological, and environmental fields, including detection of metal ion, anion, neutral molecules and biomolecules. Fluorescent technique has several special features over other methods such as high sensitivity, high selectivity, cost-effectiveness in instrumentation and operational simplicity with ability to allow visual detection and optical imaging [20].

Fluorescence is the emission of light typically occurring with aromatic compounds or highly conjugated molecules. The fluorescence processes that occur between the absorption and emission of light can be usually described by the Jablonski diagram (Figure 1.13). Upon the absorption of light energy, the molecule is excited to excited states (S_1 or S_2) and forms an excited molecule. The molecule rapidly relaxes to the lowest vibrational level of S_1 which this process is called internal conversion. The final process, the molecule returns to ground state (S_0) via emission of a longer wavelength photon. The time required to complete this process takes nano-second [21].
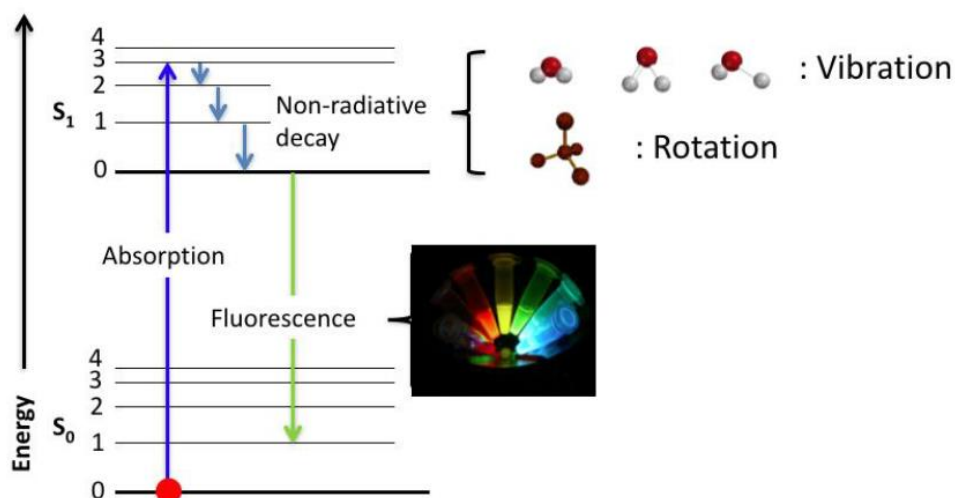
Figure 1.13 Simple Jablonski diagram illustrating fluorescent processes.

Sensing modes

Most of the fluorescent chemosensors contains of two main components: one is a receptor unit for selective binding of the analytes, the other is a fluorophore unit provides the means of signaling this bonding, whether by fluorescence turn-on, turn-off and wavelength shift. Fluorescent turn-on mode is fluorescent sensor that gives enhanced fluorescence signal upon interaction with an analyte (Figure 1.14a). In contrast, turn-off mode must have fluorophore unit which is high emission intensity and low emission intensity upon interaction with an analyte (Figure 1.14b). For the wavelength shift mode, the sensing molecule may change its electronic structure or at least its geometry upon the interaction with analyte that leads to a new fluorescence signal at different wavelength (Figure 1.14c). The ideal sensors should not be affected by environmental interference (signal-selectivity), such as photochemical reactions, concentration and matrixes (polarity, temperature, pH, etc.).
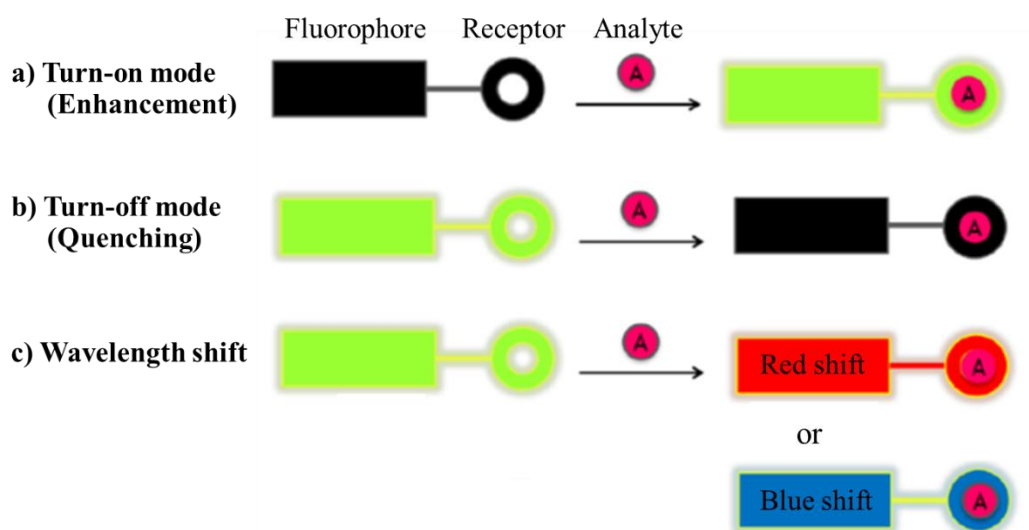
Figure 1.14 Modes of fluorescence responses.

Quinoline-based fluorescence sensors

Quinolines are one of the most interesting classes of heterocyclic compounds forming fluorescent complex with metal ions. The prime example is tris-(8-hydroxyquinoline) aluminum AlQ3 which is highly fluorescent in both solution and solid state that it has been used as a standard green emissive material for organic light-emitting diodes (OLEDs) [22-27]. Quinoline and its derivatives, mainly 8-hydroxyquinolines and 8-aminoquinoline, are important fluorescence sensor for detecting metal ions [28-30]. Derivatives of 8-aminoquinoline with an aryl sulfonamide are the first and most widely applied fluorescent chemosensors for Zn^{2+} in biological sample (Figure 1. 15) [31]. They are highly selective sensor for Zn^{2+} in the presence of high concentration of Ca^{2+} and Mg^{2+}, which is very important for in vivo application. However, their poor water solubility has limited their applications [32].
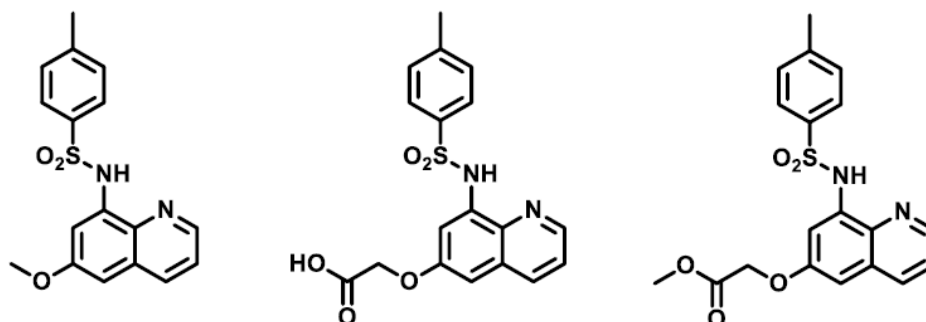
Figure 1.15 Derivative of 8-aminoquinoline with an aryl sulfonamide.

Some examples of literature related to quinoline-based fluorescence sensors are as follows:

In 2011, Rastogi et al. [28] presented a novel fluorescent nanosensor for Zn^{2+} detection using a derivative of 8-aminoquinoline (N-(quinolin-8-yl)-2-(3 (triethoxysilyl)propylamino)acetamide (QTEPA) grafted on silica nanoparticles (SiNPs). These functionalized SiNPs were used to demonstrate specific detection of Zn^{2+} in tris-HCl buffer (pH 7.22), in yeast cell (Saccharomyces cerevisiae) suspension, and in tap water. This sensor selectively detects Zn^{2+} ions with submicromolar detection to a limit of 0.1 μM (Figure 1.16). The sensor shows good applicability in the determination of Zn^{2+} in tris-HCl buffer and yeast cell environment. Further, it shows enhancement in fluorescence intensity in tap water samples.
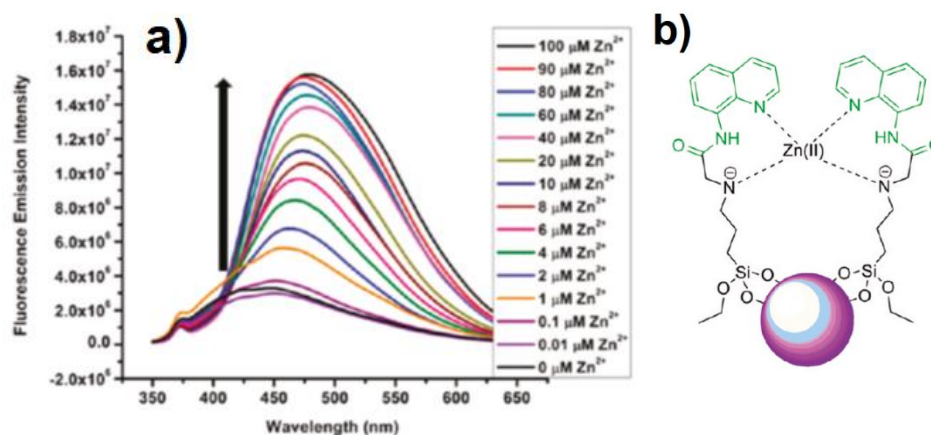
Figure 1.16 a) Fluorescence emission spectra, in the presence of Zn^{2+} from 0.01 to 100 µM, and b) hypothetical figure showing capture of one Zn(II) by two fluorophores grafted on SiNPs.

In 2015, Areti et al. [32] presented A water-soluble glucopyranosyl conjugate, L, has been demonstrated to have switch-on fluorescence enhancement of ~75 fold in the presence of La^{3+} among the nine lanthanide ions studied in the HEPES buffer at pH 7.4. A minimum detection limit of 140 nM (16 ± 2 ppb) was shown by L for La^{3+} in the buffer at physiological pH. The utility of L has been demonstrated by showing its sensitivity toward La^{3+} on Whatman filter paper strips. The reversible and reusable action of L has been demonstrated by monitoring the fluorescence changes as a function of the addition of La^{3+} (Figure 1.17). The chemo-ensemble, $[2L+La^{3+}]$, is shown responsible for providing intracellular fluorescence imaging in HepG2 cells. The inexpensive Whatman cellulose filter paper strips coated with L can be used for the detection of La^{3+} from various samples as a use and discard method. From the concentration dependence studies, the detection limit of L toward La^{3+} on Whatman cellulose paper is 10 ± 1 µM (1.3 ppm).
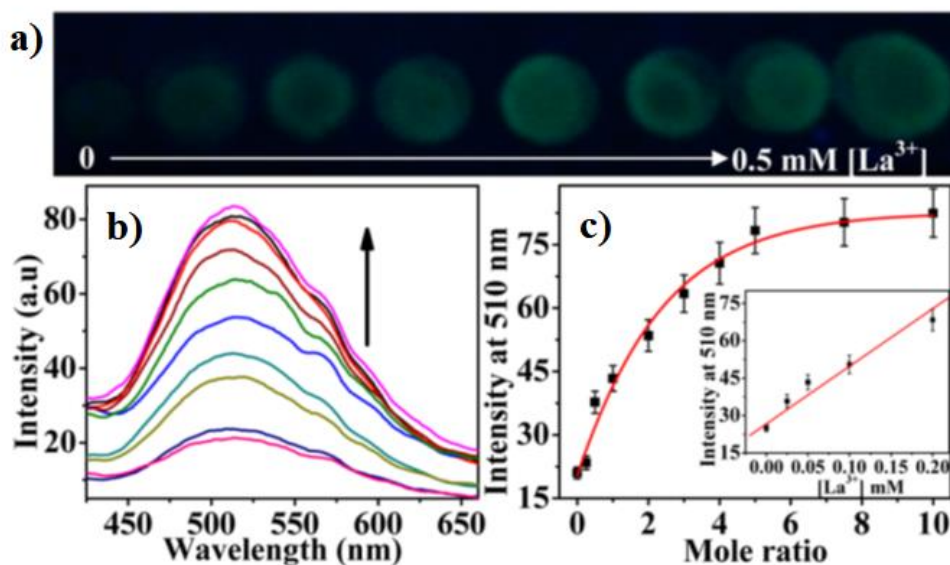
Figure 1.17 a) Photograph of all the samples used in the titration on Whatman cellulose filter paper under 365 nm UV light. b) Spectra obtained in the fluorescence titration of L (λex = 360 nm) with La^{3+} on Whatman cellulose filter paper. c) Plot of intensity vs [La^{3+}]/[L] mole ratio at 510 nm. Inset: The linear concentration region for the intensity vs [La^{3+}] for the receptor L.

In 2018, Boonkitpatarakul et al. [33] investigated the amide derivatives of 8-aminoquinoline with two types of amino acid pendants, i.e. glycine (1) and β-alanine (2), are evaluated for fluorescence sensing of various metal ions. In Tris-HCl aqueous buffer solution, the derivative containing glycine exhibits selective fluorescence enhancement with Zn^{2+}. The fluorescence turn-on signal at a longer wavelength is a result of the binding between N-8-aminoquinolinylglycinamide and Zn^{2+} which is promoted by the deprotonation of the amide proton. However, both Zn^{2+} and Cd^{2+} induce the turn-on signal in ethanol solution. Simultaneous detection of Zn^{2+} and Cd^{2+} are possible by using paper chromatographic separation and the ligand as a visualizing agent. The fluorescence imaging of either Zn^{2+} or Cd^{2+} in plant tissue is demonstrated (Figure 1.18). The conjugation of the ligand with dimethylaminophenylacetylene effectively tunes the emission color of the ligand while retaining the sensing selectivity. Therefore, N-8-aminoquinolinylglycinamide is a simple yet effective binding probe for Zn^{2+} and Cd^{2+} with excellent fluorescence signal transduction.
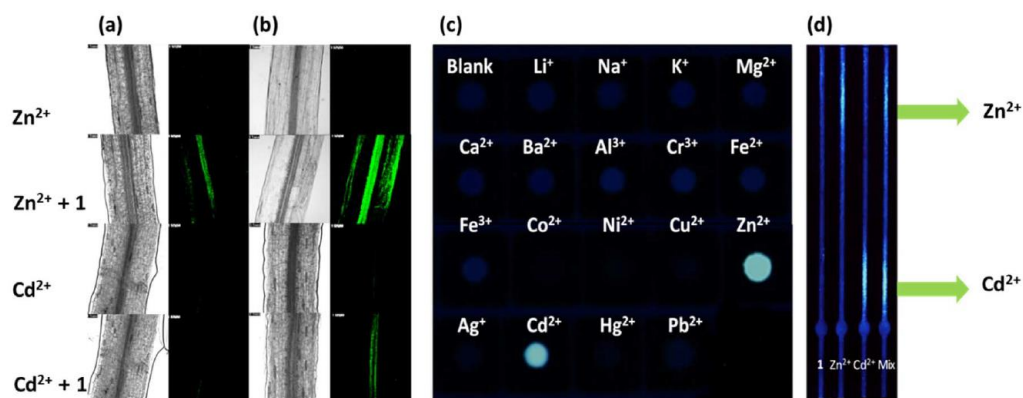
Figure 1.18 Fluorescence images of Chinese cabbage (Brassica rapa.) sprout tissue samples treated with Zn^{2+} (100 μM) and Cd^{2+} (100 μM), (a) washed with Milli-Q water and (b) washed with ethanol, before and after addition of 1 (100 μM, 10 μL). (c) Photographic image of metal ion (0.1 mM) detected by 1 (1 mM) on wax patterned filter paper. and (d) Photographic image for dual detection of Zn^{2+} and Cd^{2+} (1 nmol) by 1 (1 mM) using paper chromatography for separation after elution with CH3NH2 4% (v/v). Images (c) and (d) were taken under black light illumination.

In 2019, Song et al. [34] reported a quinoline-based fluorescent probe for discriminative sensing of Zn^{2+} and Cd^{2+} has been synthesized by inserting an amide group into the 8-aminoquinoline fluorophore and a propargylamine chelating site. This easily-available chemosensor displayed selective and distinct ratiometric fluorescence responses to Zn^{2+} in almost totally water solution through its amide tautomer binding form, and to Cd^{2+} in CH_3CN aqueous medium through its imidic acid tautomer binding form, respectively (Figure 1.19). Moreover, the in situ prepared probe 1–Zn^{2+} complex could act as a relay fluorescent sensor selectively toward pyrophosphate (PPi) and adenosine 5′-triphosphate (ATP) anions via further complexation. Thus, with good specificity, low detection limits and fast response time, a highly efficient fluorescence platform for simultaneous multi-analyte detection has been developed by using the uncomplicated single molecule.
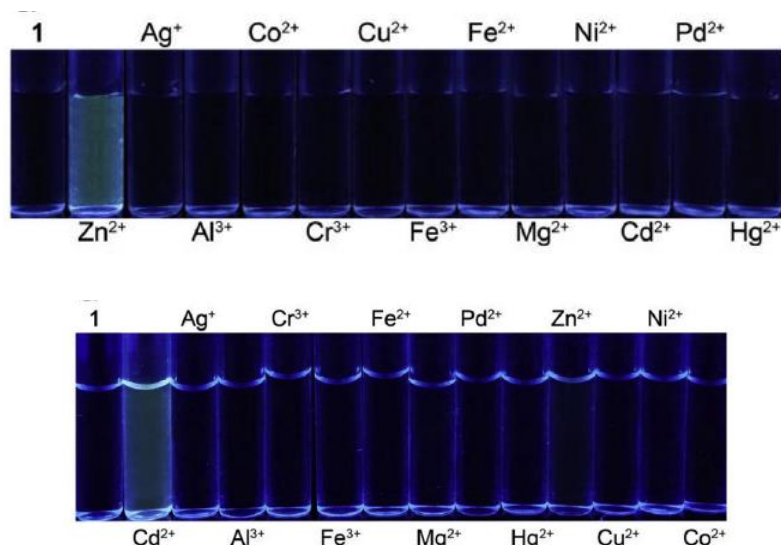
Figure 1.19 Fluorescence change of quinoline-based fluorescent probe under UV lamp (365 nm).

1.7 Bacterial cellulose-based sensors and adsorbent for metal ion detection

Recently, development of bacterial cellulose-based sensors has gain more attention due to their well define structures, mono-dispersity, simpler synthesis and purification allowing better understanding of structure-property relationships. Some examples of literature related to bacterial cellulose-based sensors for detecting metal ion are as follows:

In 2015, Pourreza et al. [35] presented a new strategy for green, in-situ generation of silver nanoparticles using flexible and transparent bacterial cellulose nanopapers. In this method, adsorbed silver ions on bacterial cellulose nanopaper are reduced by the hydroxyl groups of cellulose nanofibers, acting as the reducing agent producing a bionanocomposite "embedded silver nanoparticles in transparent nanopaper" (ESNPs) (Figure 1.20). The fabricated ESNPs were investigated and characterized by field emission scanning electron microscopy (FE-SEM), UV–visible spectroscopy (UV–vis), Fourier-transform infrared spectroscopy (FT-IR), thermo-gravimetric analysis (TGA) and energy-dispersive X-ray spectroscopy (EDX). The important parameters affecting the ESNPs were optimized during the fabrication of specimens. The resulting ESNPs were used as a novel and sensitive probe for the optical sensing of cyanide ion (CN$^-$) and 2-mercaptobenzothiazole (MBT) in water

samples with satisfactory results. The change in surface plasmon resonance absorption intensity of ESNPs was linearly proportional to the concentration in the range of 0.2–2.5 mg.mL^{-1} and 2–110 mg.mL^{-1} with a detection limit of 0.012 mg.mL^{-1} and 1.37 mg.mL^{-1} for CN$^-$ and MBT, respectively.
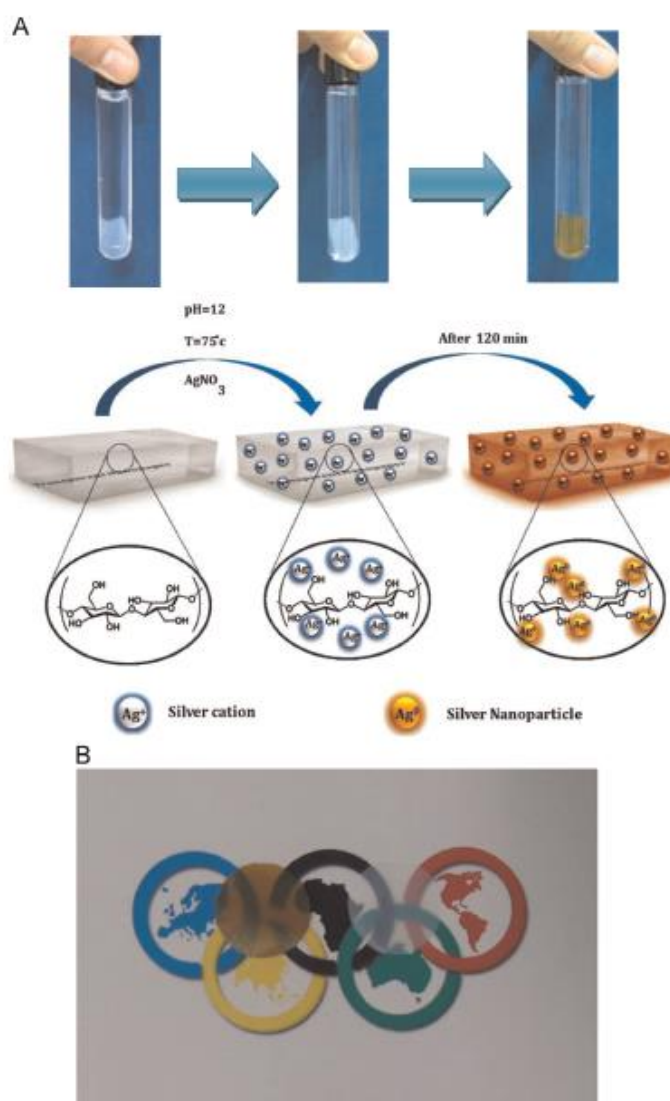
Figure 1.20 A) schematic representation for fabrication of ESNPs and B) a transparency demonstration of dried films of (left) fabricated ESNP and (right) bare nanopaper, on top of "Olympic symbol".

In 2015, Sai et al. [36] presented bacterial cellulose (**BC**)–silica composite aerogels (**CAs**) with interpenetrating network (IPN) microstructure are prepared through a permeation sol–gel process followed by freeze drying. The IPN structure is constructed by diffusing the precursor into a three-dimensional (3D) **BC** matrix followed by permeating the catalyst into the **BC** network gradually to promote the in situ condensation of precursor to form a SiO_2 gel skeleton from outside to inside. The precursor used here is Na_2SiO_e instead of traditional tetraethoxysilane. This IPN structure could offer excellent mechanical properties to aerogels, and is essential to prepare flexible aerogels by freeze drying. The **BC**–silica **CAs** exhibit low density (as low as 0.011 $g.cm^{-3}$) and high specific surface area (as high as 534.5 $m^2.g^{-1}$). Furthermore, the contact angle of the hydrophobization modified **CAs** is as high as 145°. The outstanding hydrophobicity and the large specific surface area endow the hydrophobic **CAs** with excellent oil absorption capability on the water surface. Moreover, the hydrophobic **CAs** that had absorbed oil could be washed and recycled (Figure 1.21).

Figure 1.21 The photos show the oil absorption capability of the hydrophobic CAs. 17 mg hydrophobic CAs were placed on the water surface with 150 mL vegetable oil

colored with a red dye. Then, the hydrophobic CAs with oil could be washed by alcohol to achieve recycling.

In 2015, Gonçalves et al. [37] presented the feasibility of bacterial cellulose (**BC**) as a novel substrate for retinal pigment epithelium (RPE) culture. Thin (41.6 ± 2.2 μm of average thickness) and heat-dried **BC** substrates were surface-modified via acetylation and polysaccharide adsorption, using chitosan and carboxymethyl cellulose. All substrates were characterized according to their surface chemistry, wettability, energy, topography, and also regarding their permeability, dimensional stability, mechanical properties, and endotoxin content. Then, their ability to promote RPE cell adhesion and proliferation in vitro was assessed. All surface-modified **BC** substrates presented similar permeation coefficients with solutes of up to 300 kDa. Acetylation of **BC** decreased it's swelling and the amount of endotoxins. Surface modification of **BC** greatly enhanced the adhesion and proliferation of RPE cells. Although similar proliferation rates were observed among the modified substrates, the acetylated ones showed higher initial cell adhesion (Figure 1.22). This difference may be mainly due to the moderately hydrophilic surface obtained after acetylation.
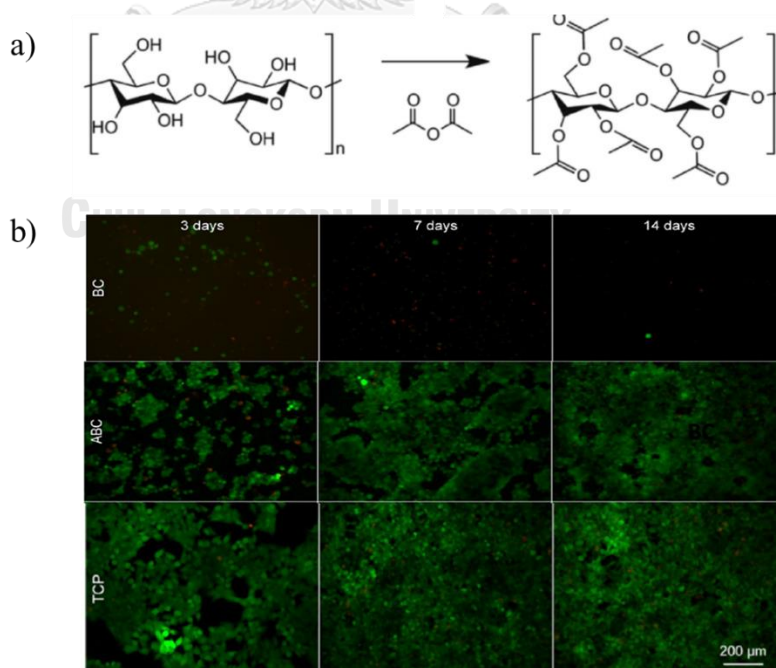
Figure 1.22 a) Scheme of **BC** acetylation reaction b), Representative LIVE/DEAD fluorescence micrographs of HTERT-RPE1 cells cultured for 3, 7, and 14 days on

unmodified **BC**, acetylated **BC** (ABC), and tissue culture polystyrene (TCP, control surface).

In 2015, Hettegger et al. [38] presented the modification of cellulosic materials is of great interest in materials research. Wet bacterial cellulose sheets were modified by an alkoxysilane under mild conditions to make them accessible to click chemistry derivatization. For this purpose (3-azidopropyl)triethoxysilane was grafted covalently onto the cellulosic surface. To demonstrate subsequent click chemistry functionalization, a new fluorophore based on fluorescein was synthesized and clicked to the silane-modified bacterial cellulose (Figure 1.23). The new method renders bacterial cellulose and other never-dried cellulosic materials such as pulps or fibers, susceptible to direct and facile functionalization in an aqueous medium without the need to work in water-free organic phases or to employ extensive protecting group chemistry and functional group interconversion. The clicking of this compound to the azide-equipped cellulose proceeded neatly. The introduction of azidoalkyl groups onto wet (bacterial) celluloses using the current silane grafting approach represents a general and promising way to introduce different functional molecules to cellulose surfaces with opportunities that reach far beyond the plain fluorophore example presented. Regarding the increasing awareness of green chemical procedures, the mild and environmentally friendly conditions.
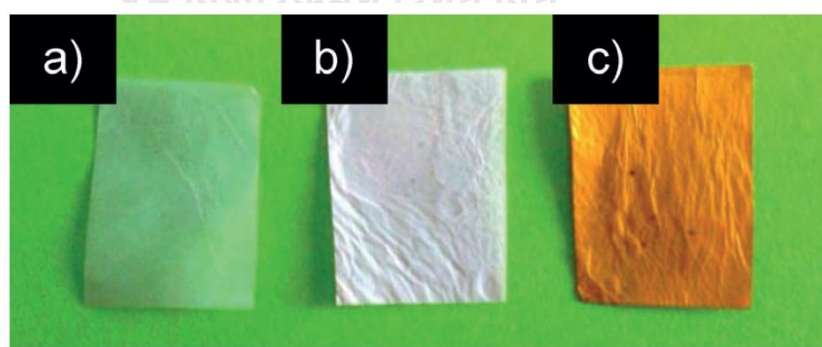
Figure 1.23 Photograph of different **BC** derivatives. a) Dried, milky, and opaque **BC**. b) **BC**-N_3 (preactivated) and c) silanized **BC** 5 after click reaction with chromophore.

In 2015, Sai et al. [39] reported the cellulose nanofibers of bacterial cellulose aerogel (**BCA**) are modified only on their surfaces using a trimethylsilylation reaction with trimethyichlorosilane in liquid phase followed by freeze-drying. The obtained hydrophobic bacterial cellulose aerogels (**HBCAs**) exhibit low density (≤6.77 mg/cm^3), high surface area (≥169.1 m^2/g), and high porosity (≈ 99.6%), which are nearly the same as those of **BCA** owing to the low degrees of substitution (≤0.132). Because the surface energy of cellulose nanofibers decreased and the three-dimensional web-like microstructure, which was comprised of ultrathin (20−80 nm) cellulose nanofibers, is maintained during the trimethylsilylation process, the **HBCAs** have hydrophobic and oleophilic properties (water/air contact angle as high as 146.5°) that endow them with excellent selectivity for oil adsorption from water (Figure 1.24). The **HBCAs** are able to collect a wide range of organic solvents and oils with absorption capacities up to 185 g/g. Hence, the **HBCAs** are wonderful candidates for oil absorbents to clean oil spills in the marine environment.
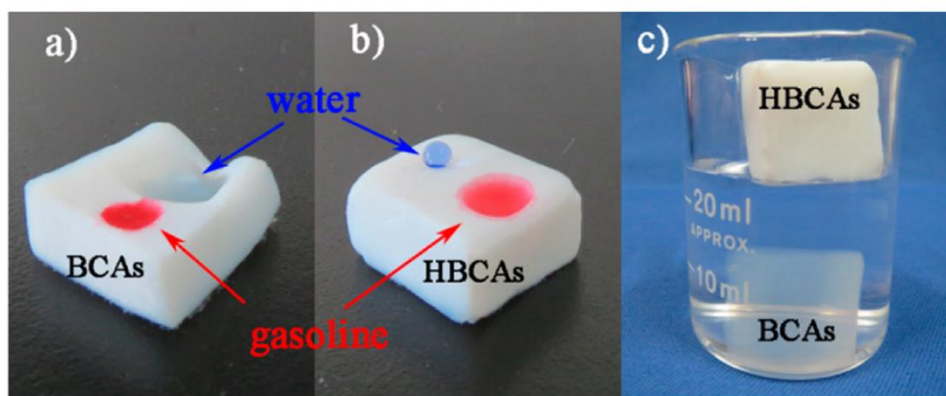
Figure 1.24 Water and gasoline were colored blue (Methyl Blue) and red (Oil Red), respectively, and dropped on the surface of a) BCA and b) HBCA-3. c) The HBCA-3 floated on water, while BCA sank into water.

In 2016, Lamboni et al. [40] reported bacterial cellulose (**BC)** was functionalized with silk sericin (SS) that has cytoprotective and mitogenic effects. The composites obtained by solution impregnation were stabilized by hydrogen bonds, and SS could be released in a controlled manner. The constructs were highly porous with interconnected pores allowing for high water uptake that varied with the SS concentration used for sample preparation (Figure 1.25). While SS did not disrupt the stability of the **BC** network, soluble SS diffusing from the composites did not influence keratinocyte growth but enhanced fibroblast proliferation, which would further optimize the wound healing process and improve extracellular matrix production, accelerating healing. Further, improved cell viability was observed upon the composites. Because of their attractive structure and properties, these **BC**−SS biomaterials represent potential candidates not only for wound dressing applications but also for tissue engineering.
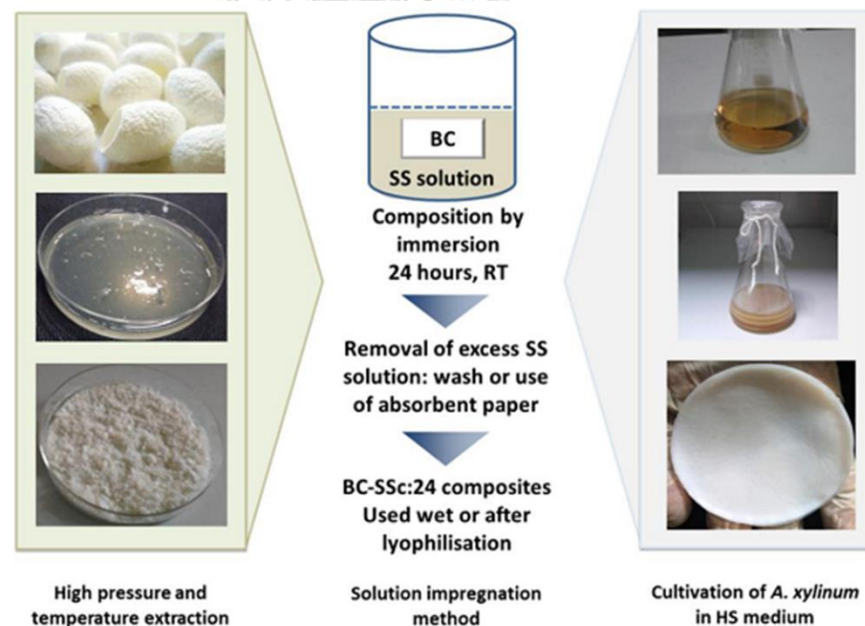
Figure 1.25 Preparation of SS powder, **BC** pellicles, and **BC**−SS composites.(c = [SS] in % w/v, 1, 2, 3; HS = Hestrin and Schramm).

1.8   Objective and scope of this research

The main goal of this thesis is to develop and modify **BC** by immobilization of 8-aminoquinoline derivatives on **BC** and use the modified **BC** as a sensor and adsorbent for metal ion detection. To achieve this goal, the following working scopes are set:

1. Use 8-aminoquinoline derivatives ligand as a sensitive fluorescent metal ion sensor.

2. To select the suitable chemical reaction for the immobilization of ligand on **BC** and produce at least one indicator and adsorbent.

3. To evaluate the adsorption responses of ligand immobilized on **BC**, the modified **BC** is potentially useful for analysis and separation of Zn^{2+} and Cd^{2+} in water such as waste-water treatment system**.**

จุฬาลงกรณ์มหาวิทยาลัย

CHULALONGKORN UNIVERSITY
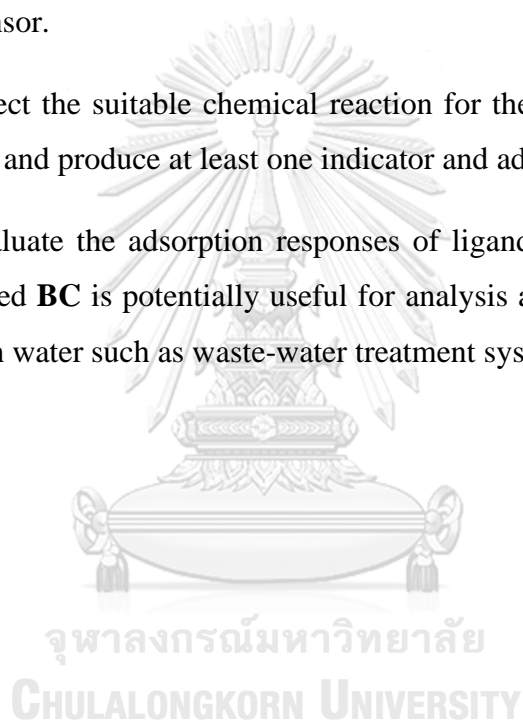
1.9 Oil marker detection

The petroleum industry is one of the world largest businesses that create numerous domestic and international transactions of petroleum products in the market. Petroleum oils are involved in social and military security that their transactions are usually controlled and taxed by government. The tax rates are dependent on the types of the petroleum oils and their application purposes. There are several legal problems related to tax avoidance, for instance, smuggling of untaxed oil or mixing of oil taxed at a high rate with that taxed at a low rate. To detect and prevent these adulterated oils, different oil markers have been added to petroleum oils with different tax rates [41-43]. The markers are usually oil soluble dyes which can be detected by naked eyes or absorption spectrometers. Usually, the marker is colorless in its initial state that can be developed into a color form during the detection process. The dye marker is usually prepared as a solution and added into petroleum oil at a minimal amount, typically 5-20 ppm, to avoid any undesirable effect in the engine combustion process [44, 45]. Therefore, the detection method must be sensitive enough to detect the marker at this concentration level. In general, a dye marker is extracted into an aqueous layer and quantified by UV-visible absorption spectroscopy [44, 46, 47] and fluorescence spectroscopy [48] techniques. Mass spectrometer has also been studied for this purpose due to it extremely high sensitivity and selectivity [49] but its applications for on-site analysis is limited by the cost and size of the instrument system.

Recently, smart phone cameras have become very common photographing devices and the associated technology including digital image sensors such as CCD and CMOS [50-54] and processing software [55-58] have been advanced that they can be used as a versatile portable optical sensor. The utilization of smart phone in chemical analysis offers many advantages including portability, accessibility, imaging, data recording, data processing and data transferring abilities [19, 59-62]. Furthermore, software applications can be readily developed to facilitate and simplify the whole detection and data analysis processes [63-65]. The applications of digital

imaging with various designs of paper-based sensors have been developed [66-69]. The combination of digital imaging with paper-based sensing platform are easy to use but there is still room for improvement in terms of its sensitivity and reproducibility.

In this study, a development of new sensitive analytical method for convenient detection of a gasoline marker on paper strips using a smart phone camera and an image processing software is reported. Phenolphthalein (PhP), a commercially available acid-base indicator, was used as a dye marker for commercial gasoline samples to demonstrate the sensitivity of this new technique. PhP is colorless in its initial neutral state and turns pink-purple color upon interaction with base. To preclude the liquid extraction step, filter paper strips were used in this work as a solid support for the reaction between PhP and base, and for capturing the PhP marker in its color form. Three sample testing methods, namely, dropping, dipping and counter-flowing methods, were comparatively studied (Figure 1.26). The color images of the paper strips were recorded by a smart phone camera and converted to digital color data by ImageJ application.
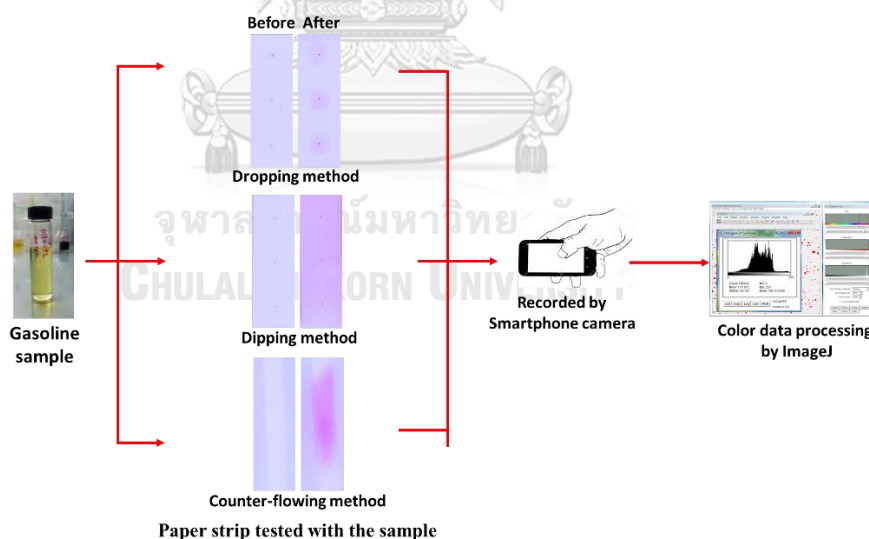
Figure 1.26 Simplified diagram of gasoline marker detection process by a smartphone camera.

Oil marker has been extensively used in several research fields. Some oil marker for petroleum oil have been reported herein.

In 2003, Suwanprasop et al. [46] presented petroleum markers 1-20 were synthesized either by a coupling reaction of n-alkylaniline (which was prepared from nitration and reduction reactions of n-alkylbenzene) with a diazonium salt of aniline derivatives or by a coupling reaction of a diazonium salt of n-alkylaniline with aniline or phenol derivatives (Figure 1.27). These synthetic markers provided invisible color in high-speed diesel fuel at an effective usable level (3-5 ppm), but gave visible colors when detected by extraction with 50% (v/v) 1,2-diaminoethane in a solution containing propane-1,3-diol and methanol (2:3, v/v). Marker contents in fuel oil could be successfully quantified with a VIS spectrophotometer. The markers did not alter the physical properties of the diesel fuel (as revealed by tests performed according to ASTM methods), and they were also stable in diesel fuel over a period of at least 3 months, suggesting that these synthetic dyes could readily be applied as petroleum markers in commercial fuel oils.
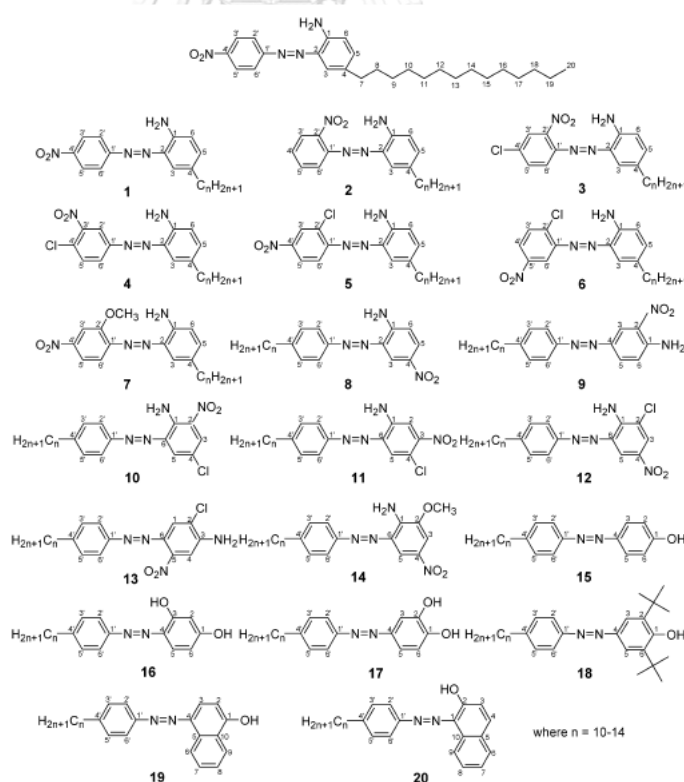
Figure 1.27 Structures of petroleum markers **1**-**20**.

In 2004, Suwanprasop et al. [47] presented marker dyes **1**-**15** for petroleum products were synthesized by coupling reaction of a naturally occurring *n*-alkylphenol, cardanol, with aniline and its derivatives (Figure 1.28). These synthetic marker dyes provided invisible color in gasoline and high-speed diesel fuel at an effective usable level (2-5 ppm) but gave visible colors when detected by extraction with 50% (v/v) 1,2-diaminoethane in a solution containing ethane-1,2-diol and methanol (1:1, v/v). Dye contents in fuel oils could be simply quantified with a vis spectrophotometer. The ASTM test methods revealed that the general physical properties of the dyed fuel oils were similar to those of the undyed fuel oils. These synthetic dyes were found to be stable in fuel oils up to at least 3 months, suggesting that these marker dyes could be readily applied as markers for commercial fuel oils. The dyes present in this report have the advantages not only of using an inexpensive agricultural byproduct from the manufacture of cashew nuts as the source of the starting material (cardanol), but also of having the nonpolar aliphatic side chain of cardanol, rendering the marker dyes well soluble in fuel oils.

Cardanol

OH

(CH$_2$)$_7$R
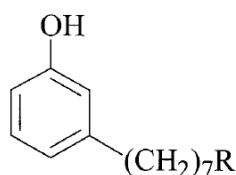
a R = (CH$_2$)$_7$CH$_3$

b R = CH=CH(CH$_2$)$_5$CH$_3$

c R = CH=CHCH$_2$CH=CH(CH$_2$)$_2$CH$_3$

d R = CH=CHCH$_2$CH=CHCH$_2$CH=CH$_2$

Figure 1.28 Structure of cardanol.

In 2007, Trindade et al. [44] presented an electroanalytical method based on square-wave voltammetry (SWV) for the determination of quinizarine (QNZ) in a mixture of Brittone-Robinson buffer 0.08 mol L^{-1} with 30% of acetonitrile. The QNZ can be used for its determination as color marker in fuel samples. All parameters were optimized and analytical curves can be constructed for QNZ concentrations ranging from 2.0×10^{6} mol L^{-1} to 1.4×10^{-5} mol L^{-1}. The method offers a limit detection of 4.12×10^{-7} mol L^{-1} and a standard deviation of 4.5% (Table 1.1). The method was successfully applied for determining QNZ in gasoline and diesel oil. The methodology was fast and simple, but with a sensitivity that was adequate for the determination of QNZ in spiked fuel, involving a simple step of sample pretreatment and resulting in short analysis times. Thus, the proposed method can be suggested as a good alternative for the routine quality control of this marker in fuel samples.

Table 1.1 Quantitative parameters for the assay of QNZ by the proposed method and reported methods

Parameter	Proposed method	Reported method [7]
Studied conc. range (mol L^{-1})	$(2.0-20.0) \times 10^{-6}$	$(2.0-41.3) \times 10^{-6}$
Intercept	-0.194	nr
Slope	7.2×10^{5}	nr
Correlation of coef. (r)	0.999	nr
LOD (mol L^{-1})	4.12×10^{-7}	8.25×10^{-7}
LOQ (mol L^{-1})	1.38×10^{-6}	nr

nr: Not revealed value.

In 2009, Le Goff et al. [70] presented Solvent Yellow 124 (SY124, N-ethyl-N-[2(isobutoxyethoxy)ethyl]-4-(phenylazo)aniline) is used as a common low tax fuel marker in European Union member countries. It is added to these fuels which may also contain traditional dyes, to prevent misuse. SY124 is produced industrially in solution (typically aromatic hydrocarbons) and its purity can vary from batch to batch. This is particularly a problem for the petroleum industry which risks large fines if SY124 levels are found to be below 6 mg/L or above 9 mg/L. A new reference material for SY124 (Figure 1.29), certified for purity was prepared to address this problem. A SY124 certified reference materials (CRM) was prepared from a commercially procured solution of SY124.
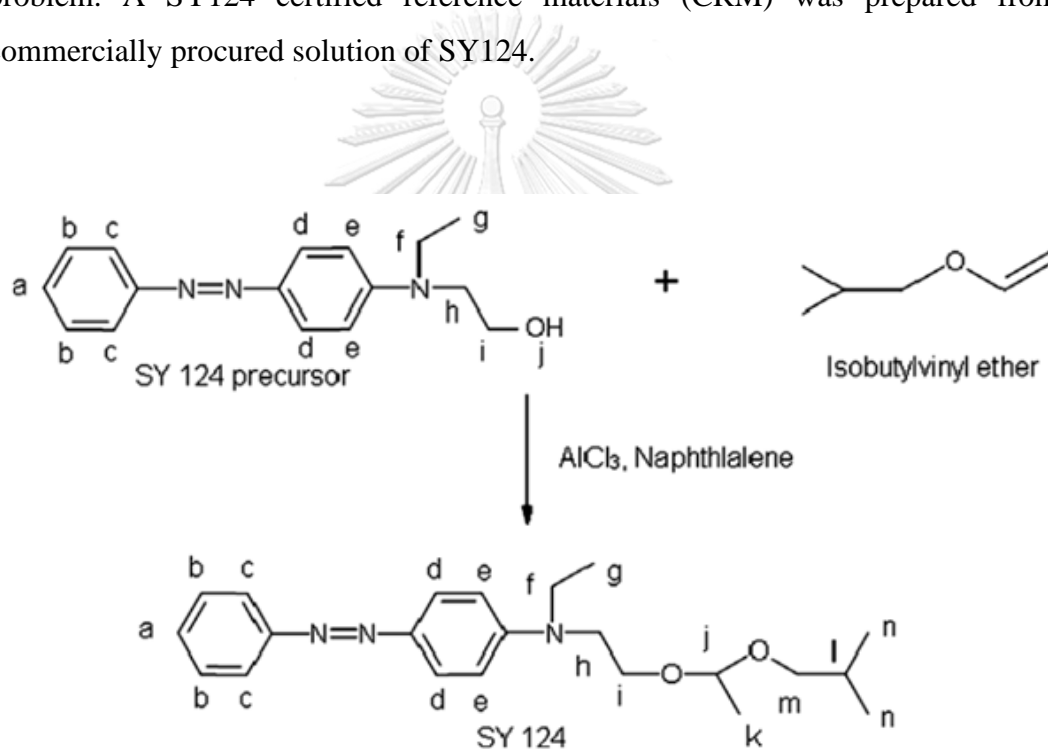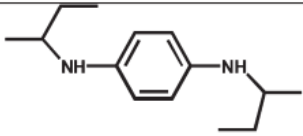
Figure 1.29 Reaction between SY 124 precursor and isobutylvinyl ether to form SY124.

In 2010, Alberici et al. [71] presented the effectiveness of the N,N'-di-sec-butylp-phenylenediamine (1) as a antioxidant (Table 1.2) to improve the oxidative stability of soybean, sunflower and canola biodiesel. Results indicate that the induction period for oxidation of soybean and canola biodiesel is significantly improved with the addition of only 0.2 ppm of the 1, reaching the oxidative stability specification. For sunflower biodiesel, 2.0 ppm of the 1 was necessary. This additive is also shown to be efficiently detected by the easy ambient sonic-spray ionization mass spectrometry technique, indicating that 1 and its analogues and derivatives could also be used as versatile artificial markers of biodiesel. to identify types production sites, or specific producers. For tax control, for instance, large industrial biodiesel producers could be required to add a specific diamine marker able to trace producers and production sites.

Table 1.2 Common commercial antioxidant used in fuels

Commercial name	Composition	Chemical structure
Santoflex MF: $C_{14}H_{24}N_2$ MW: 220,4 g mol^{-1}	N,N'-Di-sec-butyl-p-phenylenediamine	

In 2018, Langley et al. [49] presented a new ultrahigh-performance supercritical fluid chromatography-mass spectrometry (UHPSFC-MS) method has been developed using electrospray ionization (ESI) to detect and quantify a new fiscal fuel marker, ACCUTRACE S10, that was used as a replacement for ultraviolet-visible (UV-vis) fuel markers, such as quinizarin, Euromarker, and Solvent Red 24. It is UV-invisible, is doped at a low level (2.5 ppm) and was designed for detection using modern gas chromatography-mass spectrometry (GC-MS) instrumentation. The new UHPSFC−MS method has proven to be a quick, robust, and quantitative assay for the determination of the ACCUTRACE S10 fuel marker. The method has an analysis time of 8 min and is approximately 5 times faster than the recommended GC−MS method. UHPSFC−MS is compatible with injections of neat fuel (containing S10) (Figure 1.30). The novel UHPSFC-MS method uses this phenomenon, allows injection of undiluted fuels, and affords detection and quantitation at doping and tank dilution levels.
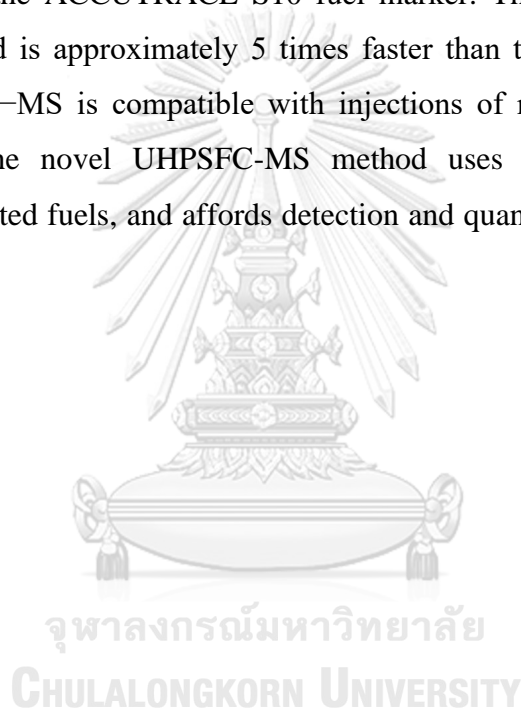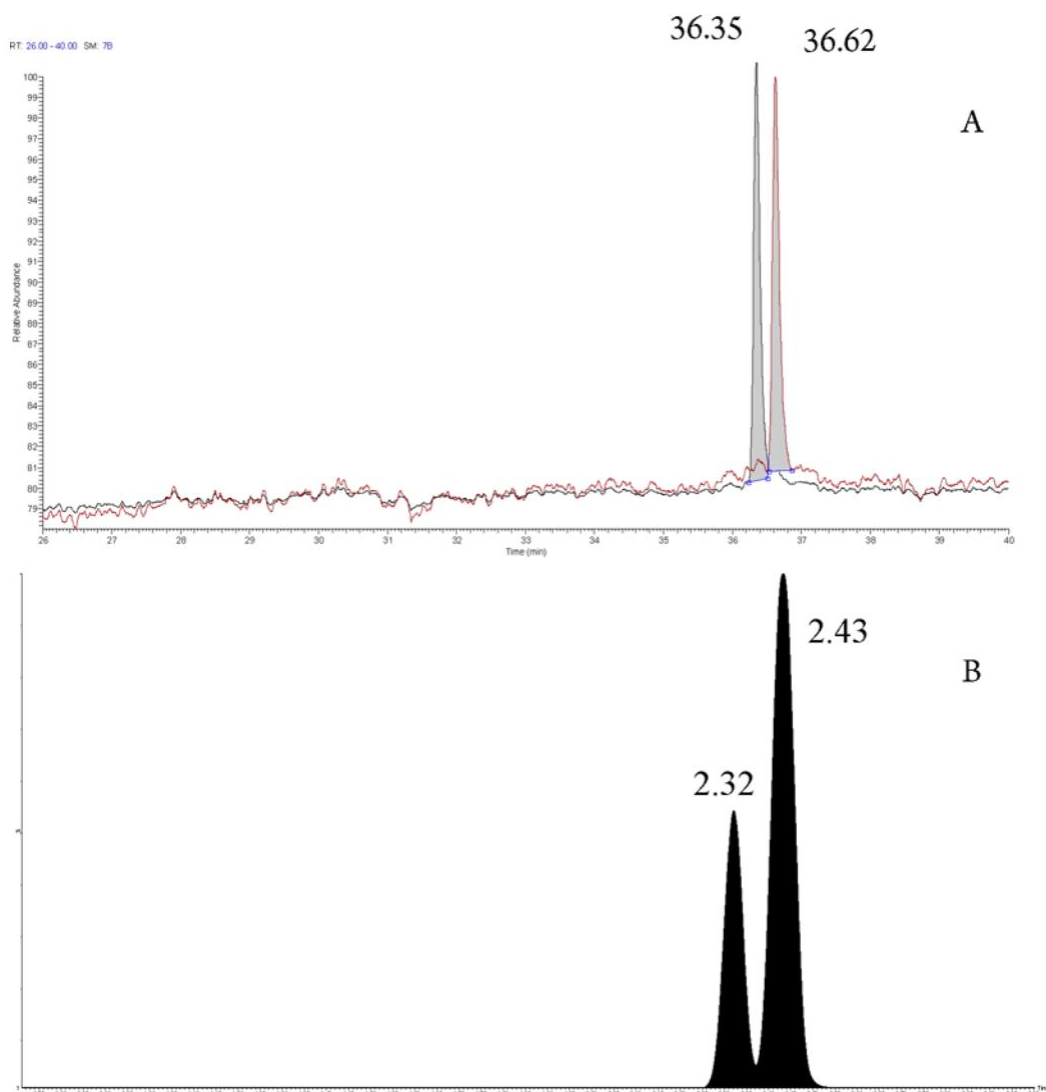
Figure 1.30 SIM chromatograms of molecular species for (A) GC−MS and (B) UHPSFC−MS showing chromatographic separation of ACCUTRACE S10-d21 and ACCUTRACE S10, respectively (labeled S10 eluting earliest in both cases).

1.10   Objectives and scope of this research.

The aim of the work presented in this thesis is to study and develop reliable and sensitive analytical method for determination of PhP in gasoline. To achieve this goal, the following working scopes are set:

1.   To produce of simple paper indicator.

2.   To study the detection methods of oil marker in gasoline i.e., dropping technique, dipping technique and counter-flowing technique.

3.   To detect quality of the oil marker that are present in the fuels, using smart phone camera to read and record,

4.   To detect quantity of the oil marker that are present in the fuels, using the ImageJ application to evaluate.
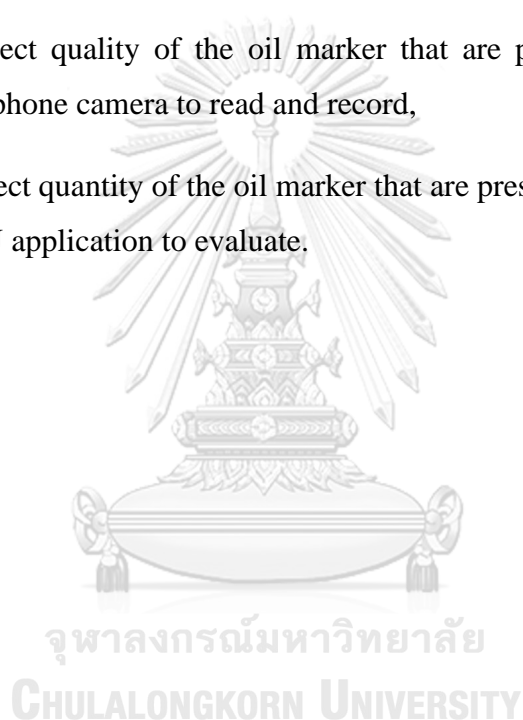
CHAPTER 2
EXPERIMENTS

2.1 Chemicals and Equipment

Chemicals:

- Acetonitrile (MeCN), RCI Labscan, Bangkok, Thailand

- Acetone, RCI Labscan, Bangkok, Thailand

- Sodium hydroxide (NaOH), Merck, Darmstadt, Germany

- Potassium carbonate (K_2CO_3), Merck, Darmstadt, Germany

- Phenolphthalein (PhP), Sigma Aldrich, MO, USA.

- Methanol (MeOH), RCI Labscan, Bangkok, Thailand

- Ethanol (EtOH), Merck, Darmstadt, Germany

- N-methyl-2-pyrrolidone (NMP), Merck, Darmstadt, Germany

- Chloroacetyl chloride, Merck, Darmstadt, Germany

- 8-Aminoquinoline, TCI, Japan

- Pyridine, Sigma Aldrich, MO, USA.

- Chloroform ($CHCl_3$), Merck, Darmstadt, Germany

- Tetrabutyl ammaonium iodide (TBAI), Sigma Aldrich, MO, USA

- Cesium carbonate (Cs_2CO3), Sigma Aldrich, USA

- Dimethylformamide (DMF), RCI Labscan, Bangkok, Thailand

- Dichloromethane (CH_2Cl_2), RCI Labscan, Bangkok, Thailand

- (3-Aminopropyl)triethoxysilane (APTES), TCI, Japan

- Salicylaldehyde, Fluka (Switzerland)

- tert-Butanol (t-BuOH), PanReac AppliChem, Germany

- Toluene, RCI Labscan, Bangkok, Thailand

- Commercial gasoline (octane 95), A local gas station, Thailand.

- Nitrogen gas (N_2), Linde, Thailand

Equipment:

- Rotary evaporator, R200, Buchi , Switzerland

- Ultrasonicator, Elma, Germany

- Balance (AB204-S, Mettler Toledo)

- UV Lamp (365 nm), TUV 15W/G15 T18 lamp, Philips, Holland

- Magnetic stirrer, Fisher Scientific, USA

- Hot plated magnetic stirrer, IKA, Germany

- Blender, Waring Commercial, USA

- Syringe filter, Verticlean, PTFE, 13 mm, 0.45 µm

- Freeze Dryer, Labconco, MO, USA

- Oven, Memmert, Germany

2.2 Analytical instrument

Elemental (C, H, N) analyses were performed on a PE 2400 series II analyzer (Perkin-Elmer, USA). Fourier transform infrared spectra were acquired on Nicolet 6700 FT-IR spectrometer (Nicolet, USA) equipped with an ATR universal accessory. The spectra were taken in absorbance mode over the wavenumber range of 650–4000 cm-1, with a scanning resolution of 4 cm^{-1} and after 16 scans for each sample. ^{1}H-NMR spectra were acquired from sample solutions in DMSO-d6 on Varian Mercury NMR spectrometer (Varian, USA) at 400 MHz. UV-visible absorption and emission spectra were obtained on an Agilent 8453 UV-visible Spectroscopy System. The absorption spectra were acquired from solutions of the PhP in a quart cuvette (Starna

29- F/Q/ 10) with 1 cm light path recorded in the range from 200 nm to 800 nm at ambient temperature. The concentrations of metal ions w determined by Inductively Coupled Plasma-Atomic Emission Spectrometry (ICP-AES) model iCAP 6500 series (Thermo Fisher scientific).

2.3 Preparation of bacterial cellulose (BC)

The cultivation of Acetobacter xylinum was achieved using naturally fermented coconut-water as the incubation system. 100 mL of fermented coconut-water as well as 2.0 g of sucrose, 1.5 g of agar, 0.2 g of disodium hydrogen phosphate solution, 0.3 g of ammonium sulfate and 0.05 g of magnesium sulfate was well mixed to form uniform medium. The pH of the medium was adjusted to 4.5 by acetic acid, followed by high temperature sterilization for 30 min. Thereafter, Acetobacter xylinum was activated at 30 °C for 48 h, and then 5 mL of the suspension was inoculated in the same medium with the volume of 100 mL. The cultivation of Acetobacter xylinum was conducted at 30 °C for 14 days. After the incubation period, bacterial cellulose (**BC**) was formed as a white thick pellicle (~1 cm thickness) floating at the top of the medium. The **BC** pellicle was lifted from the medium and washed thoroughly in running tap water.

2.3.1 Purification of bacterial cellulose (BC)

The harvested **BC** pellicles were subjected to cleaning steps to remove the bacteria, microbial cell attached to the pellicle, and the medium by drowning in deionized water for 3 days. After that, it was treated by 1 M NaOH at 100 °C for 6-8 hours to eliminate remaining medium and cells, and subsequently washed with excess deionized water to remove the alkali completely and neutralize the pH. The purified **BC** was cut to small cubes with a $1 \times 1 \times 1$ cm^3 of dimension (Figure 2.1a) and stored at 4 °C for future use. As this **BC** cubes have inhomogeneous density, they were homogenized by mincing with a high speed blender (over 10,000 rpm) for 3 minutes to obtain the homogenized **BC** slurry, as shown in Figure 2.1b. The homogenized **BC** was transferred into a closed container and kept in a refrigerator at 4 °C for future use.

The aqueous media of the homogenized **BC** was repeatedly replaced with tert-butanol (at least 10 times). The **BC** suspension was then frozen at -20 °C for 24 hours and was then subjected to a freeze-dry process. Drying was performed for 48 hours at a temperature of -60 °C in a vacuum of 0.50 mbar. After the freeze-dry process, the resulting freeze-dried **BC** foam (Figure 2.1c) was kept in a desiccator for further use.
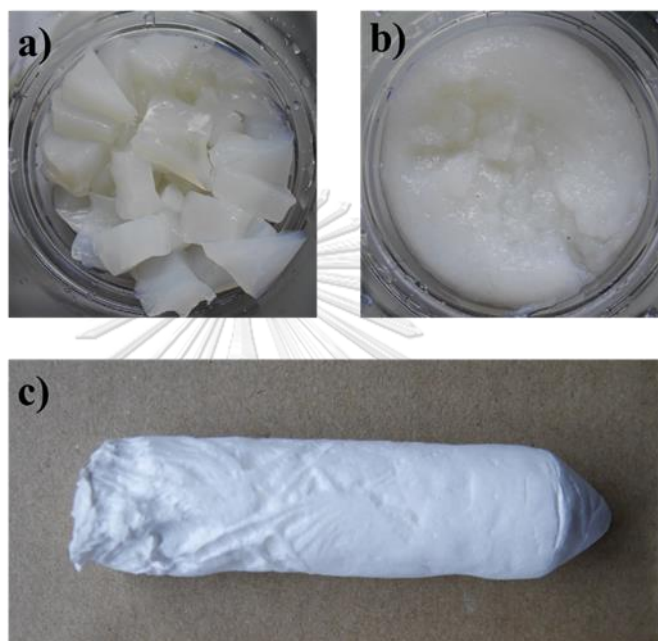
Figure 2.1 a) Purified **BC** cubes, b) homogenized **BC** slurry in aqueous media and c) freeze-dried **BC** foam.

2.4 Synthesis of (2-chloro-N-(quinolin-8-yl)acetamide

8-aminoquinoline (288 mg, 2.0 mmol) and pyridine (222 mg, 2.8 mmol) were dissolved in chloroform (10 mL), stirred in an ice bath, and 2-chloroacetyl chloride (461 mg, 2.4 mmol) in chloroform (5 mL) was then added dropwise over a 1 h period. After stirring for 2 h at room temperature, the solvent was removed under reduced pressure to obtain a white solid residue, which was purified by silica gel column chromatography using dichloromethane as the eluent to afford 2-chloro-N-(quinol-8-yl)acetamide (QA-Cl) [28, 72, 73]. Yield: 374 mg (84%), mp: 131.6~132.6 °C. 1H NMR (400 MHz, DMSO) δ 10.70 (s, 1H), 8.95 (dd, J = 4.3, 1.7 Hz, 1H), 8.63 (d, J = 7.7 Hz, 1H), 8.44 (dd, J = 8.3, 1.6 Hz, 1H), 7.73 (d, J = 8.2 Hz, 1H), 7.66 (dd, J = 8.3, 4.2 Hz, 1H), 7.61 (t, J = 8.0 Hz, 1H), 4.61 (s, 2H).

2.5   Immobilization of fluorophore on bacterial cellulose

Four methods for immobilization of **AZQ** onto **BC** i.e., attachment via APTES linker, direct incubation, and using nucleophilic substitution with K_2CO_3 and Cs_2CO_3 as a base were investigated. These experimental procedures are described as follows.

2.5.1   Immobilization of QA on BC using APTES as a linker

Under stirring, APTES (0.244 mL, 1.04 mmole) was added to *tert*-butanol (5 mL) followed by an addition of **BC** foam (50 mg, 0.308 mmole). The mixture was magnetically stirred at room temperature under nitrogen gas. After 48 hours, the resulting slurry was centrifuged. After the first centrifugation (4000 rpm, 10 min) the supernatant was removed. The precipatete was redispersed-recentrifuged in methanol and deionized water for 5 cycles each. The modified **BC** was recovred as a solid residue. Subsequently, the silane-modified **BC** was added into a mixture of 2-chloro-*N*-(quinolin-8-yl)acetamide (70 mg, 0.317 mole) and K_2CO_3 (0.256 g, 1.85 mmole) in acetonitrile (40 mL). After reflux at 100 °C for 4 hours, the mixture was centrifuged, and the solid residue was washed by dichloromethane for 5 times and ethanol 5 times to afford the **QZ** modified **BC** [28].

2.5.2   Immobilization of QA on BC using direct incubation

2-chlorin-N-(quinolin-8-yl)acetamide (0.1225 g, 0.555 mmole) was dissolved in *tert*-butanol (10   mL), sonicated for 30 minutes at 50 °C, and allowed to room temperature. The **BC** foam (0.09 g, 0.555 mmole) was then added into the solution and stirred for 48 hours at room temperature. The mixture was frozen at -22 °C for 24 hours and followed by a freeze-drying process for 48 hours at -60 °C in vacuum of 0.50 mbar to give **QA/BC** foam. The **QA/BC** foam was incubated in a oven at 100 °C for 1 hour. The cured-**BC** sample was washed by methanol (50 mL) for 10 times to remove unreacted ligand [38].

2.5.3   Immobilization of QA on BC using K_2CO_3 as a base

BC foam (0.3 g, 1.85 mmole), potassium carbonate (1.534 g, 11.1 mmole) and 2-chloro-N-(quinolin-8-yl)acetamide 204, 408 and 816 mg (0.925, 1.85 and 3.70 mmole) were dissolved in acetonitrile (50 mL) and refluxed at 100 °C for 4 hours.

The resulting slurry was washed by Soxhlet extraction for 72 hours by using methanol (2 liters) with fresh solvent replacement every 24 hours to remove untrated ligand.

In this investigation, three amounts of 2-chloro-N-(quinolin-8-yl)acetamide i.e. 0.925 mmole, 1.85 mmole and 3.70 mmole were evaluated to give three types of the **QA** modified **BC** foam samples coded as **BC:QA** 1:0.5, **BC:QA** 1:1 and **BC:QA** 1:2, respectively.

2.5.4 Immobilization of QA on BC using Cs₂CO₃ as a base

BC foam (0.5 g, 3.08 mmole), cesium carbonate (6.0317 g, 18.51 mmole), tetrabutyl ammaonium iodide (TBAI) (0.6838 g, 1.85 mmole), and 2-chloro-N-(quinolin-8-yl)acetamide (0.6808 g 3.08 mmole) were dissolved in dimethylformamide (100 mL), and stirred at room temperature for 4 hours. The resulting slurry was washed by Soxhlet extraction for 72 hours by using methanol (2 liters) with fresh solvent replacement every 24 hours to remove untrated ligand [74].

2.6 Film fabrication

The **QA** modified **BC** were fabricated to paper-thin sheet by poured wet **QA** modified **BC** sample onto moistened filter paper of suction filtration that cover on buchner funnel. The mixture was then vacuum filtrated to prepare **BC** sheet. After almost dried, the **BC** sheet was peeled off from the filter paper, it was dried in oven at 100 °C for 1 hour to obtain **BC** solid film.

2.7 CHN analysis and degree of substitution (%DS)

The CHN analysis of **BC** sample was determined by elemental analyzer (THERMO FLASH 2000). The **%DS** was calculated from %N using the following equation.

Equation

$$\%\textbf{DS} = \frac{\%\text{N in } \textbf{QA} \text{ modified } \textbf{BC}}{\text{Theroitical } \%\text{N in the 100\% substitution}} \times 100$$

The theoretical %N in the 100% substitution was calculated from $C_{17}H_{18}N_2O_6$ which represent the chemical formula of fully **QA** monosubstituted on every repeating unit of **BC**.

2.8 Adsorption study

For the adsorption study, the **QA** modified **BC** was fabricated to plate sheet, after that incubate these films sheet (0.3 g) into Zn^{2+} and Cd^{2+} solutions (1 mM, 10 mL) at room temperature for 24 hours. After incubated, the **AQ** modified **BC** was removed. The metal ion solution was filtered by syringe filter and determined the remain amount of metal ion concentration in the filtered solution by ICP-AES technique.

2.9 Sensing study

Fluorescent test

For fluorescence test, the **QA** modified **BC** sample (0.3 g) was incubated in Zn^{2+} and Cd^{2+} solution (1 mM, 10 mL). After 30 minutes, the fluorescence images of the **BC** samples were photographically recorded by a digital camera under black light (365 nm) illumination.

2.10 Gasoline sample preparation

The PhP stock solutions (1.793×10^5 ppm) were prepared in three solvents, i.e. ethanol, acetone and NMP. Each PhP stock solution was added into commercial gasoline to give a gasoline sample containing 6 ppm of PhP dye marker and 50 ppm of the stock solution. This gasoline sample was diluted with the commercial gasoline to give five more gasoline samples containing lower concentrations of PhP (5, 4, 3, 2 and 1 ppm).

2.11 Substrate selection

The four types of substrates i.e. filter paper (Whatman No. 1 and No. 3) and cotton yarns (3 ply and 12 ply or 0.18 g/m and 3.83 g/m, respectively) were tested as the indicator substrate, at least three pieces of replicate samples were prepared for each indicator. These indicator substrates were immersed entirely in a gasoline sample

(1 mL) and the other end was dipped into a NaOH solution (0.5 mL). The indicator substrate was left to allow for the gasoline sample and NaOH solution to travel along the paper strip for 15 minutes. The color image of the tested substrate was photographed at 6 cm distance under white light illumination (1600 lux) in a light control box. The camera was set manually using shutter speed of 1/250 second, ISO 50, F/1.7 and white balance of 5500 K.

2.12 Detection methods

2.12.1 Dropping technique

A piece of filter paper (Whatman No. 3) was cut into multiple 1×3 cm^2 strips each of which contained 3 dots marked with 1 cm apart. Then, the filter paper strip was soaked with a base solution. The base soaked paper strips were allowed to dry in the air for 1 hour and kept in a desiccator for at least 24 hours prior to use. The gasoline sample (6 µL) was dropped on the 3 dots marked on the base coated paper strip. The image of the tested strip was photographed at 6 cm distance under white light illumination (1600 lux) in a light control box. The camera was set manually using shutter speed of 1/250 second, ISO 50, F/1.7 and white balance of 5500 K. The 3 marked dots on the indicator strips provided three replicates of the images for each test.

2.12.2 Dipping technique

The base coated paper strip was prepared and stored in a same way as the dropping technique described above. The indicator strip was immersed entirely in a gasoline sample (1 mL) for 1 minute. The image of the tested strip was photographed in the same manner described for the dropping method and the 3 marked dots on the indicator strips provided three replicates of the images for each test.

2.12.3 Color data processing

For the direct dipping and dropping methods, an image on the indicator strip was cropped into a circular shape with diameter of 80 pixels centered at the marked dots. Each indicator strips thus provided three replicates of the circle images. The RGB color values of the cropped image were converted to CMYK values by using the

RGB to CMYK plugin of ImageJ processing program. For the counter-flowing method, the wand (tracing) tool was selected in the magenta channel with the thresholding function enabled. The image pixels with the magenta value above the threshold value, determined based on histogram shape by the program, were automatically cropped.

2.12.4 Counter-flowing technique

The filter paper (Whatman No. 3) was cut into narrow strips (0.1 or 0.2 × 6 cm^2). One end of the paper strip was dipped into a gasoline sample (0.5 mL) and the other end was dipped into a NaOH solution (0.5 mL). The indicator substrate was left to allow for the gasoline sample and NaOH solution to travel along the paper strip for 15 minutes. The color image of the tested strip was photographed at in the same manner described for the dropping method. The test for each sample were performed in three replicates using three indicator strips.

2.13 Light control box and light source

All photographics were taken by a smart phone camera (Samsung Galaxy Note 8) with 1440 × 2560 pixels of resolution. The smart phone camera was set in the same condition during image capture (shutter speed of 1/250 second, ISO 50, F/1.7 and white balance of 5500 K). To reduce environmental variability, all photographs were taken in a light control box with white light (LED strip), with the smart phone placed on the box at the same height for each sample.

CHAPTER 3
RESULTS AND DISCUSSION

In this research work, cellulose was studied as a substrate for optical chemical sensors. High surface area and light weight of cellulose is suitable for development of highly sensitive and portable sensors. The first part deals with bacterial cellulose-based sensors and adsorbent for metal ion detection and the second part is related with paper-based sensors for oil marker detection. The results and discussion of these two developments will be presented and discussed here.

3.1 Bacterial cellulose-based sensors and adsorbent for metal ion detection

In this part of research work, bacterial cellulose (**BC**) was used as a solid substrate and 2-chloro-N-(quinolin-8-yl)acetamide (**QA**) was used as a sensitive fluorescent ligand for metal ions to develop a metal ion sensor and adsorbent. The development involves the immobilization of **QA** on **BC** and characterization by fluorescence test, ATR-IR spectroscopy, ligand leaching test, elemental analysis and metal ion adsorption.

Four immobilizations techniques studied in this work included using (3-aminopropyl) triethoxysilane (APTES) as a linker, using direct incubation, and using nucleophilic substitution with K_2CO_3 and Cs_2CO_3 as a base. The **BC**-**QA** conjugated products from the immobilization were initially tested with Zn^{2+} solution. The fluorescence appearance on the solid sample suggested the immobilization success while the fluorescence appearance in the solution suggested the immobilization failure.

3.1.1 Immobilization of QA-Cl on BC using APTES as a linker

In this study, surface of **BC** foam was first functionalized with APTES by condensation reaction in *tert*-butanol at room temperature for 48 hours under nitrogen gas (Figure 3.1). The resulting APTES modified **BC** was reacted with **QA-Cl** and K_2CO_3 in the presence of acetonitrile at 100 °C for 4 hours to give **QA** modified **BC** sample.
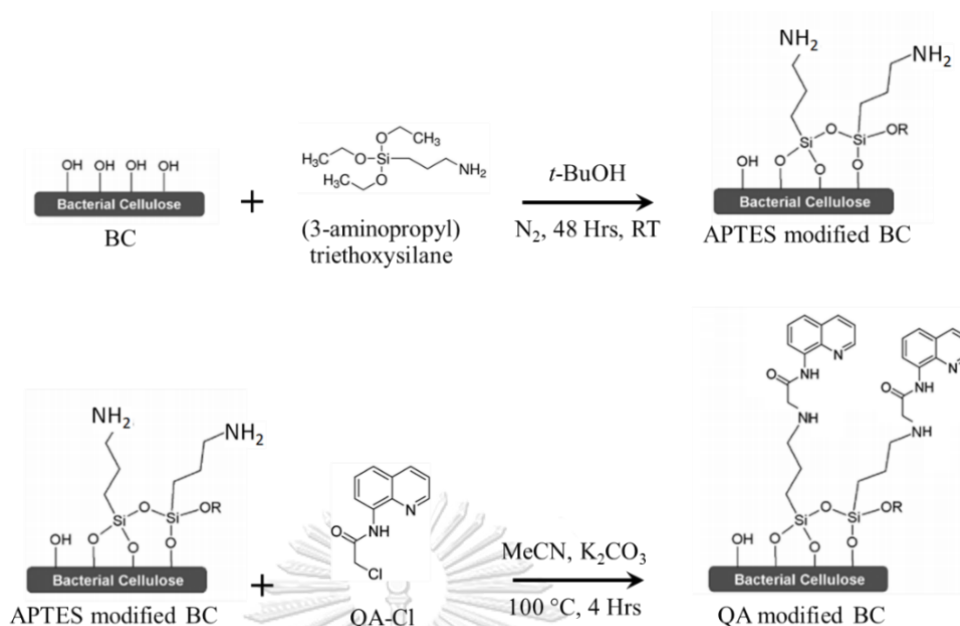
Figure 3.1 Immobilization of **QA** ligand on **BC** using APTES as a linker.

The **QA** modified **BC** sample was added with Zn^{2+} solution and observed its fluorescence appearance under UV light (365 nm). The observation showed that the **QA** modified **BC** sample was not fluorescent, but the solution gave strong green fluorescence (Figure 3.2). These results indicated that the immobilization of **QA** ligand on **BC** via APTES linker was not successful as the **QA** ligand diffused out of the solid sample into the solution. This immobilization technique required two-stepped reactions in which the success of the first step cannot be proven, another immobilization technique using a single step reaction was studied and discussed in the next section.
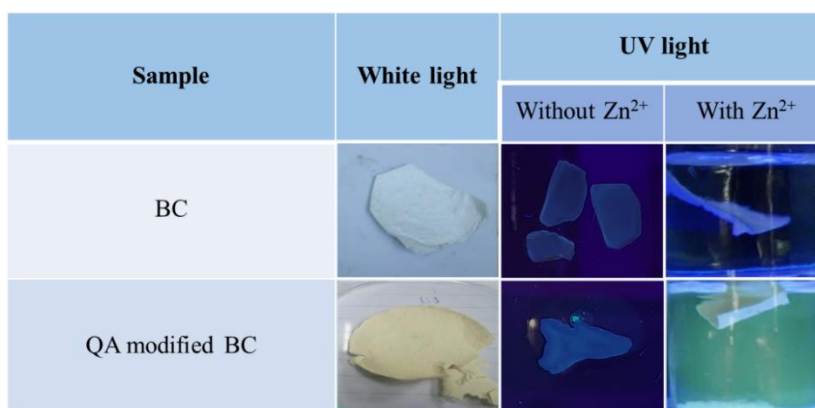
Figure 3.2 **BC** and **QA** modified **BC** samples under white light and UV light before and after addition of Zn^{2+} solution.

3.1.2 Immobilization of QA-Cl on BC using direct incubation

In this study, **BC** foam was mixed with **QA-Cl** in *tert*-butanol at room temperature for 48 hours. The resulting **BC** mixed with **QA-Cl** was incubated at room temperature and 100 °C for 1 hours to give **QA** modified **BC** sample (Figure 3.3).
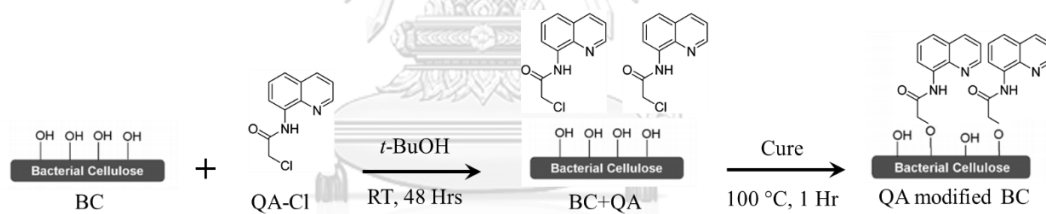
Figure 3.3 Immobilization of **QA** ligand on **BC** using direct incubation.

After curing at room temperature, the color of **QA** modified **BC** sample turned light yellow, the color of **QA** ligand (Figure 3.4b). However, the curing at 100 °C caused the color of the sample turned into intense yellow (Figure 3.4c). The intense yellow color indicated that there was a reaction of **QA-Cl** occurred. The sample was washed by methanol for 10 times to give white solid powder (Figure 3.4d). This white solid powder was tested with Zn^{2+} solution and it showed no fluorescence for both solid sample and solution under UV light (Figure 3.4e). The results indicated that **QA** ligand was no longer presence in the **BC**. Therefore, **QA-Cl** was not condensed with **BC** substrate, but it might react intramolecularly to form a cyclic quinolinium salt (Figure 3.5).
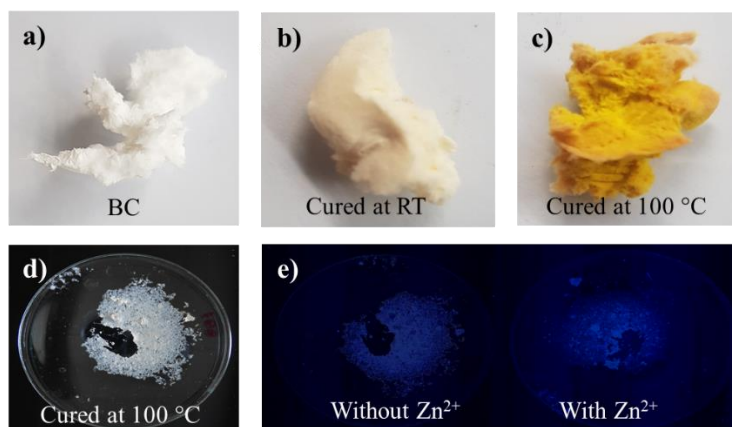
Figure 3.4 **BC** foam a) before and after cured with **QA**-**Cl** at b) room temperature and c) 100 °C. **BC** foam cured with **QA**-**Cl** at 100 °C d) after washing and dry, e) in water and in Zn^{2+} solution under UV light.

QA-Cl	**Quinolinium salt**
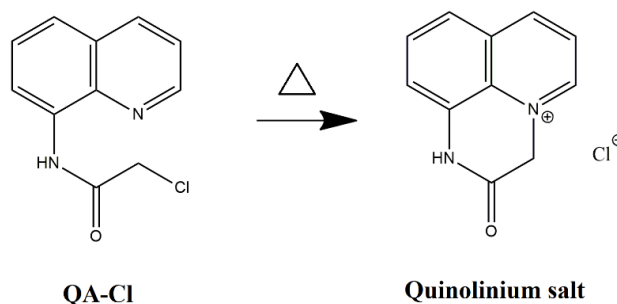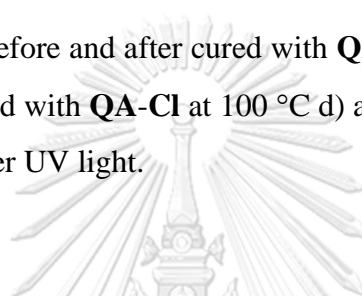
Figure 3.5 Intramolecular cyclization of **QA**-**Cl** to form quinolinium salt.

The IR-spectrum of **BC** foam cured with **QA-Cl** at 100 °C after washing and dry was showed similar pattern with **BC** but did not show any peaks of **QA-Cl**. The results confirmed that, after washing, the sample no longer contained the **QA** ligand (Figure 3.6).
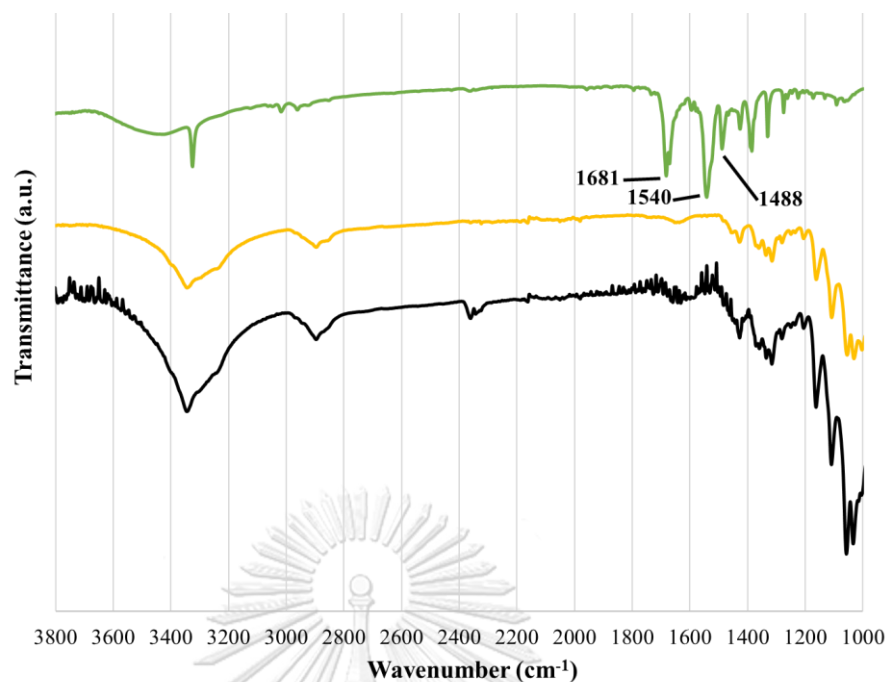
Figure 3.6 FTIR-ATR transmittance spectra of –**QA**-**Cl**, –**BC**, and –**BC** mixed **QA**-**Cl** incubated at 100 °C after washing.

Due to the unsuccessful immobilization of **QA** using the direct incubation method, the nucleophilic substitution reaction of **QA-Cl** using basic condition was investigated and discussed in the next section.

3.1.3   Immobilization of QA-Cl on BC using K$_2$CO$_3$ as a base

In this study, surface of **BC** foam was reacted with **QA-Cl** by nucleophilic substitution reaction using K$_2$CO$_3$ as a base in acetonitrile at 100 °C for 4 hours. The reaction was expected to give the **QA** modified **BC** by forming an ether linkage between **QA** ligand and **BC** (Figure 3.7).
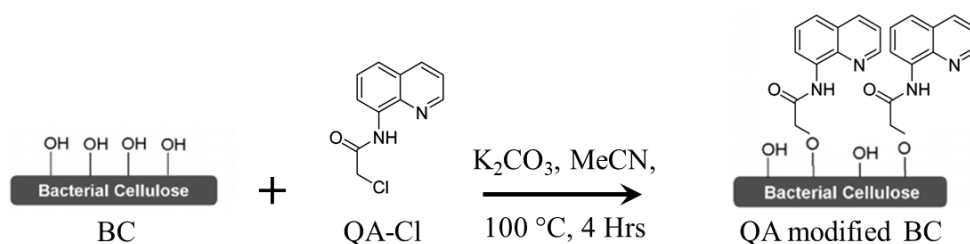
Figure 3.7 Immobilization of **QA** ligand on **BC** by using K$_2$CO$_3$ as a base.

The **QA** modified **BC** sample was washed by Soxhlet extraction in methanol for 72 hours, with fresh solvent replacement every 24 hours, to give light yellow solid (Figure 3.8a). This light yellow **QA** modified **BC** sample was tested with Zn^{2+} solution. Upon addition of Zn^{2+} solution, the solid **BC** sample showed strong green fluorescence, but the solution gave no fluorescence under UV light (Figure 3.8b). These results indicated that the modified **BC** sample contained the **QA** ligand. To confirm that **QA** ligand attached on **BC** via chemical bond rather than physisorption, the Soxhlet extractant at every 24 hours was also tested with Zn^{2+} solution. Only the extractant from the first 24 hours showed green fluorescence under UV light (Figure 3.8c). The results indicated that **QA** ligands present in the modified **BC** sample after 72 hours of Soxhlet extraction was likely attached to **BC** via chemical bonds.
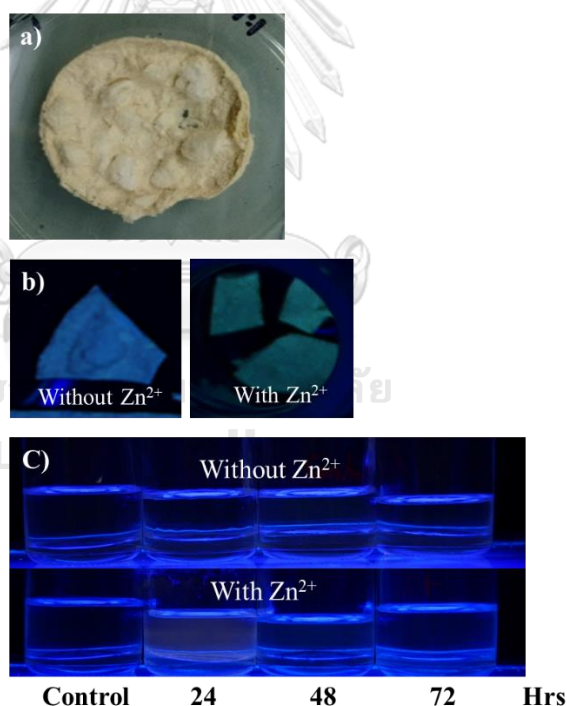
Figure 3.8 a) **QA** modified **BC** samples under white light and b) UV light before and after addition of Zn^{2+} solution. c) Soxhlet extractant under UV light before and after addition of Zn^{2+} solution (final concentration = 1 mM).

The spectrum of **QA** modified **BC** contained peaks at 1680, 1540 and 1488 cm^{-1} belonging to C=O stretching, N–H bending and aromatic C=C stretching of **QA** ligand, respectively. The peaks at 3600-3000, 3000-2800, 1430-1300 and 1200-1000 cm^{-1} in the spectrum of **QA** modified **BC** were corresponding to the O–H stretching, C–H stretching, CH$_2$ bending, C–O stretching in carbohydrate chains of **BC**, respectively (Figure 3.9). The IR-spectrum thus confirmed the presence of **QA** ligand in the modified **BC** sample.
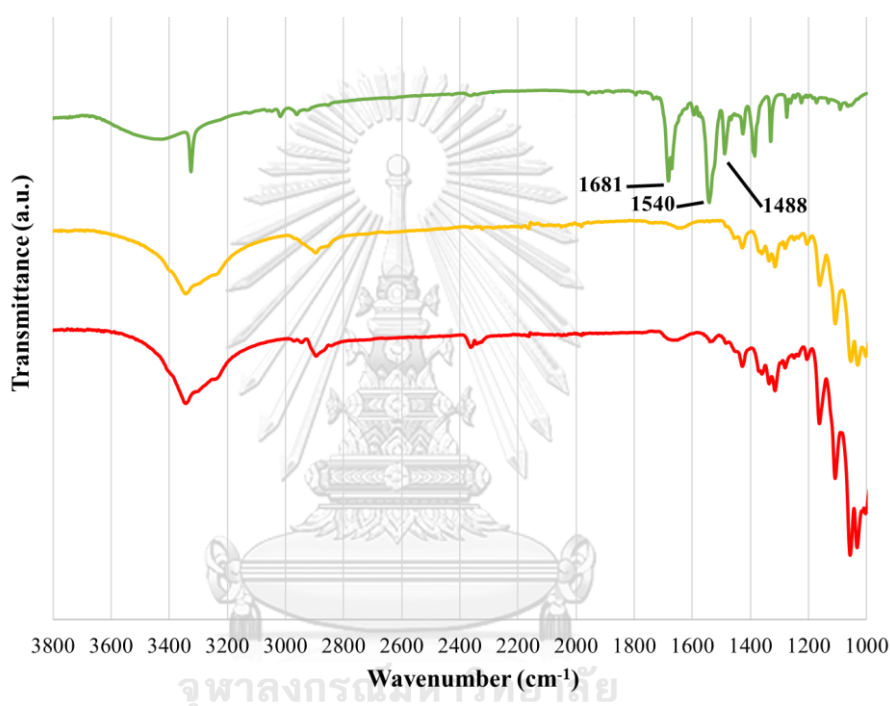
Figure 3.9 FTIR-ATR transmittance spectra of –**QA-Cl**, –**BC**, and –**QA** modified **BC** sample prepared by using K$_2$CO$_3$ as a base.

As **QA** contains N atoms, the nitrogen content in the **QA** modified **BC** can be used for calculation of the ligand content or degree of substitution (**%DS**). Theoretically, the completed substitution (**%DS** = 100%) of **QA** should give the nitrogen content of 8.09%. From CHN analysis, the **QA** modified **BC** samples gave different DS depending on the mole ratio of **BC:QA-Cl** used in the immobilization reaction (Table 3.1). The **%DS** increased with the increasing amount of **QA-Cl** from 23% to 63% when the **QA**-**Cl** was increased from 0.5 to 2.0 equivalents. However, the **QA** modified **BC** sample prepared from 1 equivalent of **QA-Cl** gave less

yellowish color sample (Figure 3.10) with only slightly lower **%DS** (58%) than that prepared from 2 equivalent of **QA**-**Cl**. Therefore, the **QA** modified **BC** sample prepared from 1 equivalent of **QA**-**Cl** was used for further metal ion adsorption study.

Table 3.1 C, H, and N contents of **BC** and **QA** modified **BC** from CHN analysis and calculated degree of substitution (**%DS**)

Sample	C	H	N	%DS
BC (calculated from $C_6H_{10}O_5$)	44.45	6.22	0	-
100% **QA** substituted **BC** (calculated from $C_{17}H_{18}N_2O_6$)	58.95	5.23	8.09	100
BC	43.42	6.16	0	-
BC:QA 1:0.5	48.90	6.26	1.86	23
BC:QA 1:1	52.26	6.24	4.66	58
BC:QA 1:2	53.51	6.15	5.06	63

Figure 3.10 **QA** modified **BC** prepared from different mole ratio of **BC**:**QA**-**Cl**.

3.1.4 Immobilization of QA-Cl on BC using Cs₂CO₃ as a base

In this section, a stronger base, Cs_2CO_3 was used in place of K_2CO_3 for the nucleophilic substitution reaction of **QA-Cl** with **BC** in the presence of tetrabutyl ammonium iodide (TBAI) phase transfer catalyst (Figure 3.11) according to the procedure for ether synthesis reported in the literature work [74].
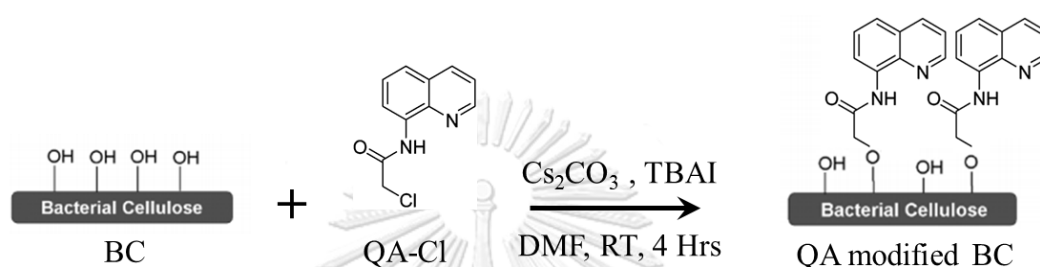
Figure 3.11 Immobilization of **QA** ligand on **BC** by using Cs_2CO_3 as a base.

The **QA** modified **BC** sample was washed by Soxhlet extraction in methanol for 72 hours, with fresh solvent replacement every 24 hours, to give white solid (Figure 3.12a). This white **QA** modified **BC** sample was tested with Zn^{2+} solution and it showed no fluorescence for both solid sample and solution under UV light (Figure 3.12b). The results indicated that **QA** ligand was no longer presence in the **BC** sample and **QA-Cl** did not react with **BC** in this reaction condition. The Soxhlet extractant tested with Zn^{2+} solution also confirmed that **QA** ligand was completely extracted with in the first 24 hours (Figure 3.12c)
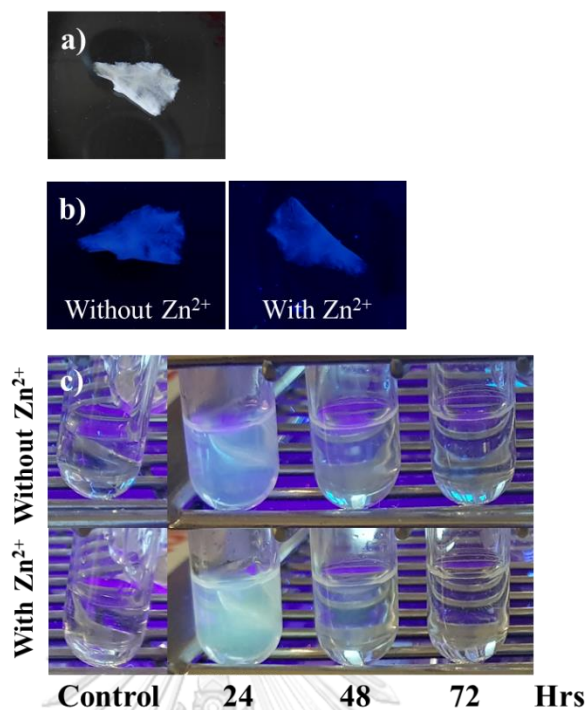
Figure 3.12 a) **QA** modified **BC** samples under white light and b) UV light before and after addition of Zn^{2+} solution. c) Soxhlet extractant under UV light before and after addition of Zn^{2+} solution (final concentration = 1 mM).

The IR-spectrum of **QA** modified **BC** sample showed similar pattern with **BC** but did not show any peaks of **QA-Cl**. The results confirmed the absence of **QA** ligand in the sample after Soxhlet extraction and the unsuccessful immobilization of **QA** (Figure 3.13).
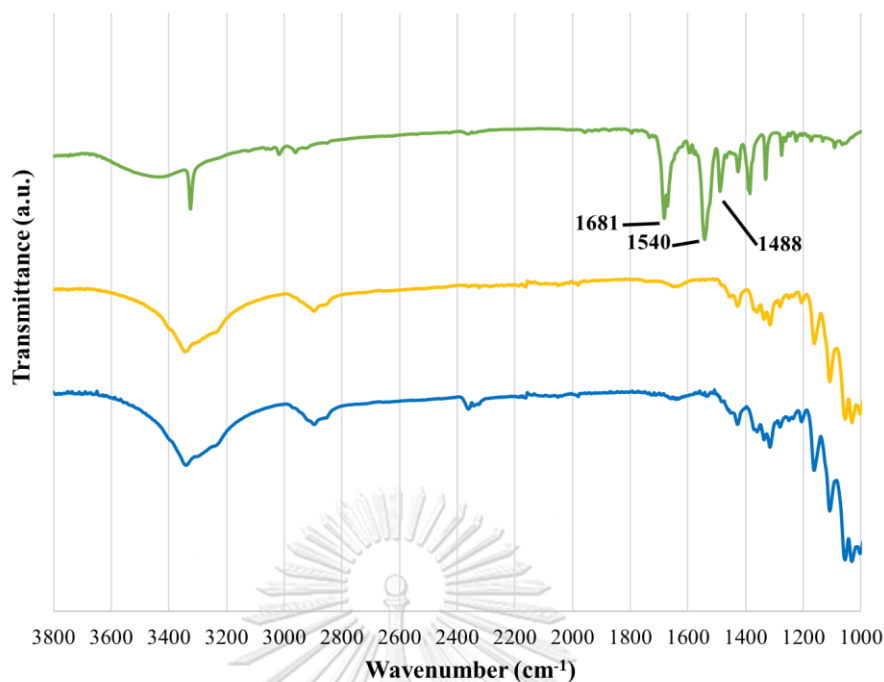
Figure 3.13 FTIR-ATR transmittance spectra of –**QA-Cl**, –**BC**, and –**QA** modified **BC** sample prepared by using Cs_2CO_3 as a base.

3.1.5 Metal ion adsorption study

The metal ion adsorption of **QA** modified **BC** sample was studied by inductively coupled plasma atomic emission spectroscopy (ICP-AES). In this work, **QA** modified **BC** sample prepared with K_2CO_3 as a base (section 3.1.3) was used as an adsorbent for Zn^{2+} and Cd^{2+} in water. The **BC** sample was prepared as a paper-thin sheet and immersed in the metal ion solutions for 24 hours. The ICP-AES analysis showed that both Zn^{2+} and Cd^{2+} were adsorbed over 99% (Table 3.2). The adsorption capacities of **QA** modified **BC** sample was calculated from the milligram of Zn^{2+} and Cd^{2+} adsorbed per gram of the modified **BC**. The values were 38.2 and 56.8 mg/gram for Zn^{2+} and Cd^{2+}, respectively. It has high of adsorption capacities in comparison with other works previously reported [75]. Although this **QA** modified **BC** showed higher adsorption capacity for Cd^{2+}, the sample did not give any fluorescence unlike the sample adsorbing Zn^{2+}. Therefore, the modified **BC** can be used as fluorescence sensor and adsorbent for Zn^{2+} but it can be used as only adsorbent for Cd^{2+}.

Table 3.2 ICP-AES study of Zn^{2+} and Cd^{2+} removal from aqueous solutions (10 mL) by **BC** and **QA** modified **BC**

Metal ion	Adsorbent	BC sample (g)	Initial concentration (M)	Final concentration (M)	Removal (%)	Adsorption capacity (mg/g)
Zn^{2+}	BC	0.0236	1.00×10^{-3}	1.02×10^{-3}	0	0
	QA modified BC	0.0171	1.00×10^{-3}	1.94×10^{-6}	99.8	38.2 ($\pm$1.5)
Cd^{2+}	BC	0.0219	1.00×10^{-3}	1.00×10^{-3}	0	0
	QA modified BC	0.0197	1.00×10^{-3}	3.20×10^{-6}	99.7	56.8 ($\pm$2.1)

3.2 Paper-based sensors for oil marker detection

To detect and prevent these adulterated oils, different oil markers have been added to petroleum oils with different tax rates. The oil marker detection method must be sensitive enough to detect the marker at ppm concentration level. In general, a dye marker is extracted into an aqueous layer and quantified by UV-visible absorption spectroscopy and fluorescence spectroscopy techniques. In this research section, filter paper strips were developed as the cellulose-based sensing platform for detection of a petroleum dye marker. Phenolphthalein (PhP) was used as the dye marker in gasoline samples. PhP was captured on the paper strips and converted into its pink-purple color state by a base. Three sample testing techniques namely dropping, dipping and counter-flowing methods, were studied. The color images of the tested strips were photographed by a smartphone camera under controlled white light illumination. The RGB digital color values of the images were determined and converted into the CMYK color values color by ImageJ processing program. The magenta color values were used for evaluating the detection sensitivity of the detection methods.

3.2.1 Dropping and dipping methods

The indicator strips for the direct dipping and dropping methods were studied included test for background color from samples and reagents, selection of solvents for preparation of PhP solutions and selection of bases for detection of PhP.

a) Test for background color from samples and reagents

First, the perturbation of gasoline sample for the filter paper (Whatman No. 3) were test. A piece of filter paper (Whatman No. 3) was cut into multiple 1×3 cm^2. The filter paper strip was soaked with gasoline or gasoline sample. While another piece of filter paper was soaked with a base solution (NaOH or K_2CO_3). Then the base coated filter paper was dipped into gasoline (Figure 3.14).
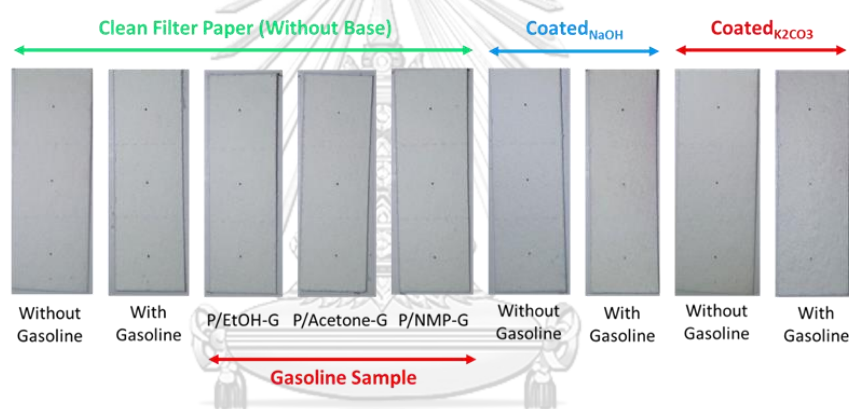
Figure 3.14 Photographic Images of filter paper without base coated exposing to gasoline and gasoline samples containing PhP (6 ppm). Filter paper with/without base (2.0 M) coated exposing with/without gasoline, all images were taken at 5 minutes of drying time.

It is noteworthy, the filter paper coated with NaOH has higher data color than the other. Due to its strong basic properties, it slightly damaged the filter paper causing intense yellowish, after preparation by dipping in NaOH solution and drying process. However, after the filter paper with base coated exposing with gasoline gave similar color with other sample. The MCYK data color show approximate same data color, there were no significant differences as show in figure 3.15. It was concluded that the coated with base or soaked with gasoline is not perturb the color of the filter paper.
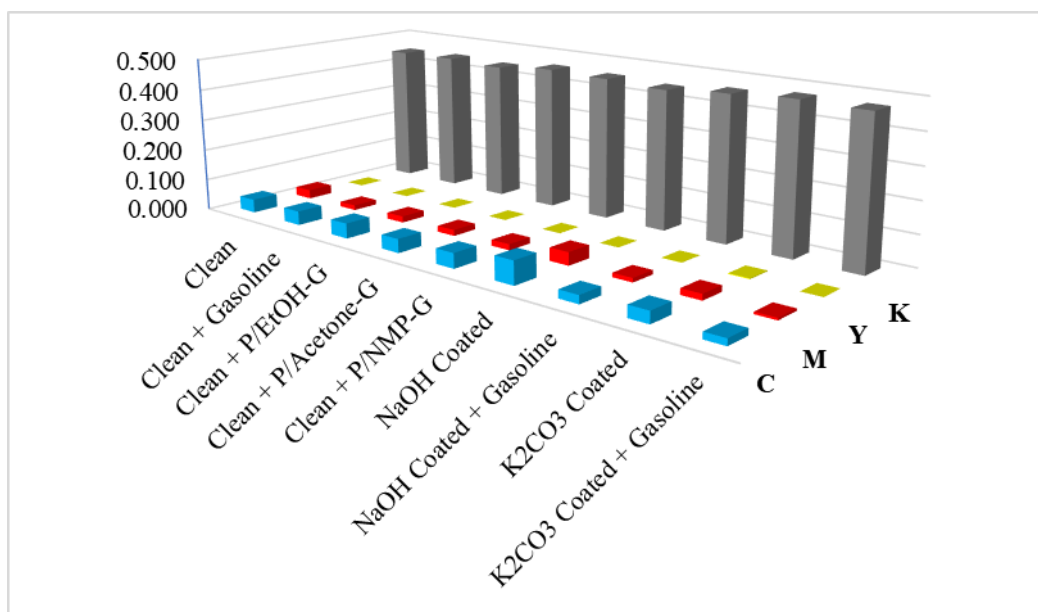
Figure 3.15 CMYK color values of filter paper without base coated exposing to gasoline and gasoline samples containing PhP (6 ppm). Filter paper with/without base (2.0 M) coated exposing with/without gasoline, all images were taken at 5 minutes of drying time.

b) **Selection of solvents for preparation of PhP solutions**

First, the effects of solvents used for the preparation of PhP stock solutions prior to mix with the commercial gasoline on the color appearance of the dye was studied. In this investigation, three solvents i.e. ethanol, acetone and NMP were evaluated to give three types of the gasoline samples coded as P/EtOH-G, P/Acetone-G and P/NMP-G, respectively. When the paper strips coated with NaOH base tested with the gasoline samples either by dropping or dipping method, gasoline sample P/EtOH-G consistently gave higher magenta color values than the P/NMP-G and P/Acetone-G, respectively (Figure 3.16). The color development of PhP is associated to the polarity and protic properties of the solvent. Generally, the color of PhP is better developed in more polar and protic solvents such as water or alcohols [76-78]. In this study, ethanol provided higher magenta color values than the other solvents and it is more favorable solvent for the preparation of PhP marker solution. Furthermore, ethanol is also commonly used for mixing with gasoline as an alternative automotive fuel and compatible with most current gasoline combustion engines.
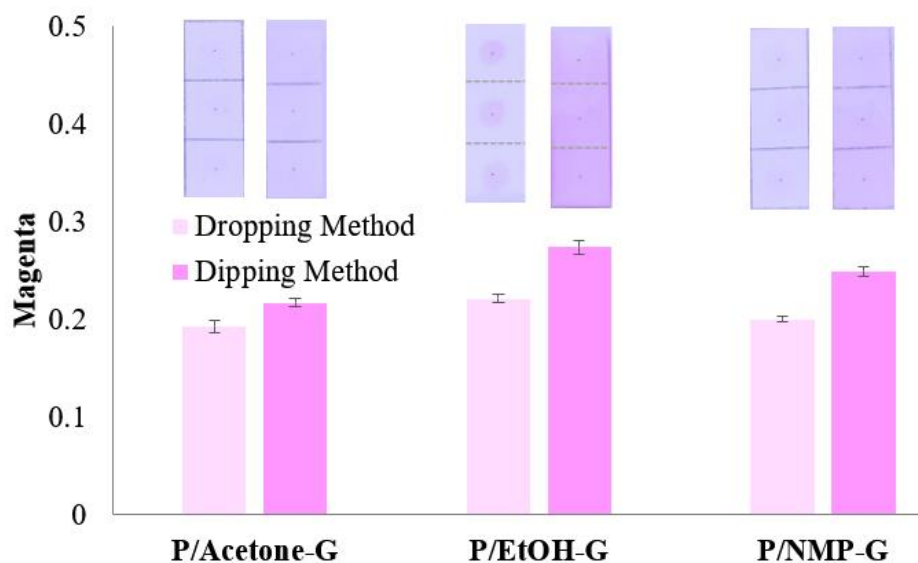
Figure 3.16 Magenta color values and representative photographic images of indicator strips coated with NaOH (2.0 M) after exposing to gasoline samples containing PhP (6 ppm) by dropping and dipping methods. Each color value was obtained from image taken at 5 minutes of drying time and presented as average value with standard deviation error bar of 3 replicated strips.

c) **Selection of bases for detection of PhP**

Next, effects of the type of base used for the preparation of the indicator strips on the detection sensitivity were investigated by the dipping and dropping methods. The indicator strips were prepared from paper substrate coated with NaOH and K_2CO_3 were compared. The indicator strips were tested with the gasoline sample P/EtOH-G containing of PhP (6 ppm). In the dropping method, the gasoline sample (6 µL) was dropped on the dot marked on the paper strip. In the dipping method, the paper strip was immersed entirely in the gasoline sample for 1 minute. It found that the indicator strips coated with NaOH generally showed higher magenta color values than those of the indicator strips coated with K_2CO_3 (Figure 3.17). The pH of the indicator surfaces, estimated by universal pH paper, were ~10 for NaOH-coated and ~8 for K_2CO_3-coated indicator strips. The results agree well with the pH dependence of the PhP color transition range. It is purple in the pH range of 8.2-10.0 and colorless at the pH below or above this range [17].

The sensitivity difference between the dropping and dipping sample testing methods was also observed. The results showed that the dipping method consistently exhibited higher magenta color value than that of the dropping method (Figure 3.17, 3.21a and b). These results reflected the amount of PhP captured on the indicator strips. For the dipping method, the entire indicator strip was exposed to the gasoline sample for 1 minute that probably allowed PhP to be accumulatively captured on the indicator strip for the entire immersing period. On the other hand, the amount of PhP marker per area of the detection zone in the dropping method was likely to be lower due to the diffusion of the limited amount (6 µL) of the gasoline sample dropped on the indicator strip.
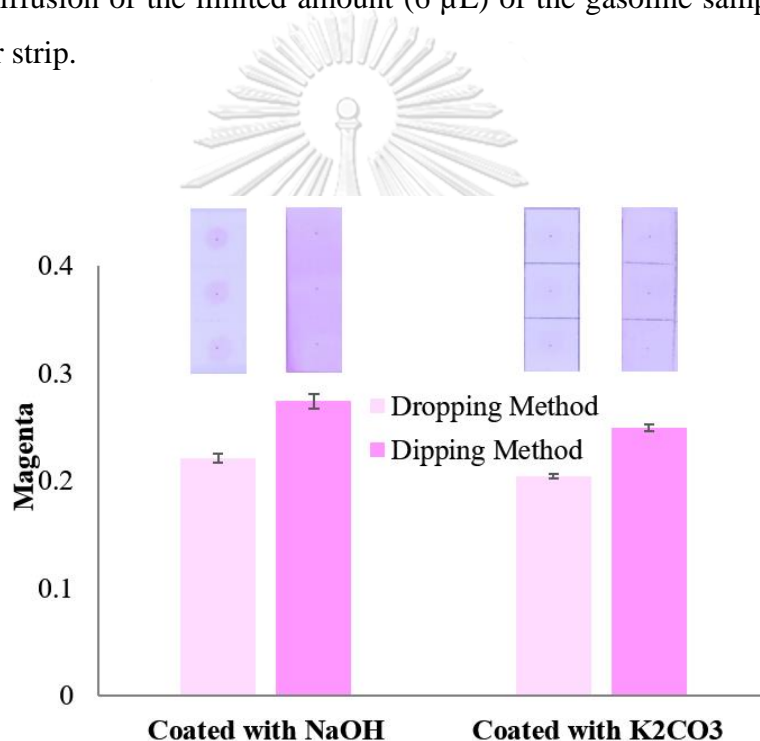
Figure 3.17 Magenta color values and representative photographic images of indicator strips coated with NaOH and K_2CO_3 (2.0 M) after exposing to gasoline samples P/EtOH-G containing PhP (6 ppm) by dropping and dipping methods. Each color value was obtained from image taken at 5 minutes of drying time and presented as average value with standard deviation error bar of 3 replicated strips.

Because pH directly affects the color development of php, the concentration of base used for the color development can affect the final color of the indicator strips. To determine the optimum amount of NaOH on the substrate, the concentration of

NaOH solution used for coating filter paper strips were varied from 0.5 to 3.0 M. The gasoline sample P/EtOH-G containing PhP (6 ppm) was used as a representative sample in all detection experiments. For the dropping and dipping methods, the highest magenta color values were obtained at 2.0 M of NaOH solution (Figure 3.18). The paper strips prepared with 3.0 M NaOH was a little fragile that was difficult to be handled. The high concentration of the strong base was probably break some of the intermolecular and intramolecular hydrogen bondings among cellulose chains in the filter paper. Furthermore, the indicator strips coated with 3.0 M NaOH solution was rather damp because the high content of NaOH readily absorbed the air humidity. Consequently, the optimum concentration of NaOH solution used for developing of the PhP color in dropping and dipping methods was 2.0 M.
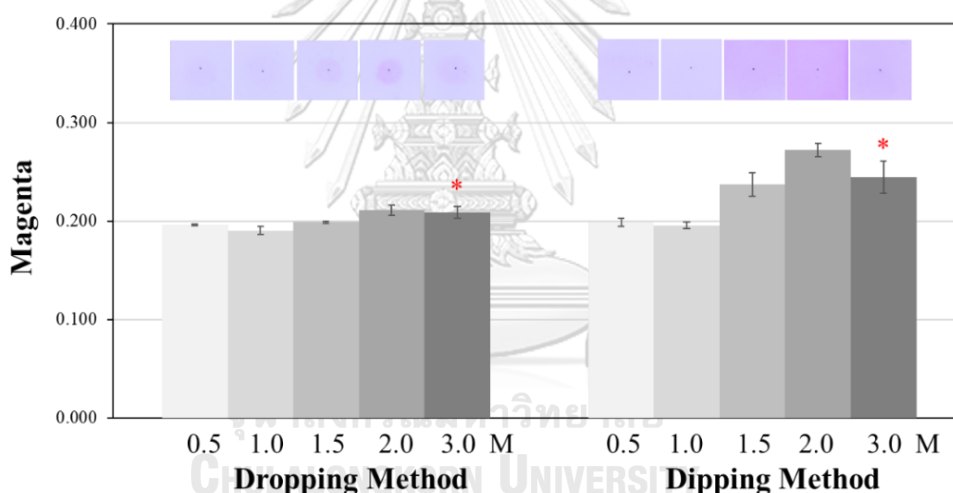
Figure 3.18 Effects of NaOH concentration on magenta color values of indicator strips obtained from dropping and dipping methods tested with gasoline sample P/EtOH-G containing PhP (6 ppm). Each color value was obtained from image taken at 5 minutes of drying time and presented as average value with standard deviation error bar of three replicated strips. * Paper strips were damp and difficult to be handled.

3.2.2 Counter-flowing method

Besides two simple sample testing methods (dropping and dipping), they have investigated a new sample testing technique, the "counter-flowing" method, with an aim to increase the marker detection sensitivity. In this new technique, one end of a solid substrate strip was dipped into a gasoline sample containing PhP and the other end was dipped into a NaOH solution. The gasoline sample and NaOH solution were allowed to diffuse along the substrate strip and meet midway of the strip (Figure **3.19**). Via this counter-flowing concept, the PhP dye will be adsorbed, reacted with base and accumulated in its color state at the interface.

After dipping both end of the indicator strip into the gasoline sample and NaOH solution, the sample and the solutions travelled to meet each other at 10 minutes and the purple color of PhP was clearly observed at 15 minutes (Figure 3.19b). The indicator strip was taken out after 15 minutes, allowed for air dry and photographed every 5 minutes. The magenta color value was evaluated by ImageJ application. It is important to note that the shape of the magenta color area in the images is rather irregular. To reduce the impact of human biases, the ImageJ wand tool was applied with auto threshold to select the area of the uniform color for determination of the magenta color values.
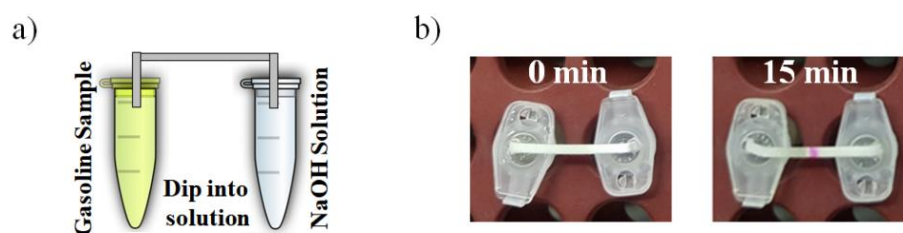
Figure 3.19 (a) Diagram of experimental setup for detection of PhP gasoline marker in counter-flowing method and (b) examples of photographic images of indicator strip at starting time and after 15 minutes.

a) **Effects of NaOH**

As the color of PhP depends on pH, the concentration of base used for the color development can affect the final color. The concentration of NaOH solution used for diffusion in counter-flowing method on the filter paper strips were varied as 0.5, 1.0, 1.5, 2.0 and 3.0 M. The gasoline sample P/EtOH-G containing PhP (6 ppm) was used as a representative sample in all detection experiments. The results showed that 3.0 M NaOH solution gave the highest magenta color value (Figure 3.20), however the paper strips became weak and easily broken during the detection process. The high concentration of strong NaOH base probably perturbs the intermolecular and intramolecular hydrogen bonding among cellulose chains in the filter paper. Consequently, the optimum concentration of NaOH solution used for developing of the PhP color in counter-flowing method is 2.0 M.
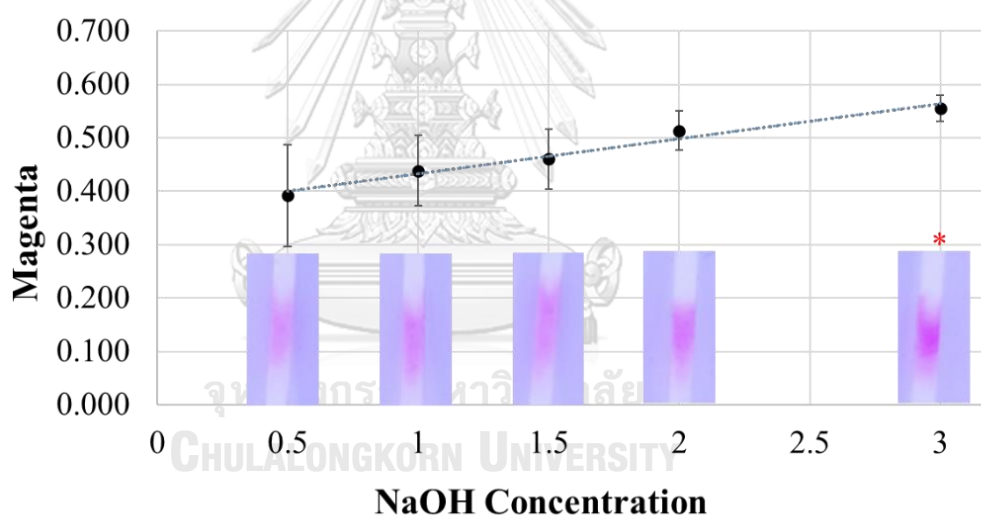
Figure 3.20 Magenta color values and photographic images of indicator strips tested with gasoline sample P/EtOH-G containing PhP (6 ppm) using varied concentrations of NaOH in counter-flowing method. Each color value was obtained from images taken at 5 minutes of drying time and presented as average value with standard deviation error bar of 3 replicated strips. * Paper strips were damp and difficult to be handled.

For comparison, the representative results from the counter-flowing method are compared with those obtained from the dropping and dipping methods described previously (Figure 3.21). Interestingly, the magenta color value from the counter-flowing method was significantly higher than those from the other two methods that strongly suggested the higher sensitivity of the counter-flowing method. This new counter-flowing concept can probably allow the accumulation of the PhP dye marker at the immiscible solvent interface to form narrow purple band during the continuous flowing of the gasoline sample and base solution from the opposite direction. To confirm this hypothesis, quantification of PhP marker in gasoline using these sample testing methods were studied to determine their detection limits.
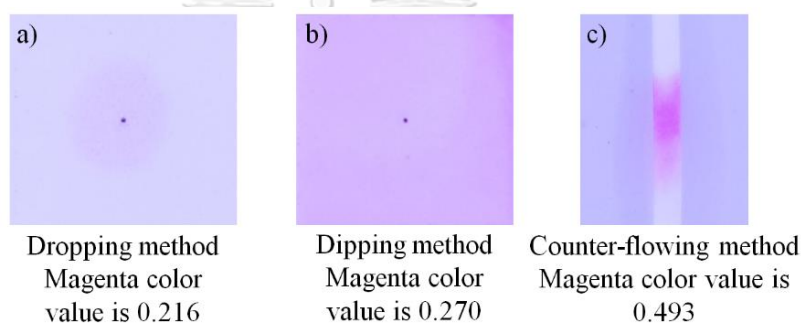
Figure 3.21 Photographic images and magenta color values of indicator strips tested with gasoline samples P/EtOH-G containing PhP (6 ppm) in various detection methods. NaOH solution (2.0 M) was used for coating of paper strips in dropping and drying methods and for diffusion on paper strip in counter-flowing method. All images were taken at 5 minutes of drying time.

b) **Substrate selection**

For naked eye detection, capturing PhP on cellulose materials is very economical and sensible because cellulose can provide highly sensitive detection via adsorption and accumulation as already observed and suggested in the previous section. For the substrate selection, filter paper (Whatman No. 1 and No. 3) and cotton yarns (3 ply and 12 ply or 0.18 g/m and 3.83 g/m, respectively) were tested to study different types of substrates. Gasoline samples P/EtOH-G containing PhP (6 ppm) and NaOH solution (2 M) were used in demonstrating model study for detection of the oil dye marker on different types of substrates by the proposed counter-flowing method.

The results shown in Figure 3.22 indicated that filter paper (Whatman No. 3) gave the most vivid pink-purple color with the highest and most consistent magenta color value. The results may be attributed to higher porosity and greater thickness of No. 3 filter paper in comparison with the No. 1 filter paper. For cotton yarns, both 3 ply and 12 ply of cotton yarns gave pale and inconsistent purple color due to their woolly and twinning structure. The color appeared on the yarns were rather non-uniform from side to side that was difficult for reproducibility of image recording. Overall, the the filter paper (No. 3) was the most suitable indicator substrate for detection of the gasoline oil marker in this work and it is used in all subsequent experiments.
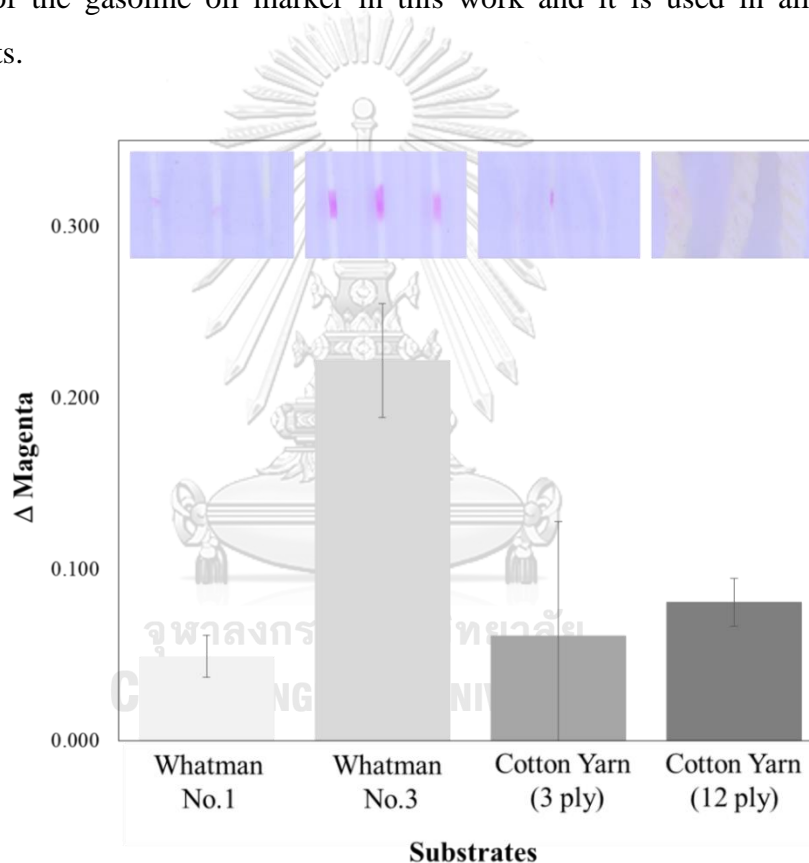
Figure 3.22 Image of magenta color values and photographic images of 3 replicate indicator strips made from different cellulose substrates tested with gasoline sample P/EtOH-G samples containing PhP (6 ppm) using NaOH solution (2.0 M) as color developing agent in counter-flowing method. Each color value was obtained from image taken at 5 minutes of drying time and presented as average value with standard deviation error bar of three replicated strips.

3.2.3 Effect of drying time

The difference between magenta color values (ΔM) of the indicator strips with and without PhP were used for comparison of the time dependence of the colorimetric responses in each detection method. The plot between ΔM and drying times, prior to the image photographing, showed relatively stable color values of the indicator strips up to at least 20 minutes of drying time in the dropping and dipping methods (Figure 3.23). In the counter-flowing method, the higher ΔM values were observed from the beginning and gradually increased with the drying time.
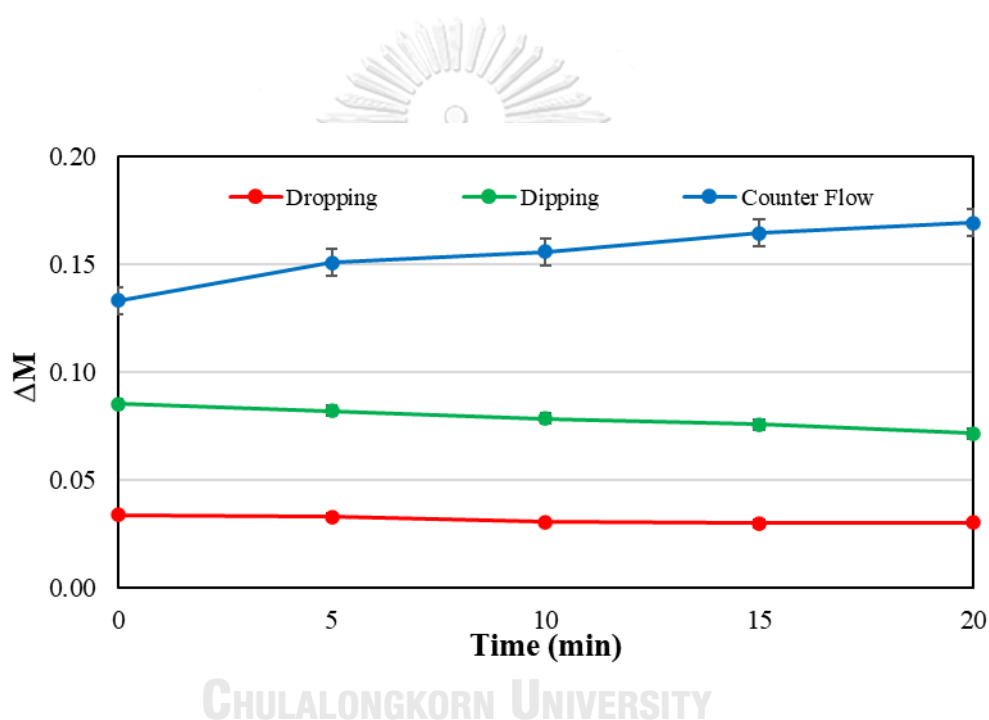
Figure 3.23 ΔM color values of indicator strips tested with gasoline sample P/EtOH-G containing PhP (4 ppm) with NaOH (2.0 M), obtained from the images taken at varied drying time in different detection methods. Each ΔM value was average value with standard deviation error bar of 3 replicated strips.

3.2.4 Quantitative detection of PhP marker

Under most regulation, it is important to demonstrate that the detection method can be used to detect the oil marker at lower concentration in case if the marked petroleum product was diluted with the unmarked product. The quantitative analyses of PhP marker with dropping, dipping and counter-flowing techniques were performed by using P/EtOH-G containing PhP from 0 to 6 ppm as the gasoline samples (Figure 3.24). The difference between magenta color (ΔM) values of the indicator strips with and without PhP were determined from the images of tested strips at 5 minutes drying time. The plots of ΔM values against the PhP concentrations from all three methods are presented in Figure 3.25. The slopes of the plots from these methods were in the order of the counter-flowing > dipping > dropping methods, that suggested their relative sensitivity. The limit of detection (LOD) of each method was calculated from $3 \times SD$/slope, where (SD) is the standard deviation of 6 strips tested with PhP free P/EtOH-G (blank). The LOD of the counter-flowing, dipping and dropping methods were 0.31, 0.56 and 0.62 ppm, respectively, which confirmed the sensitivity order of these methods. It is also important to note that the plot from the counter-flowing method gives best linearity with $R^2 = 0.9860$ while that from the dropping method gives the poorest linearity with $R^2 = 0.8994$ (Table 3.3). The linearity of the plot reflects the sensitivity and dynamic range of the detection methods. From LOD and R^2 values, the counter-flowing method provided the highest sensitivity and linear dynamic range for the detection of PhP petroleum oil marker by the smartphone camera.

Figure 3.24 Images derived from gasoline sample P/EtOH-G containing PhP (1-6 ppm) using a) dropping, b) dipping and c) counter-flowing method with 2.0 M NaOH. Each sample were tested in three replicates, all images were taken at 5 minutes of drying time.

Figure 3.25 Magenta color difference (ΔM) values derived from quantitative detection of gasoline sample P/EtOH-G containing PhP (1-6 ppm) using dropping, dipping and counter-flowing methods with 2.0 M NaOH. Each sample was tested in three replicates. * Data derived from test of gasoline sample P/EtOH-G containing 3 ppm PhP kept for 6 months using counter-flowing method.

To evaluate the stability of PhP in gasoline sample, P/EtOH-G containing PhP (3 ppm) was analyzed after 6 months of storage by UV-vis absorption spectroscopy and counter-flowing method. No significant change of the absorption spectrum was observed upon storage (Figure 3.26) and the ΔM values obtained from the counter-flowing method was about the same as the original value of the fresh sample (Figure 3.25). The results clearly demonstrated the applicability of both PhP as a gasoline marker and the counter-flowing method as a sensitive technique for detection of the marker by a smartphone camera. Another beneficial advantage of the counter-flowing detection method is that it uses simple filter paper strip which can be kept in ambient atmosphere indefinitely unlike the other two methods which required the NaOH coated paper strips needed to be kept in a closed and dry container and usable for only a few months. However, the higher sensitivity of the counter-flowing method was achieved with a cost of slightly longer operation time (Table 3.3).
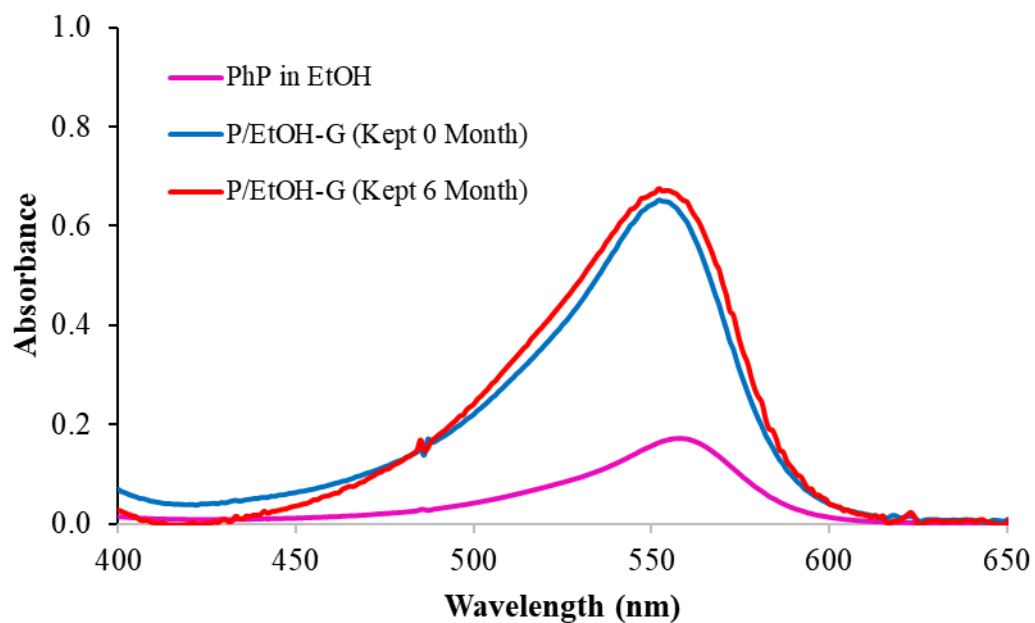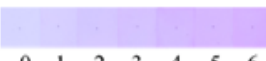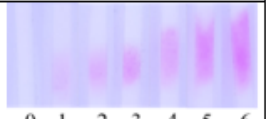
Figure 3.26 UV-vis absorption spectrum of PhP in EtOH (*9* ppm) and gasoline sample P/EtOH-G containing PhP (9 ppm) before and after kept for 6 months.

Table 3.3 The properties of indicator strips were prepared from dropping, dipping and counter-flowing method by using the gasoline sample P/EtOH-G with NaOH (2.0 M)

Feature	Method of detection		
	Dropping	Dipping	Counter-Flowing
Naked eye detection	0 1 2 3 4 5 6 down to 3 ppm	0 1 2 3 4 5 6 down to 2 ppm	0 1 2 3 4 5 6 down to 1 ppm
Limit of detection (LOD)	0.62 ppm	0.56 ppm	0.31 ppm
Linearity R^2	0.8994	0.9552	0.9860
Operation time	~5 min simple operation	~10 min simple operation	~20 min careful operation
Storage and stability of indicator strips	NaOH coated paper can be kept in a close and dry container for a few months	NaOH coated paper can be kept in a close and dry container for a few months	Filter paper can be kept indefinitely in ambient atmosphere
%RSD for color measurement	0.27 - 1.18	0.43 - 2.85	2.04 – 6.63

The color changes demonstrated above were evaluated based on the magenta color which is an intuitive choice for the color appearance of the base developed PhP. To demonstrate the consistency and generality of the color data processing in this work, it have also evaluated the color changes by applying a more common total color difference (ΔE) according to the CIE 1976 (CIE76) color system. The RGB data was processed into L*a*b* color system using an ImageJ plugin and converted to ΔE by following formula,

$$\Delta E = \sqrt{(L_2^* - L_1^*)^2 + (a_2^* - a_1^*)^2 + (b_2^* - b_1^*)^2}$$

where L* is luminance, a* is color on a green-red scale, and b* color on a blue-yellow scale. The ΔE values linearly increased with the PhP concentration consistent with the trend of ΔM values (Figure 3.27). These results demonstrated that ΔE may be used in place of ΔM if needed, especially for the detection of other dyes with different colors.

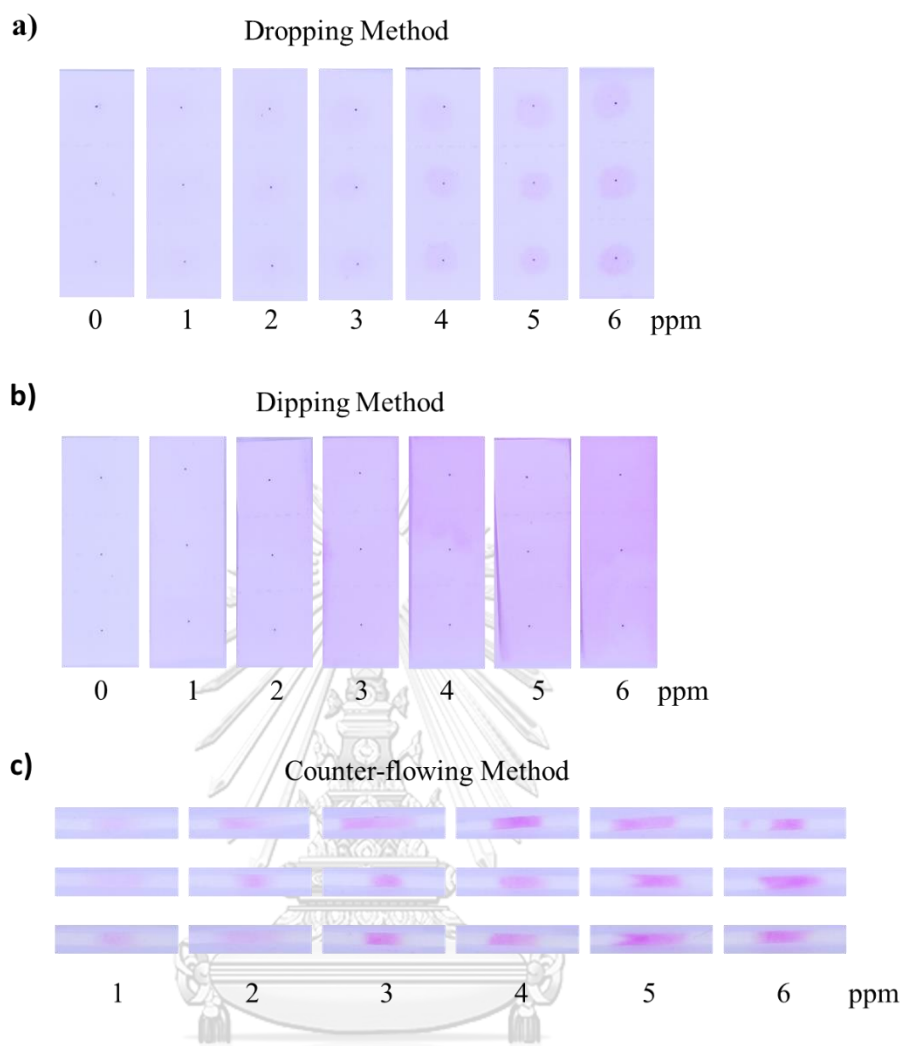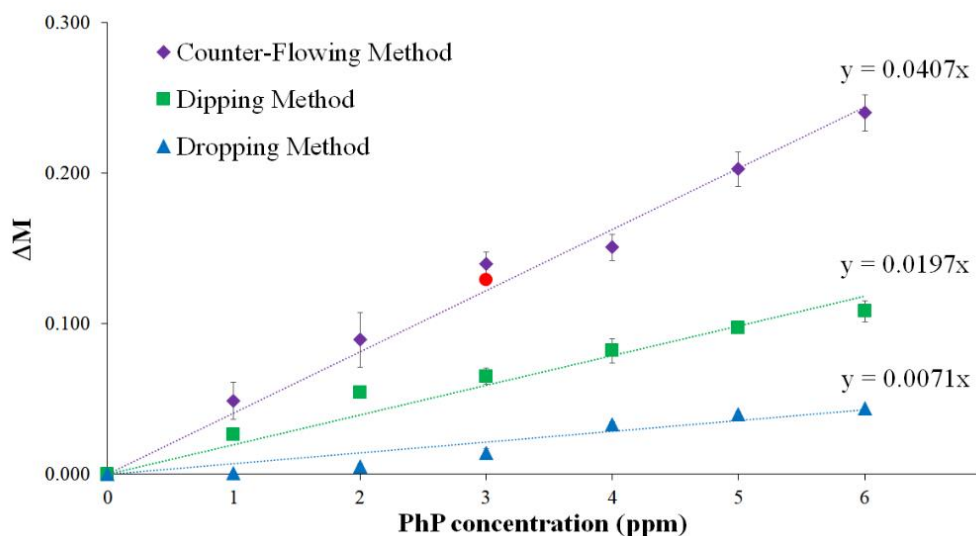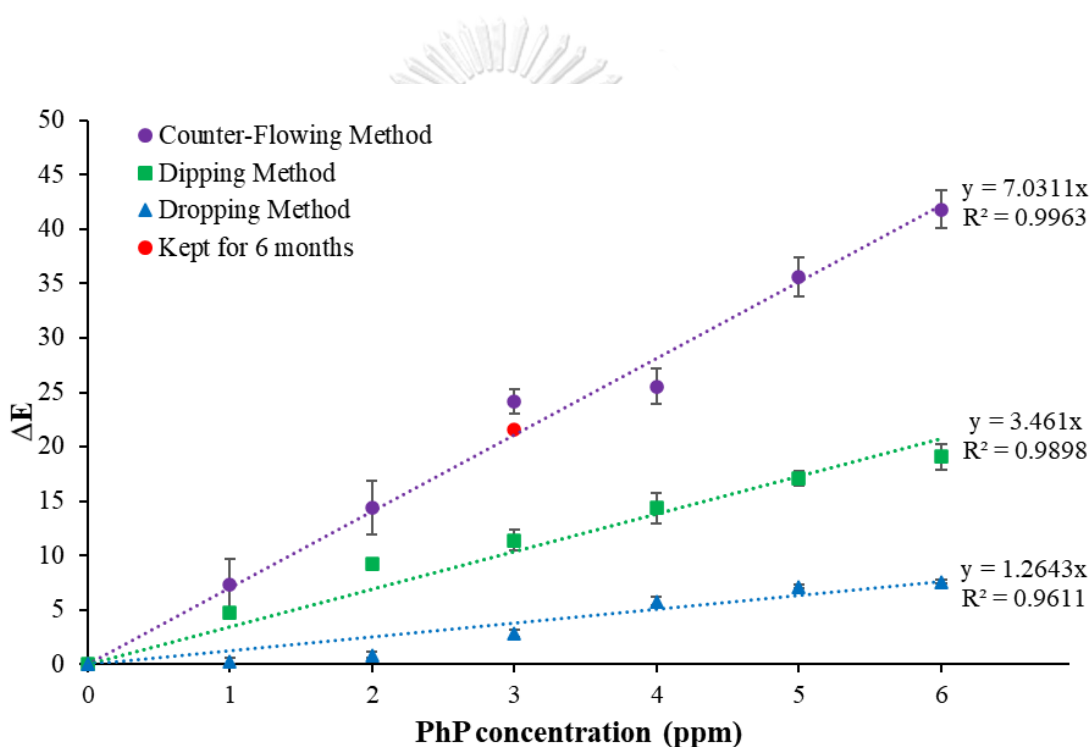Figure 3.27 The total color difference (ΔE) difference values derived from quantitative detection of gasoline sample P/EtOH-G containing PhP (1-6 ppm) using dropping, dipping and counter-flowing methods with 2.0 M NaOH. Each sample was tested in three replicates. • Data derived from test of gasoline sample P/EtOH-G containing PhP (3 ppm) kept for 6 months using counter-flowing method.

CHAPTER 4
CONCLUSION

Bacterial cellulose-based sensors and adsorbent for metal ion detection

BC was utilized as a substrate for immobilization of a 2-chloro-N-(quinolin-8-yl)acetamide (**QA-Cl**). The **QA** modified **BC** metal ion sensor and adsorbent was archived by using nucleophilic substitution with K_2CO_3 as a base. The immobilization of **QA** on **BC** was demonstrated by the green fluorescence observation from the **QA** modified **BC** sample when tested with Zn^{2+} solution. ATR-IR spectroscopy and elemental analysis also confirmed the presence of **QA** in the **QA** modified **BC** sample after 72 hours Soxhlet extraction. The metal ion adsorption study by ICP-AES showed that **QA** modified **BC** has the adsorption capacity of 38.2 and 56.8 mg/g for Zn^{2+} and Cd^{2+}, respectively. The metal ions in aqueous solution (10 mL) containing either 1 mM of Zn^{2+} or Cd^{2+} was effectively removed (over 99%) by less than 20 mg of **QA** modified **BC** sample.

จุฬาลงกรณ์มหาวิทยาลัย

CHULALONGKORN UNIVERSITY

Paper-based sensors for oil marker detection

In this work, paper-based sensors for oil marker detection were successful developed as a sensitive technique for convenient detection of a gasoline marker, phenolphthalein (PhP), on filter paper strip using digital imaging and processing. The PhP marker solution prepared in highly polar and protic solvent such as ethanol prior to mixing with gasoline samples gave intense purple color upon contact with NaOH base on the paper strips. The color developed on paper strips was conveniently recorded by a smart phone camera and processed into magenta color value in the CMYK color system using an ImageJ plugin. Three sample testing methods i.e. dipping, dropping and counter-flowing gave limit of detection of PhP at 0.56, 0.62 and 0.31 ppm, respectively. The counter-flowing method thus has the highest sensitivity, and it can easily detect 1 ppm of PhP in the gasoline with naked eye observation. This is by far among the most sensitive optical detection techniques of oil markers in comparison with other works previously reported (Table 4.1). The PhP marker was stable in gasoline samples for at least 6 months without significant change in concentration and UV-vis absorption spectrum. Most importantly, this work has demonstrated that the counter-flowing method provides a concurrent preconcentration and detection technique for convenient sensitivity enhancement that is potentially useful not only for the detection of an oil marker but also other analytes in water immiscible media. Further development of a smartphone application for image processing used in this work can also simplify the detection method for on-site analyses by non-technical operators.

Table 4.1 Comparison of the counter-flowing method used in this work with other methods for detection of oil markers previously reported in literatures

Marker Solution		Conc. (ppm)	Oil Type	Method	Stability	Ref.
Dye	Solvent					
Quinizarine	Acetonitrile	3-5	• Gasoline • Diesel	Square-wave Voltammetric, UV-vis Spectrophotometry (liquid extraction)	> 4 months	44
n-Alkylbenzene and Aniline Derivatives	Propane-1,3-diol and methanol	3-5	• Hi-Speed diesel	UV-vis spectrophotometry (liquid extraction)	> 3 months	46
Cardanol and Aniline Derivatives	Ethane-1,2-diol and methanol	2-5	• Gasoline • Hi-Speed Diesel	UV-vis spectrophotometry (liquid extraction)	> 3 months	47
Phthalocyanines and Naphthocyanines	Aromatic hydrocarbon	10	• Gasoline	Spectrofluorometer (liquid extraction)	>3 months	48
3-s-butyl-4-decyloxyphenyl methanetriyltribenzene	Methanol	2.5	• Gasoline • Diesel	UHPSFC-MS (liquid extraction)	> 3 months	49
N-ethyl-N-[2(isobutoxyethoxy)ethyl]-4-phenylazo)aniline)	Solvent-free	6	• Diesel	GC-FID HPLC-DAD (liquid extraction)	-	70
Quinizarine	-	<3	• Gasoline - Octane 95 - Octane 98 - Octane 100	UV-vis spectrophotometry (liquid extraction)	-	79
Phenolphthalein	Ethanol	1-6 (LOD = 0.31)	• Gasoline	Smartphone Photography (no liquid extraction needed)	> 6 months	This work

REFERENCES

1.   Chang, C.; Zhang, L., Cellulose-based hydrogels: Present status and application prospects. *Carbohydr. Polym.* **2011,** *84* (1), 40-53.

2.   Habibi, Y.; Lucia, L. A.; Rojas, O. J., Cellulose Nanocrystals: Chemistry, Self-Assembly, and Applications. *Chem. Rev.* **2010,** *110*, 3479–3500.

3.   Yan, H.; Chen, X.; Song, H.; Li, J.; Feng, Y.; Shi, Z.; Wang, X.; Lin, Q., Synthesis of bacterial cellulose and bacterial cellulose nanocrystals for their applications in the stabilization of olive oil pickering emulsion. *Food Hydrocoll.* **2017,** *72*, 127-135.

4.   Iguchi, M.; Yamanaka, S.; Budhiono, A., Bacterial cellulose—a masterpiece of nature's arts. *J. Mater. Sci.* **2000,** *35*, 261-270.

5.   Chawla, P. R.; Bajaj, I. B.; Survase, S. A.; Singhal, R. S., Microbial Cellulose Fermentative - Production and Applications. *Food Technol. Biotechnol.* **2009,** *47* (2), 107-124.

6.   Atsushi Okiyarna; Hideyuki Shirae; Hideo Kana; Yamanaka, S., Bacterial cellulose I. Two-stage fermentation process for cellulose production by Acetobacter aceti. *Food Hydrocoll.* **1992,** *6* (5), 471-477.

7.   Gelin, K.; Bodin, A.; Gatenholm, P.; Mihranyan, A.; Edwards, K.; Strømme, M., Characterization of water in bacterial cellulose using dielectric spectroscopy and electron microscopy. *Polymer* **2007,** *48* (26), 7623-7631.

8.   Sani, A.; Dahman, Y., Improvements in the production of bacterial synthesized biocellulose nanofibres using different culture methods. *J. Chem. Technol. Biotechnol.* **2010**, *85*, 151-164.

9.   Shi, Z.; Zhang, Y.; Phillips, G. O.; Yang, G., Utilization of bacterial cellulose in food. *Food Hydrocoll.* **2014,** *35*, 539-545.

10.   Carreira, P.; Mendes, J. A.; Trovatti, E.; Serafim, L. S.; Freire, C. S.; Silvestre, A. J.; Neto, C. P., Utilization of residues from agro-forest industries in the production of

high value bacterial cellulose. *Bioresour. Technol.* **2011,** *102* (15), 7354-7360.

11.   https://en.wikipedia.org/wiki/RGB_color_model *(accessed june 24, 2021).*

12.   https://en.wikipedia.org/wiki/CMYK_color_model *(accessed june 24, 2021).*

13.   https://en.wikipedia.org/wiki/Color_difference *(accessed june 24, 2021).*

14.   Cate, D. M.; Dungchai, W.; Cunningham, J. C.; Volckens, J.; Henry, C. S., Simple, distance-based measurement for paper analytical devices. *Lab Chip.* **2013,** *13* (12), 2397-2404.

15.   Eden Morales-Narva´ ez; Hamed Golmohammadi; Tina Naghdi; Hossein Yousefi; Uliana Kostiv; Daniel Hora´ k; Nahid Pourreza; Merkoci, A., Nanopaper as an Optical Sensing Platform. *ACS Nano* **2015,** *9* (7), 7296-7305.

16.   Guan, L.; Tian, J.; Cao, R.; Li, M.; Cai, Z.; Shen, W., Barcode-like paper sensor for smartphone diagnostics: an application of blood typing. *Anal. Chem.* **2014,** *86* (22), 11362-11367.

17.   Rathod, B. B.; Murthy, S.; Bandyopadhyay, S., Is this Solution Pink Enough? A Smartphone Tutor to Resolve the Eternal Question in Phenolphthalein-Based Titration. *J. Chem. Educ.* **2019,** *96* (3), 486-494.

18.   Choodum, A.; Kanatharana, P.; Wongniramaikul, W.; NicDaeid, N., A sol–gel colorimetric sensor for methamphetamine detection. *Sens. Actuator B-Chem.* **2015,** *215*, 553-560.

19.   Li, X.; Li, J.; Ling, J.; Wang, C.; Ding, Y.; Chang, Y.; Li, N.; Wang, Y.; Cai, J., A smartphone-based bacteria sensor for rapid and portable identification of forensic saliva sample. *Sens. Actuator B-Chem.* **2020,** *320*, 128303-128313.

20.   Lakowicz, J. R., *Introduction to Fluorescence.* Springer US: 2006; p 1-26.

21.   Higginson, K. A.; Zhang, X.-M.; Papadimitrakopoulos, F., Thermal and morphological effects on the hydrolytic stability of aluminum tris(8-hydroxyquinoline) (Alq3). *Chem. Mater.* **1998,** *10* (4), 1017-1020.

22.   Pohl, R.; Anzenbacher, P., Jr., Emission color tuning in AlQ3 complexes with extended conjugated chromophores. *Org. Lett.* **2003,** *5* (16), 2769-72.

23.   Pohl, R.; Montes, V. A.; Shinar, J.; Anzenbacher, P., Red−green−blue emission from tris(5-aryl-8-quinolinolate)Al(III) complexes. *J. Org. Chem.* **2004,** *69* (5), 1723-1725.

24.   Lee, C. B.; Uddin, A.; Hu, X.; Andersson, T. G., Study of Alq3 thermal evaporation rate effects on the OLED. *Mater. Sci. Eng. B.* **2004,** *112* (1), 14-18.

25.   Bhagat, S. A.; Borghate, S. V.; Kalyani, N. T.; Dhoble, S. J., Novel Na+ doped Alq3 hybrid materials for organic light-emitting diode (OLED) devices and flat panel displays. *Luminescence* **2015,** *30* (3), 251-256.

26.   Choong, V.-E.; Park, Y.; Gao, Y.; Mason, M. G.; Tang, C. W., Photoluminescence quenching of Alq3 by metal deposition: A surface analytical investigation. *J. Vac. Sci. Technol. A.* **1998,** *16* (3), 1838-1841.

27.   Pathak, R. K.; Dessingou, J.; Hinge, V. K.; Thawari, A. G.; Basu, S. K.; Rao, C. P., Quinoline driven fluorescence turn on 1,3-Bis-calix[4]arene conjugate-based receptor to discriminate Fe^{3+} from Fe^{2+}. *Anal. Chem.* **2013,** *85* (7), 3707-3714.

28.   Rastogi, S. K.; Pal, P.; Aston, D. E.; Bitterwolf, T. E.; Branen, A. L., 8-Aminoquinoline functionalized silica nanoparticles: A fluorescent nanosensor for detection of divalent zinc in aqueous and in yeast cell suspension. *ACS Appl. Mater. Interfaces.* **2011,** *3* (5), 1731-1739.

29.   Meng, X. M.; Wang, S. X.; Zhu, M. Z., Quinoline-based fluorescence. various aspects. *InTech.* **2012**.

30.   Fahrni, C. J.; O'Halloran, T. V., Aqueous coordination chemistry of quinoline-based fluorescence probes for the biological chemistry of zinc. *J. Am. Chem. Soc.* **1999,** *121* (49), 11448-11458.

31.   Zalewski, P. D., Flux of intracellular labile zinc during apoptosis (gene-directed cell death) revealed by a specific chemical probe, Zinquin. *Chem. Biol.* **1994,** *1* (3), 153-

161.

32.   Areti, S.; Bandaru, S.; Teotia, R.; Rao, C. P., Water-Soluble 8-Hydroxyquinoline Conjugate of Amino-Glucose As Receptor for La($3+$) in HEPES Buffer, on Whatman Cellulose Paper and in Living Cells. *Anal. Chem.* **2015,** *87* (24), 12348-12354.

33.   Boonkitpatarakul, K.; Smata, A.; Kongnukool, K.; Srisurichan, S.; Chainok, K.; Sukwattanasinitt, M., An 8-aminoquinoline derivative as a molecular platform for fluorescent sensors for Zn(II) and Cd(II) ions. *J. Lumin.* **2018,** *198*, 59-67.

34.   Song, H.; Zhang, Z., A quinoline-based ratiometric fluorescent probe for discriminative detection of Zn^{2+} and Cd^{2+} with different binding modes, and its Zn^{2+} complex for relay sensing of pyrophosphate and adenosine triphosphate. *Dyes Pigm.* **2019,** *165*, 172-181.

35.   Pourreza, N.; Golmohammadi, H.; Naghdi, T.; Yousefi, H., Green in-situ synthesized silver nanoparticles embedded in bacterial cellulose nanopaper as a bionanocomposite plasmonic sensor. *Biosens. Bioelectron.* **2015,** *74*, 353-359.

36.   Sai, H.; Xing, L.; Xiang, J.; Cui, L.; Jiao, J.; Zhao, C.; Li, Z.; Li, F.; Zhang, T., Flexible aerogels with interpenetrating network structure of bacterial cellulose–silica composite from sodium silicate precursor via freeze drying process. *RSC Adv.* **2014,** *4* (57), 30453-30462.

37.   Goncalves, S.; Padrao, J.; Rodrigues, I. P.; Silva, J. P.; Sencadas, V.; Lanceros-Mendez, S.; Girao, H.; Dourado, F.; Rodrigues, L. R., Bacterial cellulose as a support for the growth of retinal pigment epithelium. *Biomacromolecules* **2015,** *16* (4), 1341-1351.

38.   Hettegger, H.; Sumerskii, I.; Sortino, S.; Potthast, A.; Rosenau, T., Silane meets click chemistry: towards the functionalization of wet bacterial cellulose sheets. *ChemSusChem.* **2015,** *8* (4), 680-687.

39.   Sai, H.; Fu, R.; Xing, L.; Xiang, J.; Li, Z.; Li, F.; Zhang, T., Surface modification of bacterial cellulose aerogels' web-like skeleton for oil/water separation.

ACS Appl. Mater. Interfaces. **2015,** *7* (13), 7373-7381.

40.   Lamboni, L.; Li, Y.; Liu, J.; Yang, G., Silk Sericin-Functionalized Bacterial Cellulose as a Potential Wound-Healing Biomaterial. *Biomacromolecules* **2016,** *17* (9), 3076-3084.

41.   "Evaluation of the Performance of the Short-Listed Candidate Markers Regarding the Technical Requirements*"* JRC Technical Report 2017, *European Commission,* http://publications.jrc.ec.europa.eu/repository/bitstream/JRC10720/kjna 28670enn.pdf*, Retrieved on 10 February 2021.*

42.   "The colour of Australian unleaded petrol is changing to red/orange" Australian Institute of Petroleum LTD, September 2015, https://www.aip.com.au/sites /default/files/download-files/2017-09/AIP_ULP_Colour_Press_Release_and_QA.pdf, Retrieved on 10 February 2021.

43.   "Diesel fuel and kerosene; exemption for dyed fuel" US Code of Federation Title 26§48.4082-1, https://ecfr.federalregister.gov/current/title-26/chapter-I/subchap ter-D/part-48/subpart-H/subject-group-ECFR031f656bf9c8875/section-48.4082-1, Retrieved on 10 February 2020.

44.   Trindade, M. A. G.; Ferreira, V. S.; Zanoni, M. V. B., A square-wave voltammetric method for analysing the colour marker quinizarine in petrol and diesel fuels. *Dyes Pigm.* **2007,** *74* (3), 566-571.

45.   Orelup, R. B., 1988 Apr. 5. Colored petroleum markers. United States patent US 4,735,631.

46.   Suwanprasop, S.; Suksorn, S.; Nhujak, T.; Roengsumran, S.; Petsom, A., Petroleum Markers Synthesized from n-Alkylbenzene and Aniline Derivatives. *Ind. Eng. Chem. Res.* **2003,** *42* (21), 5054-5059.

47.   Suwanprasop, S.; Nhujak, T.; Roengsumran, S.; Petsom, A., Petroleum Marker Dyes Synthesized from Cardanol and Aniline Derivatives. *Ind. Eng. Chem. Res.* **2004,** *43* (17), 4973-4978.

48.   Smith, M. J., 1996 Mar. 12. Fluorescent petroleum markers. United States patent US 5,498,808.

49.   Langley, G. J.; Herniman, J.; Carter, A.; Wilmot, E.; Ashe, M.; Barker, J., Detection and Quantitation of ACCUTRACE S10, a New Fiscal Marker Used in Low-Duty Fuels, Using a Novel Ultrahigh-Performance Supercritical Fluid Chromatography–Mass Spectrometry Approach. *Energy Fuels* **2018,** *32* (10), 10580-10585.

50.   Iri, A. H.; Shahrah, M. H. A.; Ali, A. M.; Qadri, S. A.; Erdem, T.; Ozdur, I. T.; Icoz, K., Optical detection of microplastics in water. *Environ. Sci. Pollut. Res. Int.* **2021**, 1-7.

51.   Hampf, R.; Ulrich, A.; Wieser, J., Evaluation of CCD cameras for beam profile monitoring with high intensity particle beams traversing gases. *EPJ Tech. Instrum.* **2020,** *7* (1), 1-14.

52.   Trivellin, N.; Buffolo, M.; De Santi, C.; Meneghini, M.; Forzan, M.; Dughiero, F.; Zanoni, E.; Meneghesso, G., Full Optical Contactless Thermometry Based on LED Photoluminescence. *IEEE Trans. Instrum. Meas.* **2021,** *70*, 1-8.

53.   Desjardins, K.; Medjoubi, K.; Sacchi, M.; Popescu, H.; Gaudemer, R.; Belkhou, R.; Stanescu, S.; Swaraj, S.; Besson, A.; Vijayakumar, J.; Pautard, S.; Noureddine, A.; Mercere, P.; Da Silva, P.; Orsini, F.; Menneglier, C.; Jaouen, N., Backside-illuminated scientific CMOS detector for soft X-ray resonant scattering and ptychography. *J. Synchrotron. Radiat.* **2020,** *27* (Pt 6), 1577-1589.

54.   Morales, A.; Guerra, R.; Horstrand, P.; Diaz, M.; Jimenez, A.; Melian, J.; Lopez, S.; Lopez, J. F., A Multispectral Camera Development: From the Prototype Assembly until Its Use in a UAV System. *Sensors* **2020,** *20* (21), 6129-6153.

55.   Ngampeungpis, W.; Tumcharern, G.; Pienpinijtham, P.; Sukwattanasinitt, M., Colorimetric UV sensors with tunable sensitivity from diacetylenes. *Dyes Pigm.* **2014,** *101*, 103-108.

56.   Savkova, E. N., Colorimetric Research of Self-Luminous Objects in Software and Hardware Environments by the Method of Implementation of Multidimensional

Scales. *Meas. Tech.* **2020,** *63* (8), 636-644.

57.   Yoo, Y.; Yoo, W. S., Turning Image Sensors into Position and Time Sensitive Quantitative Colorimetric Data Sources with the Aid of Novel Image Processing/Analysis Software. *Sensors* **2020,** *20* (22), 6418-6433.

58.   Ballesteros, J. I.; Caleja-Ballesteros, H. J. R.; Villena, M. C., Digital image-based method for iron detection using green tea (Camellia sinensis) extract as natural colorimetric reagent. *Microchem. J.* **2021,** *160*, 105652-105657.

59.   Meredith, N. A.; Quinn, C.; Cate, D. M.; Reilly, T. H., 3rd; Volckens, J.; Henry, C. S., Paper-based analytical devices for environmental analysis. *Analyst* **2016,** *141* (6), 1874-1887.

60.   Kong, J. E.; Wei, Q.; Tseng, D.; Zhang, J.; Pan, E.; Lewinski, M.; Garner, O. B.; Ozcan, A.; Di Carlo, D., Highly Stable and Sensitive Nucleic Acid Amplification and Cell-Phone-Based Readout. *ACS Nano* **2017,** *11* (3), 2934-2943.

61.   Valeria, S.; Avila, F.; Avena, M., A Simple Strategy for Methylene Blue Determination in Human and Veterinary Dosage Forms by Digital Imaging. *J. Anal. Chem.* **2020,** *75* (7), 958-964.

62.   Rajamanikandan, R.; Lakshmi, A. D.; Ilanchelian, M., Smart phone assisted, rapid, simplistic, straightforward and sensitive biosensing of cysteine over other essential amino acids by β-cyclodextrin functionalized gold nanoparticles as a colorimetric probe. *New J. Chem.* **2020,** *44* (28), 12169-12177.

63.   Dantas, H. V.; Barbosa, M. F.; Pereira, A.; Pontes, M. J. C.; Moreira, P. N. T.; Araújo, M. C. U., An inexpensive NIR LED Webcam photometer for detection of adulterations in hydrated ethyl alcohol fuel. *Microchem. J.* **2017,** *135*, 148-152.

64.   Hou, C.-Y.; Fu, L.-M.; Ju, W.-J.; Wu, P.-Y., Microfluidic colorimetric system for nitrite detection in foods. *Chem. Eng. J.* **2020,** *398*, 125573-125581.

65.   Woolf, M. S.; Dignan, L. M.; Scott, A. T.; Landers, J. P., Digital postprocessing and image segmentation for objective analysis of colorimetric reactions. *Nat. Protoc.*

2021, *16* (1), 218-238.

66.   Yu, A.; Shang, J.; Cheng, F.; Paik, B. A.; Kaplan, J. M.; Andrade, R. B.; Ratner, D. M., Biofunctional paper via the covalent modification of cellulose. *Langmuir* **2012,** *28* (30), 11265-11273.

67.   Zhu, Y.; Xu, X.; Brault, N. D.; Keefe, A. J.; Han, X.; Deng, Y.; Xu, J.; Yu, Q.; Jiang, S., Cellulose Paper Sensors Modified with Zwitterionic Poly(carboxybetaine) for Sensing and Detection in Complex Media. *Anal. Chem.* **2014,** *86* (6), 2871-2875.

68.   Hamedpour, V.; Oliveri, P.; Malegori, C.; Minami, T., Development of a morphological color image processing algorithm for paper-based analytical devices. *Sens. Actuator B-Chem.* **2020,** *322*, 128571-128578.

69.   Fadairo, A. S.; Ekoh-Chukwukalu, J.; Adeyemi, G. A.; Abolarin, O. G.; Mkpaoro, I. M. F., A fast and cost-efficient method to detect ethanol as adulterant in gasoline. *MethodsX* **2020,** *7*, 100974-100984.

70.   Le Goff, T.; Mazlum, S.; Wood, S., Production of a Solvent Yellow 124 "euromarker" reference material certified for purity. *Fuel* **2009,** *88* (10), 2025-2031.

71.   Alberici, R. M.; Simas, R. C.; Abdelnur, P. V.; Eberlin, M. N.; de Souza, V. a.; de Sá, G. F.; Daroda, R. J., A Highly Effective Antioxidant and Artificial Marker for Biodiesel. *Energy Fuels.* **2010,** *24* (12), 6522-6526.

72.   Zhang, Y.; Guo, X.; Si, W.; Jia, L.; Qian, X., Ratiometric and Water-Soluble Fluorescent Zinc Sensor of Carboxanmidoquinoline with an Alkoxyethylamino chain as Receptor. *Org. Lett.* **2008,** *10* (3), 473-476.

73.   Sandip Banthia, A. S., A New Strategy for Ratiometric Fluorescence Detection of Transition Metal Ions. *J. Phys. Chem. B.* **2006,** *110*, 6437-6440.

74.   Dueno, E. E.; Chu, F.; Kim, S.-I.; Jung, K. W., Cesium Promoted O-Alkylation of Alcohols for the Efficient Ether synthesis. *Tetrahedron Lett.* **1999,** *40*, 1843-4846.

75.   Ouyang, D.; Zhuo, Y.; Hu, L.; Zeng, Q.; Hu, Y.; He, Z., Research on the Adsorption Behavior of Heavy Metal Ions by Porous Material Prepared with Silicate

Tailings. *Minerals* **2019,** *9* (5) 291-307.

76.   Tsubaki, K.; Tanima, D.; Nuruzzaman, M.; Kusumoto, T.; Fuji, K.; Kawabata, T., Visual Enantiomeric Recognition of Amino Acid Derivatives in Protic Solvents. *J. Org. Chem.* **2005,** *70* (12), 4609-4616.

77.   Tsubaki, K., Colorimetric recognition using functional phenolphthalein derivatives. *J. Incl. Phenom. Macrocycl. Chem.* **2008,** *61* (3-4), 217-225.

78.   Horváth, P.; Gergely, A.; Mazák, K.; Kökösi, J.; Szász, G., Novel Data on the Effect of Tetrahydrofuran as an Organic Co-Modifier in RP-HPLC. *Chromatographia* **2013,** *76* (9-10), 441-448.

79.   Haloulos, I.; Theodorou, D.; Zannikou, Y.; Zannikos, F., Monitoring fuel quality: a case study for quinizarin marker content of unleaded petrol marketed in Greece. *Accreditation Qual. Assur.* **2016,** *21* (3), 203-210.
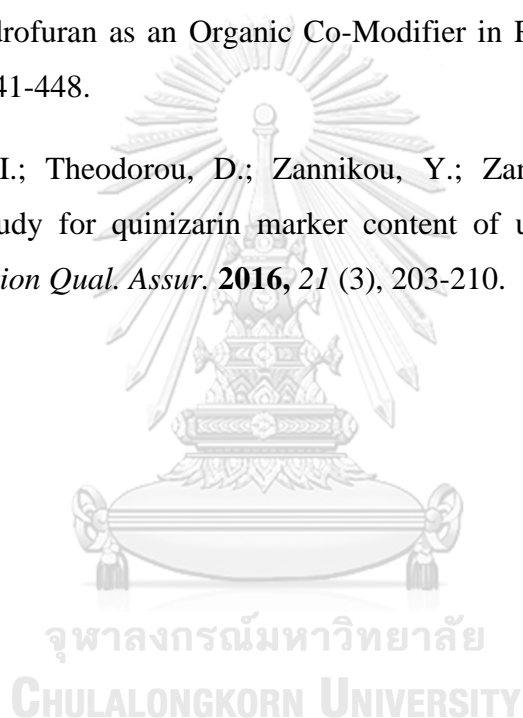
จุฬาลงกรณ์มหาวิทยาลัย
CHULALONGKORN UNIVERSITY

VITA

NAME   Jadetapong Klahan

DATE OF BIRTH   8 August 1985

PLACE OF BIRTH   Nakhon Ratchasima

HOME ADDRESS   1680 Mittraphap 15 road, nai mueang, mueang, nakhon ratchasima.

จุฬาลงกรณ์มหาวิทยาลัย
CHULALONGKORN UNIVERSITY